Numerical simulation of crack development
for Leak-Before-Break applications

Marjolein Bransen

TUDelft
Delft
University of
Technology

Department of Maritime & Transport Technology

Numerical simulation of crack development

for Leak-Before-Break applications

MASTER OF SCIENCE THESIS

For the degree of Master of Science in Offshore and Dredging
Engineering at Delft University of Technology

Marjolein Bransen

November 21, 2016

Abstract

The term Leak-Before-Break (LBB) refers to a well-established safety criterion used to assess whether cracked tanks or pipes can leak detectable amounts of fluid as a warning before catastrophic failure occurs. In this research The LBB criterion was applied to the safety assessment of spherical Liquefied Natural Gas (LNG) containment systems on ships. For this type of LNG tanks, the International Code for the Construction and Equipment of Ships Carrying Liquefied Gases in Bulk (IGC) requires several fracture mechanics analyses of fatigue crack growth.

Details on how these analyses should be carried out can be found in industry codes. Although these codes provide guidance on most aspects of an LBB assessment, they are not fully satisfactory with regard to their recommendations on how to calculate the growth of deep semi-elliptical surface cracks, on how to estimate the crack shape when the crack snaps through the tank wall and how to assess these through-thickness cracks in the stage right after breakthrough.

The aim of this research was to more accurately simulate the development of cracks for LBB applications. To do so, a new numerical calculation model have been developed for the estimation of crack growth, crack shape development and crack propagation after wall penetration. In addition, Finite Element Models (FEM) have been developed to predict the Stress Intensity Factor (SIF), a parameter that characterises the local stress distribution in the vicinity of a crack-tip and is commonly used in fracture mechanics. Finite Element (FE) analyses were conducted to evaluate existing, approximative SIF solutions for deep, semi-elliptical surface cracks and to find a new, FE-derived SIF solution for through-thickness cracks after breakthrough. Both the new FE-derived and existing SIF solutions were used in the numerical model. The results of different SIF solutions and numerical model configurations were then compared to experimental data from the literature in order to find recommendations for the enhancement of existing LBB procedures.

Table of Contents

List of Figures

List of Tables

Glossary

List of Acronyms

AFNTO   Ando, Fujibayashi, Nam, Takahashi and Ogura

API   American Petroleum Institute

BCF   Boundary Correction Factor

BS   British Standard

FE   Finite Element

FEM   Finite Element Model(s)

IGC   International Code for the Construction and Equipment of Ships Carrying Liquefied Gases in Bulk

LBB   Leak-Before-Break

LEFM   Linear Elastic Fracture Mechanics

LNG   Liquefied Natural Gas

LR   Lloyd's Register

NR   Newman and Raju

NRC   Newman and Raju Correction

SIF   Stress Intensity Factor

SINTAP   Structural Integrity Assessment Procedures for European Industry

TU Delft   Delft University of Technology

List of Symbols

Greek Symbols

Γ	Integration contour
ϵ	Strain
η	Ratio length over width, c/W
θ	Angle
μ	Shear modulus
ν	Poisson's ratio
Π	Potential energy
σ	Nominal stress
σ_y	Yield stress
$\Delta\sigma$	$\sigma_{max} - \sigma_{min}$
φ	Parametric angle of the ellipse

Latin Symbols

A	Deepest point of a semi-elliptical crack
$\mathcal{A}$	Crack area
a	General crack size/ depth of a semi-elliptical crack
a_1	Initial crack depth
a_{bb}	Assumed depth of the crack at ligament instability
C	Surface point of a semi-elliptical crack
$\hat{C}$	Constant in Paris relation
$\mathcal{C}$	Compliance
c	Half surface length of the crack
c_1	Initial crack half length
c_2	Half length of the back side of the crack after breakthrough
E	Youngs' modulus
E'	E (plane stress) ; $E/(1-\nu^2)$ (plane strain)
e	Eccentricity
$\mathcal{F}$	Work done by external forces
$f_R(.)$	Function depending on R
f_w	Finite width correction factor
f_φ	Embedded elliptical crack boundary correction factor
$\mathcal{G}$	Linear elastic energy release rate
H	(Half-) heigth
i	Iteration step number
J	Energy release rate
K	Stress intensity factor

K_c	Critical stress intensity factor (plane stress)
K_{eff}	Effective stress intensity
K_{Ic}	Critical stress intensity factor (plane strain)
ΔK	$K_{max} - K_{min}$
ΔK_{th}	Threshold stress intensity factor range
k	Step number
$\hat{m}$	Exponent in Paris relation
$m(x,a)$	Weight function
N	Number of load cycles
n	Total number of steps/ order of the stress field
n_i	Normal vector components
P	Load
Q	Square of the complete elliptic integral of the second kind
R	Load ratio ($= \sigma_{min}/\sigma_{max} = K_{min}/K_{max}$)
r	Radius
r^2	Coefficient of determination
r_p	Radius of the plastic zone around the crack-tip
T	Thickness of a solid body
T_i	Stress vector components
t	Plate thickness
$\mathcal{U}$	Elastic strain energy
u	Displacement
W	(Half-)width
$\mathcal{W}$	Strain energy density
$\{X,Y,Z\}$	Global coordinates
$\{x,y,z\}$	Local coordinates
Y	Boundary correction factor

Subscripts/Superscripts

A	At point A
a	Along direction a
bb	Before breakthrough
bt	Breakthrough
b	Bending
C	At point C
c	Along direction c/critical
D	At point D
max	Maximum
min	Minimum
m	Membrane
$*$	Condition at breakthrough

Preface

During my first days of my internship at the Global Technology Centre of Lloyd's Register (LR) in Southampton, I was given the opportunity to join a multi-day workshop on fracture mechanics related topics. A group of Lloyd's experts from all over the world shared their knowledge of a wide range of topics within this field. Some of them gave examples of the challenges they had encountered and how they had managed to deal with these issues. They also raised some current unresolved questions related to their work. One of these problems, on how to deal with crack propagation in spherical LNG tanks after a crack had appeared at the tank surface, became the starting point for a research exercise and this thesis.

The idea to apply for a graduate internship at LR came after doing an internship at a shipyard where the largest vessel in the world, the *Pioneering Spirit* was being build. Not only did this experience aroused my interest for marine engineering, it also introduced me to the importance of the work of classification societies like LR and their contribution to the safety of vessels.

I would like to express my gratitude to Rob Pijper of LR for giving me the great opportunity to work on my thesis at the Southampton office were I was surrounded by experts in marine engineering. In addition, his genuine interest in my research and my personal well-being while living in England is greatly appreciated. Of the many helpful and welcoming colleagues in Southampton, I would like to mention in particular my supervisors Richard Villavicencio and Shengmin Zhang. Their encouragements and efforts to improve my research have been a welcoming assistance to my work and it has been a great pleasure to work with them. Richard has not only helped me to retrieve data from the figures from external resources, he also spend much of his own time to read all chapters and gave valuable comments on my work. This welcoming and productive environment greatly contributed to the completion of the thesis.

Furthermore, I am also grateful for the useful translation of the article of Shingai *et al.* from Japanese to Dutch made by Lei Hendriks. He does not only have a degree in Japanese studies but also works as an engineer, which made him a great translator for this article. I am very thankful that he dedicated his free time to translate this for me.

On a more personal level, I would like to thank my friends Laurens, Moniek, Roos and my fellow students from 'the Parrotzone' for their mental support during the course of my study. Their encouragements, sense of humour and friendship have been an indispensable factor of success to the completion of my study during these seven *vette* years in Delft.

More than anyone else, I would like to thank my parents. They supported me in all possible kinds of ways. They encouraged me from a very young age to make my own choices and gave me the self-confidence that I was able to make my own decisions. The choices I made were quite often not their choices - quite the opposite in fact. My decision to study Korean Studies came to them as a surprise but nevertheless, they were proud that I became a language student. When I started taking evening classes in mathematics and physics at an adult education centre and subsequently enrolled as a student at the TU Delft, they were even more surprised. While some parents hope that their child becomes an engineer, mine might have had their doubts whether this plan would stand a chance. They might have thought that studying Dutch, history or economics would be more suitable for me. If your child follows precisely the career path that you have in mind, it is easy to be enthusiast and encouraging. But I truly admire my parents because they did so regardless of what I choose to do. By reassuring me countless times that I could count on them even if I would completely fail, I was able to flourish.

Delft, University of Technology   Marjolein Bransen
November 21, 2016

"On ne découvre pas de terre nouvelle sans consentir à perdre de vue, d'abord et longtemps, tout rivage."

— *André Gide*

Chapter 1

Introduction

A well-established safety assessment criterion in the nuclear and (petro-) chemical industry is to check that tanks and pipes have the ability to leak for a certain period of time as a warning before catastrophic failure occurs [1]. The objective of this so-called Leak-Before-Break (LBB)[1] assessment is to analyse:

1) How and how fast an initial flaw develops into an unstable crack and whether this instability occurs before or after penetrating through a tank or pipeline wall;

2) Whether a breakthrough crack leaks enough to get detected before becoming unstable;

3) Whether sufficient time is available after leakage detection to take emergency measures.

Figure 1-1 illustrates the stages of crack development in the wall of a tank or pipe. An initial crack is present in the structure, and the first step is to establish the initial crack size and shape. These could be known from inspection or could be assumed to be equal to the minimum detectable size. The next step is to determine how the shape of the crack develops while growing towards wall penetration, i.e. the crack growth phase. A sufficiently large crack becomes unstable, resulting in a sudden rupture of the material. If the crack re-stabilises after wall penetration an LBB case could be made, provided there is enough time for leak detection before the crack reaches a critical length at which the tank or pipe catastrophically fails. The crack growth phase after breakthrough is referred to as the crack propagation phase. Crack development refers to both the crack growth and propagation phase.

Under normal operating conditions the nominal stresses in tanks and pipes, taken into account a safety factor, should stay well below the yield strength of the material and failure should not occur when a small flaw is present. Furthermore, in these predominantly tensile loaded structures, buckling is not an issue either. Hence, apart from accidental loads, the main threat to cyclically loaded constructions is fatigue, damaging metallic structures even when loaded well below the yield stress. What initially may start as a small flaw, could grow into a potentially dangerous crack.

---

[1]It would have been more appropriate to refer to this criterion as 'Leak-Before-Failure' but this research follows the more commonly used 'Leak-Before-Break' terminology.
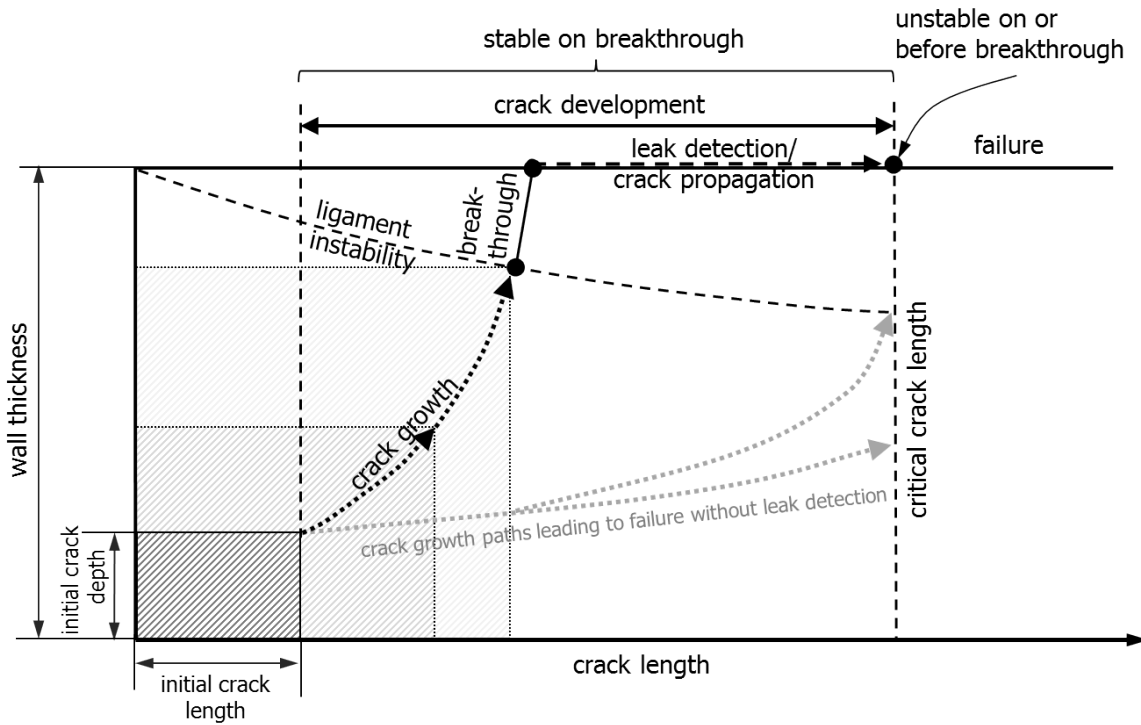
Figure 1-1: Leak-before-break diagram

In the context of welded constructions it is assumed that there are always flaws of the order of 0.1-5 mm present because the welding process introduces slag or gas intrusions, or flaws are introduced by the overuse or lack of welding material and other irregularities. For fatigue calculations, rather than studying the macroscopic features of the structure, the attention shifts to the analysis of cracks that are barely to the naked eye.

Fracture mechanics is the field of study concerned with the analysis of crack development and fatigue. Questions related to the lifetime up to catastrophic failure as well as predictions related to the size of the crack (opening) are both topics within the scope of fracture mechanics and therefore this discipline is indispensable for LBB assessments. A short overview of relevant fracture mechanics topics can be found in Appendix A.

Several codes and standards give recommendations for LBB assessments, see for instance Annex F of the British Standard (BS) [2], the recommendations of the American Petroleum Institute (API) [3] or the Structural Integrity Assessment Procedures for European Industry (SINTAP) [4]. Typically, the assessment procedure involves the determination of the load spectrum, geometry, material and temperature dependent parameters and other parameters that can tell something about crack development.

An important parameter in the field of fracture mechanics is the SIF which determines the local stress distribution around the crack-tip and can be used to predict the crack growth (see for further details Appendix A). The SIF is expressed as

$$K = Y\sigma\sqrt{\pi a} \tag{1-1}$$

in which Y is a factor that corrects for geometry, plasticity, bulging, welding, loading and/or

other factors, σ is the nominal stress and a refers to a crack size in general, like the length or depth of a crack. When reaching K_{Ic}, the critical SIF, a linear elastic material under plain strain conditions[2] starts to propagate in an unstable manner. Plasticity effects decrease the critical crack size but for stress levels well below the yield stress, it is a reasonable assumption to apply a Linear Elastic Fracture Mechanics (LEFM) model. The critical SIF depends on the temperature, material properties and production techniques and is obtained by standardised tests. From Eq. (1-1), the critical crack size is determined as

$$a_c = \frac{1}{\pi}\left(\frac{K_{Ic}}{Y\sigma}\right)^2 \tag{1-2}$$

In a recent update of the International Code for the Construction and Equipment of Ships Carrying Liquefied Gases in Bulk (IGC), section 4.18.2.6 in [5], it is required to carry out a fracture mechanics analysis of flaws in LNG containment systems. It should be verified that a crack will not reach critical dimensions before breakthrough and that it can leak detectable amounts of LNG under a recommended 15-day load spectrum before becoming critical. This IGC update underlines the importance of fracture mechanics for LBB assessments and the relevance of it for the industry, including classification societies like Lloyd's Register.

1-1 State of the art

Four different phases of crack development can be distinguished, as shown in Table 1-1. First, an initial flaw is present in the structure. This initial flaw is usually modelled as a semi-elliptical surface crack because this shape is both often observed and is generally more damaging than other shapes such as embedded cracks. The initial depth and half length of the crack are denoted as respectively a_1 and c_1. Next, in phase 2, the crack grows up to the point where either the crack becomes unstable, i.e. $K \geq K_{Ic}$, or the remaining cross section (ligament) becomes very small and the crack snaps through the wall. In phase 3, the crack is redefined as a breakthrough crack. It is still assumed that the crack shape remains semi-elliptical but the minor axis of the ellipse is now larger than the thickness of the wall. During phase 4 the crack further propagates up to the critical crack size.

The generic calculation procedure to predict crack growth or propagation is illustrated in Figure 1-2 for a general crack size a that for now refers to any sort of size parameter such as the length, radius, depth or otherwise characteristic size parameter of a crack of any shape. The procedure requires a large number of steps $k = 1, 2, 3, ..., n$ where n is the total number of calculation steps (Figure 1-3). First, as shown in sub-figure I of Figure 1-2, the SIF *range* is calculated

$$\Delta K = Y\Delta\sigma\sqrt{\pi a} \tag{1-3}$$

where $\Delta\sigma$ denotes the nominal stress range, $\Delta\sigma = \sigma_{max} - \sigma_{min}$.[3]
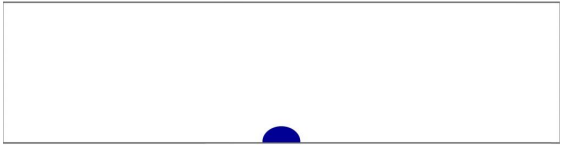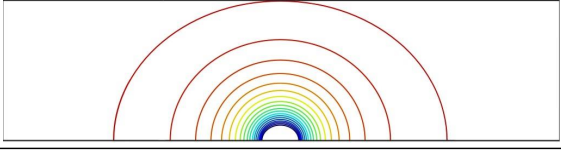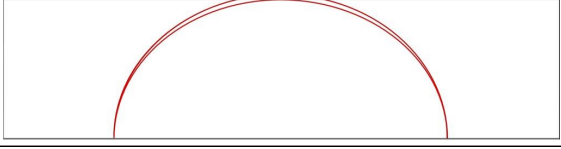
Next, (sub-figure II) ΔK is used in a crack growth relation that has the general form of

$$\frac{\mathrm{d}a}{\mathrm{d}N} = f_R(\Delta K) \tag{1-4}$$

---

[2]For plain stress conditions, the critical SIF is denoted as K_c and is somewhat higher than the K_{Ic}.

[3]Note the difference between the SIF of Eq. (1-1) and the SIF range of Eq. (1-3) that is defined as $\Delta K = K_{max} - K_{min}$.

Table 1-1: Phases of crack development

1) Initial semi-elliptical surface flaw	
2) Growth of the crack up to breakthrough	
3) Re-characterisation at breakthrough	
4) Propagation up to the critical crack size	

where $f_R(.)$ is a function that depends on the load ratio R, although R often does not directly appear in the function as a variable. More on crack growth relations can be found in Section A-4. By combining the information obtained in steps I and II, the general crack size a_k can now be related to the crack growth $(\mathrm{d}a/\mathrm{d}N)_k$ (sub-figure III). Step IV is to find the required number of cycles ΔN_k to grow the crack with Δa_k. This number of cycles is found through

$$\Delta N_k = \int_{a_{k-1}}^{a_k} \mathrm{d}N = \int_{a_{k-1}}^{a_k} \frac{\mathrm{d}a}{\mathrm{d}a/\mathrm{d}N} \tag{1-5}$$

Commonly, a 1-point integration method is used where only the value of $(\mathrm{d}a/\mathrm{d}N)_{k-1}$ is taken for the growth during the full increment Δa_k. After following steps I-IV for each k up to the desired final crack size a_n, the next step is to find the relation between a and N by the summation of ΔN_k (sub-figure V)

$$N_k = \sum_{k=1}^{n} \Delta N_k \tag{1-6}$$

Although this procedure is described for a crack with only one crack size dimension, a, the same steps I-V are applicable for crack growth with two crack sizes, growth in length and depth direction will be used as an example. Consider the semi-elliptical surface crack in Figure 1-4 where a is no longer a general crack size but denotes the depth of the crack. Furthermore c is the half surface length of the crack, A is the deepest point and C are the surface points of the crack. The entire crack is subjected to the same number of load cycles N, hence $\Delta N_{a,k} = \Delta N_{c,k}$.
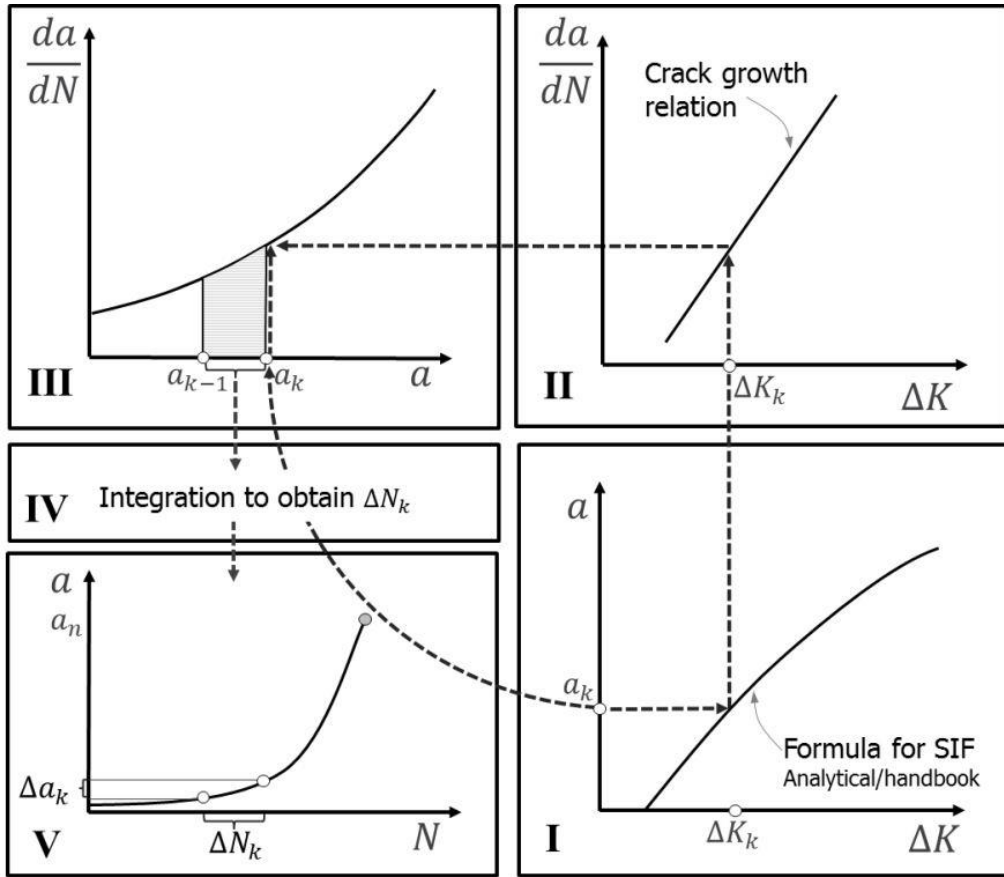
Figure 1-2: Steps to calculate the crack size versus number of stress cycles
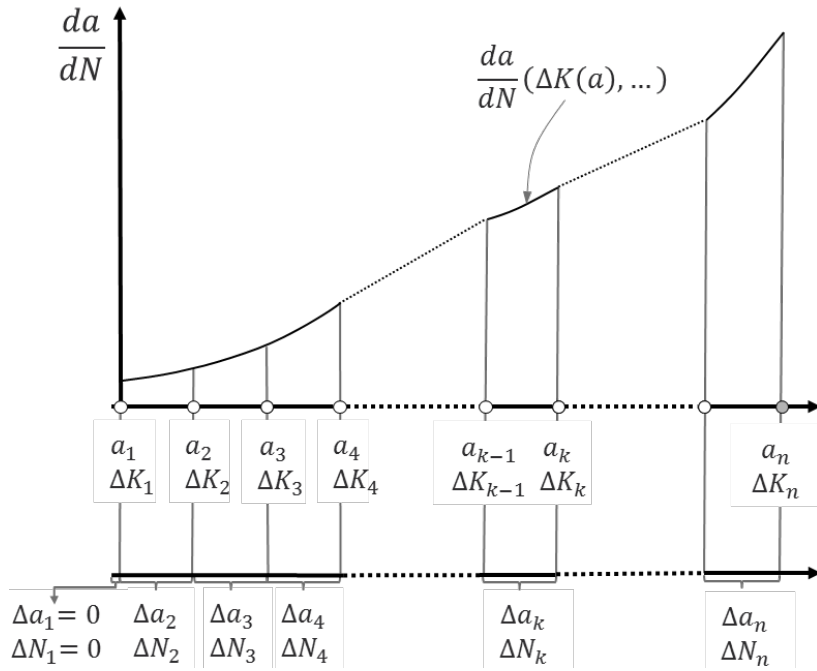
Figure 1-3: Numbering of the calculation steps in the numerical procedure
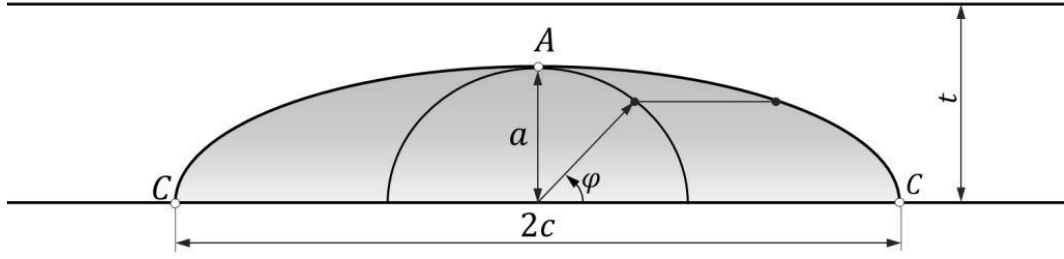
Figure 1-4: Semi-elliptical surface crack

Because generally $\Delta K_A \neq \Delta K_C$ and therefore $\mathrm{d}a/\mathrm{d}N \neq \mathrm{d}c/\mathrm{d}N$, the crack does not grow equally fast in a and c directions. To calculate these growth differences there are two options. One is to specify a fixed value of ΔN and vary both Δa and Δc as described in [6, 7].[4] The other option is to select a crack extension of $a_n - a_1$ or $c_n - c_1$ in respectively a or c direction and divide this depth or length into a large number of increments Δa or Δc. In [8], Δc is fixed into equally sized steps and the growth in a direction is subsequently calculated from $\Delta a = f_R(\Delta K_A)/f_R(\Delta K_C) \cdot \Delta c$. The same can be done by fixing Δa, as shown in Figure 1-5, and in- or decreasing Δc up to the point where $\Delta N_a = \Delta N_c$.
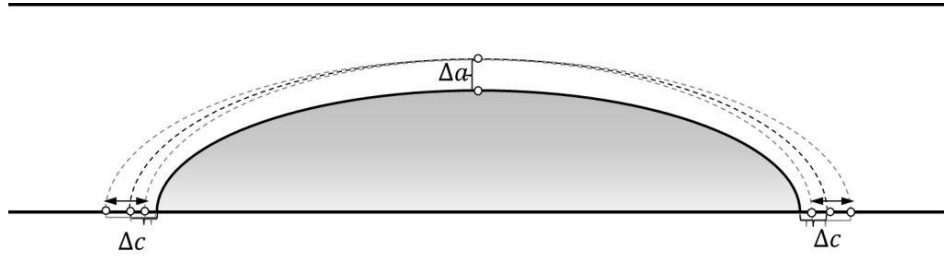
Figure 1-5: Crack growth with a fixed Δa and a variable Δc

Performing steps I-V requires an expression for the SIF throughout the crack development process. For a few geometries with specific loading conditions, an analytical solution for K is available. Analytical solutions have been derived for: a circular or elliptical crack in an infinite solid, a circular ligament in an infinite cracked solid, a straight edge crack in a semi-infinite sheet, a straight crack in an infinite sheet and an infinite row of collinear straight cracks in an infinite sheet. For all other geometries one has to rely on FE models. Collections of these FE-derived solutions can be found in the codes or in handbooks, see for instance Annex M in [2] or [9, 10, 11]. For the SIF solutions used in this thesis, see Appendix B.

The applicability of these analytical, load-specific solutions can be expanded to any other loading condition by using the *weight function method* proposed by Bueckner as cited in [12, 13].[5] Bueckner showed that the SIF can be calculated by integrating an arbitrary stress field $\sigma(x)$ (Figure 1-6) and a weight function $m(x, a)$

$$K = \int_0^a \sigma(x)m(x, a)\mathrm{d}x \tag{1-7}$$

---

[4]If fixed, ΔN , Δa or Δc are often given an equal size for each step k but this is not required.

[5]The method is applicable to any load type. If not a stress field but a point load is applied to the crack, the Dirac function can be used to express the 'stress field' as a point load in Eq. (1-7).

where x is the local coordinate in along the crack face. Throughout this research, local coordinates are indicated with $\{x, y, z\}$ and global coordinates with $\{X, Y, Z\}$, see Figure A-1. An example of the use of global coordinates can be found in Figure B-3.
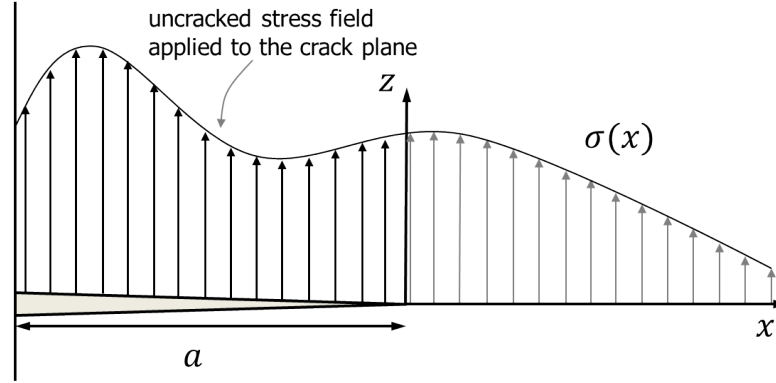
Figure 1-6: Weight function notations for a crack under an arbitrary uncracked stress field

In many cases, FE solutions can also be used to derive an - evidently - non-analytical weight function, as shown by Glinka and Shen in [14, 15]. Weight functions of a variety of crack shapes that appear in bodies of all sorts of geometries can be expressed as

$$m(x, a) = \frac{2}{\sqrt{2\pi(a - x)}} \left[1 + M_1 \left(1 - \frac{x}{a} \right)^{1/2} + M_2 \left(1 - \frac{x}{a} \right) + M_3 \left(1 - \frac{x}{a} \right)^{3/2} \right] \qquad (1\text{-}8)$$

where M_1, M_2, M_3 are constants that depend on the crack shape and the geometry of the cracked body. The benefit of a weight function is that a SIF under any load condition can be found, not only the load case for which the handbook solution is derived. The downside is that the method requires integration and weight function solutions often require a large number of constants for a reasonably accurate estimate.

Returning to the semi-elliptical surface crack of Figure 1-4, handbook solutions (e.g. [8, 16]) as well as weight functions (e.g. [17, 18]) are available. The commonly used handbook solution for this geometry is the one presented by Newman and Raju [8]. It is suitable for both membrane and bending stresses, includes multiple configuration parameters $\{W, t, a, c, \varphi\}$ and is validated by experiments. The equation can be found in Section B-1 as well. The Newman-Raju (hereafter 'NR') formula, Eq. (B-1) is derived for $0 \le a/t < 1.0$, but it is only *validated* up to $0 \le a/t < 0.8$ - for larger values validity of the solution is not established. FE results of other research do confirm the validity of the NR solution up to $0 \le a/t < 0.8$ but find errors over 10% beyond this ratio, see [16, 18].

When the depth of the semi-elliptical surface crack nearly reaches the wall thickness, the last remaining part of the ligament shears or fractures. Sharples and Clayton [19] conducted experiments with 2.5 and 50 [*sic*] meter wide stainless steel plates. These experiments showed that fatigue cracks, as long as the crack depth over length ratio is $a/c > 0.05$ right before wall penetration, cracks can grow almost up to 100% of the wall thickness. Taking into account that the applied unidirectional, in-plane tensile stress during these experiments was close to σ_y, this could be the case for cracks with even smaller a/c-ratios.

Thus, cracks do often grow beyond $a/t = 0.8$, making it desirable to have an accurate SIF estimate in this deep surface crack range of $a/t \ge 0.8$ to predict the shape development of

the crack. Research has shown that for cracks with an initial crack size of $a_1/t < 0.1$ and $a_1/c_1 > 0.05$ the length of the crack at breakthrough is predominantly influenced by the stress ratio σ_b/σ_m [20, 21]. For LBB calculations it is important to have a reliable estimate of the shape and size of the crack at breakthrough when estimating the leakage rate and number of stress cycles until reaching the critical crack size. omein To some extent, codes such as the BS, provide some guidance on how to estimate the growth of a crack from an initial crack up to a breakthrough crack. The BS prescribes Eq. (B-1) for $0 \leq a/t < 1.0$ up to the wall thickness or to the point where the SIF, combined with plasticity effects, exceeds the critical value. From this point, the crack is re-characterised in accordance with the recommendations of [22], that are shown in Figure 1-7. It is assumed that at breakthrough the surface crack length c does not change, so $2c^* = 2c_{bb}$ where * denotes the condition at breakthrough, and subscript bb the condition right before breakthrough.
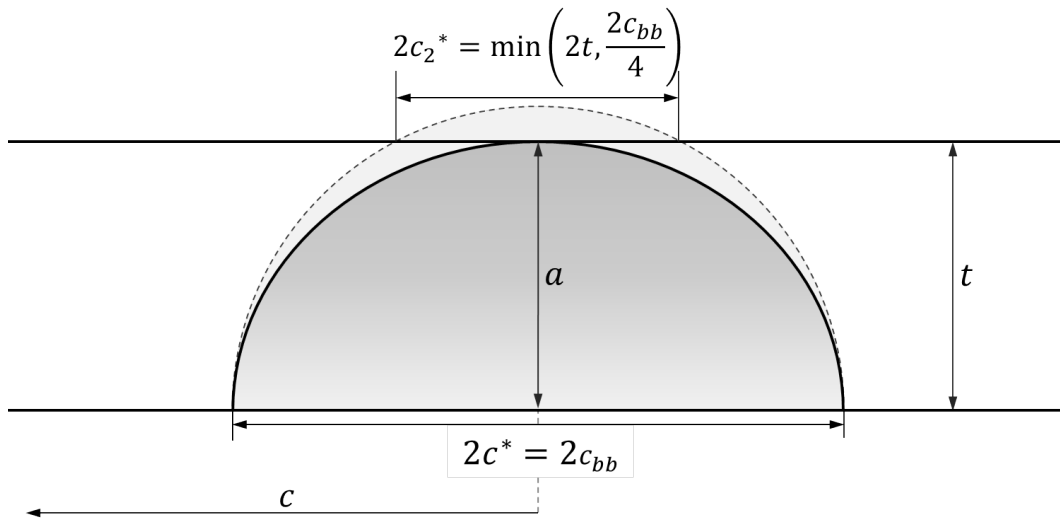
Figure 1-7: Re-characterisation of the crack at breakthrough, c.f. [2]

After breakthrough, the BS only gives qualitative information on the development of the crack shape and, to the best of this author's knowledge, no other codes or standards prescribe a calculation method for crack propagation right after breakthrough. However, review of LR's internal reports and the literature research yielded four 'unofficial' solutions that will be briefly discussed.

For the first method, described in Chapter 8 of [6], it is assumed that the NR solution may be used up to full wall thickness. Directly after breakthrough, the crack becomes immediately a straight through-thickness crack. This method overestimates the leakage rate as it predicts a larger crack at the back side compared to the actual case.

Secondly, Figure 1-8 illustrates a method developed by LR [7] that cuts the crack growth off before reaching 100% of the wall thickness and fixes the a/c-ratio afterwards. A cut-off value of $a_{bb} = 0.9t$ is used, a value that is also used in [22] and in a commercial LBB software package LBB PIPE. The critical crack size and crack propagation are calculated by using Eq. (1-2) and (1-3) where Y includes, among other factors, the analytical geometry factor for a straight centre crack of $Y = 1$.[6] As shown in Figure 1-8 the a^*/c^*-ratio is fixed

---

[6]Note that this is lower than the geometry factor of the NR equation for surface flaws between $a/t = 0.9-1.0$.

after breakthrough, which is an enhancement compared to the method of [6], where simply $c_2^* = c^*$ was used. The shorter length at the back, $2c_2$, is used to determine the crack opening area which is in its turn is used for leakage rate estimations. Length $2c_2$ is taken to avoid overestimating the leakage rate and herewith the detectability of the crack. For a short crack ($c < 5t$) under a pure tensile stress load, the crack does propagate in a similar fashion to that of Figure 1-8, as was also qualitatively described in [2, 22]. However, for longer cracks under a pure tensile stress the a/c-ratio will actually increase. If a positive bending component is present the a/c-ratio decreases, indicating that the method of Figure 1-8 will be estimate a higher leakage rate, hence a better detectability of the crack, than the actual situation. This non-conservativeness w.r.t leakage rate calculation is further aggravated by this method to deal with combined bending and membrane stress - the bending stress is added as if it were an extra tensile stress component, so $\sigma_m = \sigma_m + |\sigma_b|$. While this is a safe assumption in terms of estimating the critical crack size, the leakage rate will, as it was for the first method, be overestimated.
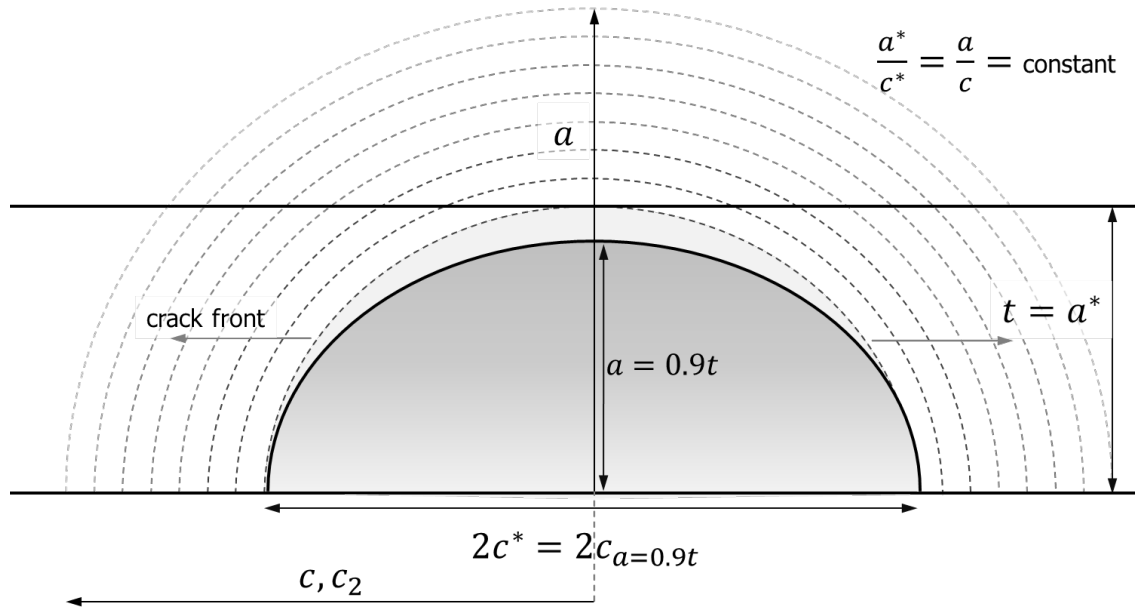
Figure 1-8: Re-characterisation of the crack at breakthrough when a^*/c^* is fixed.

A third solution to estimate the propagation is to come up with a SIF solution for this particular after breakthrough-shape and use a crack growth relation to estimate the growth. This estimate for the SIF for only tensile stresses was proposed by Ando *et al.* in [23, 24] and was further developed so that it could incorporate both bending and tensile stress conditions in [25], see also section Section B-3. Similar to the second method, the through-thickness crack is again simplified as a semi-ellipse where $a > t$, as shown in Figure 1-7 and 1-8. Their formula is not directly derived from FEM but is an assembly of other handbook solutions.

A fourth solution was found in Shingai *et al.*[7] [20]. They use a SIF solution for the semi-

---

In other words, when disregarding the influence of any other factors, the estimated crack growth rate at point C is *lower* compared to the recommendations of the BS (Figure 1-7)

[7]The article is in Japanese but the abstract, table and graphs are in English. A Dutch translation of article is available on request.

elliptical surface crack that was proposed by Shah and Kobayashi, cited in [20]. The approach followed by Shingai *et al.* is to use this SIF solution for point A and C at breakthrough throughout the propagation phase, i.e. using $a/t = 1.0$ and $\varphi = 90$ for point A and $\varphi = 0$ for point C of Figure 1-7. Since the Shah and Kobayashi formula was not intended to be used after breakthrough and their approach is not validated with test results either, this method is not considered further.

To summarise, the industrial codes offer only limited guidance for LBB assessments on how to deal with deep surface cracks or semi-elliptical through-thickness cracks. In absence of this, other solutions that are not fully satisfactory either have been proposed.

1-2   Scope of work

This research focuses on the LBB assessment of spherical aluminium LNG containment systems on ships that are commonly referred to as Moss tanks. See Figure 1-9 for a representative example of such a tank. A description of an LBB assessment applied to this example can be found in [26], in which two highly stressed locations in a Moss tank were assessed for their LBB capacity and found to be safe.
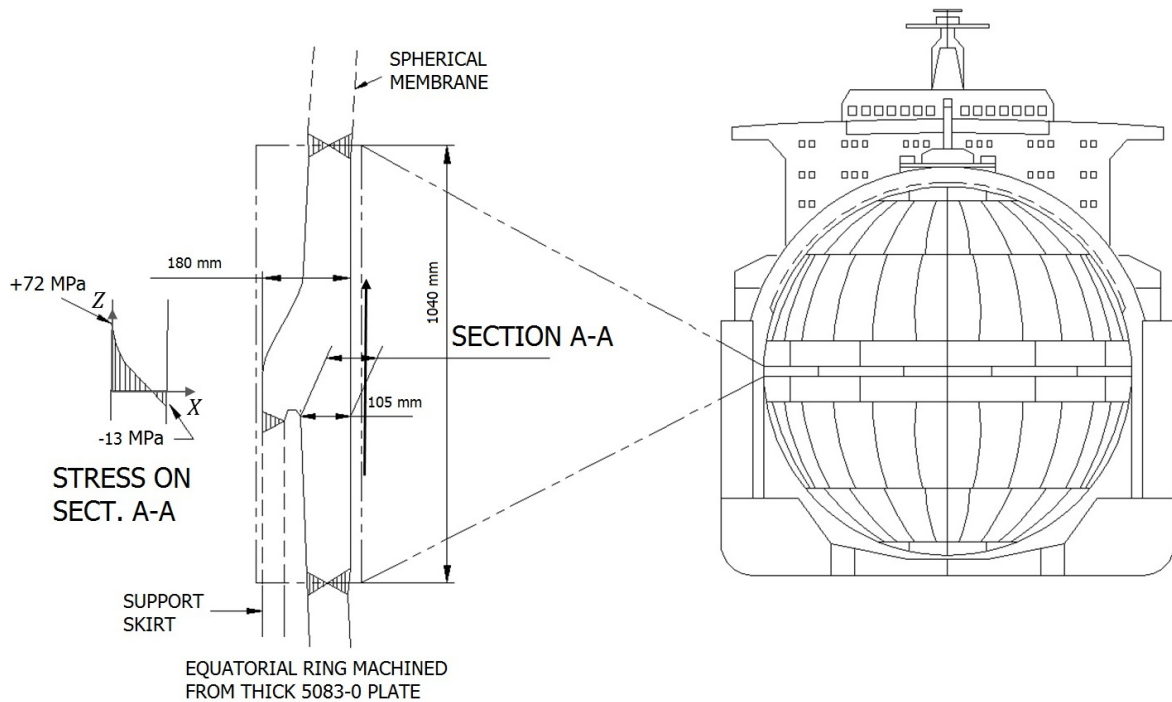
Figure 1-9: LNG spherical tank with an inner diameter of 35 m, c.f. Kaufman *et al.* [26]

Moss tanks have a radius of approximately 20 m, a wall thickness between 27-60 mm and are attached to the LNG carrier through a thick 'skirt' of approximately 170 mm thickness around the tank its equatorial ring. The LNG is stored at a temperature of -163 °C. The tank is fully insulated and a gas tight barrier covering the tank insulation should contain any leaked fluid. Although Moss tanks are equipped with gas detection devices as well, the main

leakage warning system is a so-called 'drip tray' which is installed under the tank and where the liquefied gas is collected and detected.

Fatigue damage is primarily induced by the inertial loading of the liquefied gas under the movements of the ship and by the deformation (hogging or sagging etc.) of the ship. Repeated filling and emptying of the tank barely contributes to the fatigue damage and neither is sloshing an issue because it a requirement that the tank is filled to almost 100% of its capacity.

When performing an LBB assessment, calculation steps like the determination of the stress spectrum or the estimation of material parameters, are all equally important but are considered to be given input parameters within the scope of this research. The emphasis will be on the prediction of the crack (shape) development, the first of the aforementioned three aspects of an LBB assessment. In an indirect way this also touches upon the second and third aspect: the amount of leakage is related to the crack opening area, so it is necessary to have a reliable estimate of c_2, and to determine whether there will be enough time to detect the leak or take emergency measures depends on the accuracy of the estimated relation between c and N. Howver, topics directly related to aspects 2.) and 3.) such as the estimation of the leakage rate, assessing the adequacy of the leak detection, or the expected crack propagation under a 15-day load spectrum, will not be considered. Calculations for these two aspects rely heavily on the accuracy of the assumed stress spectrum in the tank, local geometry and the availability of a reliable, experimentally obtained crack growth relation and many other values that are material-depend and situation-specific.

For this research, both a numerical calculation scheme and an FE model are developed. In order to keep the models manageable, the following simplifications are made:

- The geometry in the vicinity of the crack is simplified as an infinite, straight plate. Locally, the curvature of the tank is negligible given the large diameter of the spherical tank.

- The plate material is considered to be linear-elastic. The design stresses for plated structures like this are much lower than the yield stress, hence plasticity is not considered to have major impact unless the depth of a surface crack almost reaches the wall thickness or when high residual stresses are present.

- Damage mechanisms other than fatigue and fracture, like corrosion or impact load or dynamic effects are not considered.

- There are no other discontinuities, like welds or attachments, other than the fatigue crack.

- No multi-axial stresses but only σ_Z, the nominal stress in-plane of the plate material, is considered and it varies only in X (depth) direction, see Figure 1-9 or B-3. For brevity, subscript $_Z$ is hereafter omitted.

- The effects of nominal higher order stresses are not considered because their contribution is small w.r.t the nominal membrane and bending stresses in LNG tanks. No external pressures are modelled.

- The stresses are either of constant amplitude throughout the crack development or the amplitude is a function of the crack length at the crack initiation side.

- No crack closure effects are taken into account. A plastic zone around a crack-tip can act as a compressive, crack closing stress even when the nominal stresses are tensile.

- Differences in the crack propagation rate that exist along the thickness (in X-direction) are ignored.[8]

- Cracks grow symmetrically.

- The crack will be fully opened during all stress cycles. Roughly said, this means that the nominal stress acting on the crack area is tensile, i.e. $\sigma_{min} \geq 0$.

A minor caveat to the last point should be made: it is not true that a crack can *only* be fully opened when $\sigma_{min} \geq 0$. As an example of this, consider a semi-elliptical surface crack that is predominately subjected to a large nominal bending stress and possibly a minor - either tensile or compressive - membrane stress component. In this case, the entire crack can be opened despite that a small part of the crack face is subjected to a compressive stress. 'Membrane stress' can therefore refer to both a relatively small uniform compressive stress or a uniform tensile stress. If only the latter is considered, it is explicitly referred to as a (uniform) tensile stress.

1-3   Research objective

The first aim of this research is to predict the crack shape of surface cracks more accurately by using a different numerical calculation method than the ones described above. This new scheme will be introduced in Chapter 2 where the perceived shortcomings of other methods will be addressed. In Chapter 4 the performance of the new numerical calculation scheme is assessed in comparison with experimentally determined results of the crack shape at breakthrough. The objective is to:

1-a) Solve perceived shortcomings of other numerical calculations methods.

1-b) Improve the numerical calculation method so that it performs well in comparison with experimentally determined results.

In order to estimate crack growth before breakthrough more accurately, several FEM are build to assess the validity of two different expressions to predict the SIF. In Chapter 3, semi-elliptical surface crack FEM results of the SIF are compared to two other solutions. One is a commonly used SIF solution proposed by Newman and Raju [8], the other one was proposed by Wang [18] and is only applicable to deep surface cracks with a depth in the range of $(0.6 \sim 0.8) \leq a/t < 0.95$. In Chapter 4 the crack shapes at breakthrough estimated by first only using the NR solution and then by replacing the NR solution by the one of Wang in the range of $0.6 \leq a/t < 0.95$, will be compared to experimental results found in the literature. The goal is then to:

1-c) Assess the influence on the accuracy of the estimations for crack shape and growth when the SIF is not only predicted by the NR solution, but also by the Wang solution in the range of $0.6 \leq a/t < 0.95$.

---

[8]This crack closure effect is a 3-D phenomenon influenced by plasticity: at the material surfaces where plane stress conditions prevail, a larger plastic zone around the crack-tip is present compared to the inner material under plane strain. Hence, a closed crack opens first mid-thickness and propagates faster. Under variable amplitude loading, this effect is considerable. More on this thickness effect can be found in Chapter 11 of [6].

The second aim is to improve the accuracy of the estimated crack propagation after break-through. Of the four aforementioned solutions (straight through-thickness immediately after breakthrough; cutting growth off at $a_{bb} = 0.9t$ and fixing a^*/c^*; using an assembly of hand-book SIF equations to estimate the SIF for the crack after breakthrough; using the Shah and Kobayashi formula), the second and third will be further evaluated for their accuracy in comparison with experimental data in Chapter 4. In addition to these two methods, a new SIF formula will be proposed in Chapter 3, one that is based upon FEM of this particular semi-elliptical through-thickness shape. So the objective is to:

2) Develop a new FE-derived SIF solution for a crack after wall penetration and asses the accuracy to estimate crack propagation of both this new as well as two existing solutions in comparison with experimentally obtained data.

The results will then be used to make recommendations for improving existing LBB procedures.

Chapter 2

Numerical modelling of crack development

The generic calculation procedure to predict crack development that was briefly introduced in the previous chapter, will be discussed in more detail for each phase shown in Table 1-1 and the specific features of the numerical calculation procedure that is developed for this research will be highlighted. The next section first introduces some terminology and general aspects for the numerical modelling of crack development.

2-1   Calculation procedure, phases, steps and calculation steps

The entire process of 1.) selecting input parameters, 2.) numerically calculating crack growth, 3.) specifying the rules for re-characterisation of the breakthrough crack and 4.) numerically calculating crack propagation, is referred to as the *numerical modelling* of crack development. If only the last three aspects are considered, this is referred to as carrying out a *numerical calculation procedure* or *numerical calculation scheme*. The numerical calculation procedure is carried out by MATLAB, a program that can quickly process a large number of numerical calculations and can easily generate graphical output. The numerical model is subdivided in 4 *phases* (Table 1-1). Phase 2 and 4, respectively crack growth and propagation, can be modelled with the *steps* of Figure 1-2. The incremental steps, $k = 1, 2, 3...n$, as illustrated in Figure 1-3 are referred to as *calculation steps* to distinguish them from the steps of Figure 1-2. Within a calculation step, it is often necessary to use *iteration steps* to obtain a new value, these are denoted in the MATLAB program by i.

The basic assumption to calculate crack development, is that the crack is loaded by the same *number of load cycles*, i.e. $N_a = N_c$ or $N_c = N_{c2}$. The number of load cycles may vary each calculation step k.

As shown in Figure 1-3, $\Delta a_1, \Delta N_1$ and also Δc_1 are added as virtual increments with a value of 0 to be consistent with the MATLAB program. MATLAB does not recognize a syntax with calculation step number 0 and therefore $a_0, \Delta K_0$ cannot be attached to a value.

The specific method followed for each step of Figure 1-2 will now be further explained for the four phases.

2-2   Phase 1: Presence of an initial semi-elliptical surface flaw

Before any growth can be modelled, some input regarding crack dimensions and other inputs are required. An overview is given in Table 2-1. More input and calculation options will be discussed in the next sections.

The experimental data that will later be used to assess the numerical model, is given for finite width specimens, therefore a value for W is required to correct for a finite width. When modelling a spherical tank, the value of W should be given a value much larger than the final crack size so that is will not affect the outcome.

As pointed out in the introduction, ligament failure can occur when the crack depth reaches almost the wall thickness or when $K_{A,max} = K_c$ or $K_{C,max} = K_{Ic}$. Because the scheme only uses SIF ranges and not K_{max}, the values of K_c and K_{Ic} are converted into something that one could unofficially call 'critical SIF ranges'

$$\Delta K_c \quad = K_c - R \cdot K_c \tag{2-1a}$$
$$\Delta K_{Ic} \quad = K_{Ic} - R \cdot K_{Ic} \tag{2-1b}$$

If ΔK_A is still smaller than ΔK_c at $a = a_{bb}$ it is assumed that this very thin remaining part of the cross section fails anyhow. This research adopted $a_{bb} = 0.995t$ for all calculations, except when using the 'fixed a/c ratio' model of Figure 1-8 where it is $a_{bb} = 0.9t$.

2-3   Phase 2: Crack growth

As mentioned in the introduction, either Δa_k, Δc_k or ΔN_k should be known to calculate the crack growth for a two-dimensional crack. Δa_k is selected as the 'known' parameter in this procedure, because the distance $a_{bb} - a_1$ is known in advance, unlike $c_{bb} - c_1$.[1] Using ΔN_k as a known can be troublesome because the growth rate may vary considerable between that of an initial flaw and one that approaches criticality. Increasing ΔN_k as k increases, would solve this problem although it is hard to estimate the increase rate beforehand. Another solution is to use a small ΔN_k throughout the calculation but this is requires more computation time as the increments become increasingly small as well. Moreover, averaging the crack growth over a reasonable number of cycles better reflects the empirical nature of growth relations and the error margin of the approximative SIF solution. Again, it can be difficult to judge in advance whether a selected ΔN_k is indeed small enough yet not too small for a reliable growth estimate.

This considered, the size of Δa_k is fixed and is in most cases given an equal value for each k. Though an equal spacing rarely causes problems for growth calculations, there is an option in the model to use a logarithmically in- or decreasing Δa_k. For a rapidly increasing ΔK_A, the first option prevents that Δa_k becomes too small when approaching the wall thickness

---

[1]When ΔK_c is reached before the initially selected a_{bb}, the algorithm decreases a_{bb} until $\Delta K_A < \Delta K_c$.

Table 2-1: Input for the numerical model

Material	ΔK_{th}	Threshold SIF range
	K_{Ic}, K_c	Critical SIF (plain strain/stress)
	$\hat{C}, \hat{m}$	Parameters for crack growth model
	E, ν	Material parameters
	σ_y	Stress level at which the material yields
	NRC	Newman-Raju correction in c-direction (optional)
Geometry	a_1, c_1	Initial notch depth and length
	t, W	Plate thickness and width
	a_{bb}	Crack depth right before breakthrough if $\Delta K < K_c$
	c_{max}	Discontinue calculation at a sub-critical crack length (optional)
Loading	$\Delta\sigma_t, \Delta\sigma_b$	Constant or $\sigma = f(c)$
	R	Load ratio
Calculation	$\Delta N_{a,2}$	No. of load cycles during the first increment
	ΔN_c^*	No. of load cycles during the first increment after breakthrough
	INT	1 or 2-point integration of $\mathrm{d}a/\mathrm{d}N$ and $\mathrm{d}c/\mathrm{d}N$
	SIFM	SIF model after breakthrough (AFNTO, FIXED or FEM)
	a^*/t	Re-characterisation a^*/t instead of BS rules (optional)
	log	Use logarithmic spacing in thickness direction (optional)
	TP	Transition point to the Wang formula (optional)
	PC	Use a small scale plasticity correction for the SIF (optional)

and the increment gets 'consumed' by the crack growth within only a few cycles which causes relatively large errors when N is rounded-off. Similarly, when a large positive bending stress is present, ΔK_A decreases during crack growth. Decreasing Δa_k as k increases will then reduce computation time, as less iteration steps are required to comply with $\Delta N_a = \Delta N_c$.[2]

Step I: Relating the crack size and geometry to the SIF The SIF is estimated with the NR formula or as a combination of the NR and Wang formula. Whether or not to use the latter can be specified in the program by inserting a value for $a/t = $ TP within the validity range of the Wang formula ($0.6 \leq $ TP < 0.95); selecting a TP value in the range $0.95 \leq TP \leq 1$ will result in using the NR formula in the range $a/t \leq 1.0$, hence for each of the ΔK_k.

Though the crack is modelled by LEFM, the numerical model has an option to use a small scale yielding plasticity correction (PC). This corrects for the presence of a small plastic zone around the crack-tip by placing the crack-tip in the centre of the plastic zone, raising the stress intensity to an effective stress intensity factor K_{eff}. Details can be found in Section A-3.

---

[2]The first guess for Δc_k is based upon the previous value Δa_{k-1}, as will be explained later in this section. Since c grows much faster than a when a large positive bending component is present, an equal spacing of size of Δa_k would lead to rapidly increasing sizes of Δc_k. It would then require many iterative steps to arrive at this new, increased length increment Δc_k. A decreasing Δa_k compensates for this rapidly increasing Δc_k and therefore reduces the required number of iterative steps.

Step II: Relating the SIF to the crack growth　　The Paris relations [27]

$$\frac{\mathrm{d}a}{\mathrm{d}N} = \hat{C}_A(\Delta K)^{\hat{m}} \tag{2-2a}$$

$$\frac{\mathrm{d}c}{\mathrm{d}N} = \hat{C}_C(\Delta K)^{\hat{m}} \tag{2-2b}$$

are used to estimate the crack growth rates. One of the options is to use a different $\hat{C}_C$ in length direction in Eq. (2-2b) as suggested in [8]. It is therefore here referred to as the 'Newman-Raju correction' (NRC).

$$\hat{C}_C = 0.9^{\hat{m}} \cdot \hat{C}_A \tag{2-3}$$

Only the Paris relation is for now considered in the calculation scheme because the material parameters $\hat{C}, \hat{m}$ of the experiments that will be used for validation, have been published for this relation as well. Adding other relations does not require much effort should this be needed for a later research.

Step III and IV: Relating the crack size to the growth and obtaining $\Delta\mathrm{N_k}$　　Two different integration options (`INT`) for Eq. (1-5) are available, both shown in Figure 2-1. The first one is the conventional 1-point integration where the crack growth rate at the beginning of the increment is used throughout the increment

$$\Delta N_{a,k} = \frac{\Delta a_k}{(\mathrm{d}a/\mathrm{d}N)_{k-1}} \tag{2-4a}$$

$$\Delta N_{c,k} = \frac{\Delta c_k}{(\mathrm{d}c/\mathrm{d}N)_{k-1}} \tag{2-4b}$$
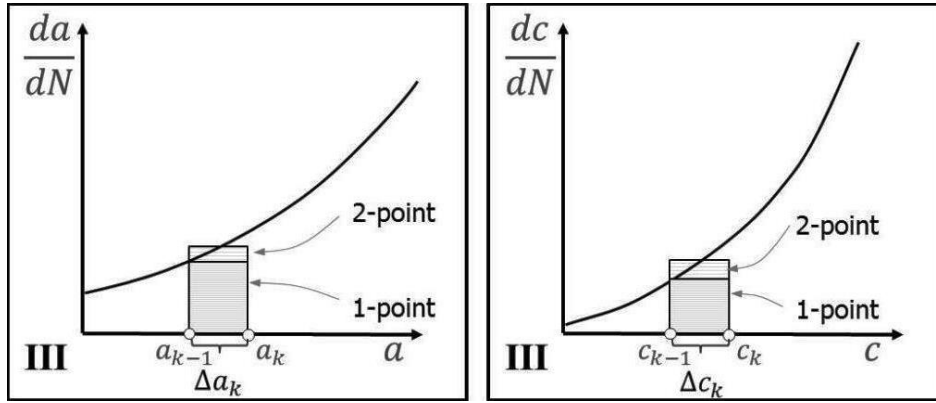
Figure 2-1: Integration methods to find ΔN, see also Figure 1-2

The 2-point integration method averages the values of the crack growth rate at the beginning and end of the increment

$$\Delta N_{a,k} = \frac{\Delta a_k}{\frac{1}{2}\Big[(\mathrm{d}a/\mathrm{d}N)_{k-1} + (\mathrm{d}a/\mathrm{d}N)_k\Big]} \tag{2-5a}$$

$$\Delta N_{c,k} = \frac{\Delta c_k}{\frac{1}{2}\Big[(\mathrm{d}c/\mathrm{d}N)_{k-1} + (\mathrm{d}c/\mathrm{d}N)_k\Big]} \tag{2-5b}$$

Both methods require knowledge of a yet unknown Δc. It is found by iteration, as is illustrated in Figure 2-2. Both ΔN and Δc are found through this calculation scheme, only for $k = 2$ the program requires an initial number of load cycles $\Delta N_{a,2}$. Depending on the input variables, $\Delta N_{a,2}$ varies in the order of $10^2 \sim 10^4$ stress cycles. The number of calculation steps before breakthrough n_{bb} is then increased up to the point that

$$\frac{(a_{bb} - a_1)/n_{bb}}{(\mathrm{d}a/\mathrm{d}N)_{k-1}} = \Delta N_{a,2} \qquad \text{(1-point integration)} \qquad (2\text{-}6a)$$

$$\frac{(a_{bb} - a_1)/n_{bb}}{\frac{1}{2}\left[(\mathrm{d}a/\mathrm{d}N)_{k-1} + (\mathrm{d}a/\mathrm{d}N)_k\right]} = \Delta N_{a,2} \qquad \text{(2-point integration)} \qquad (2\text{-}6b)$$
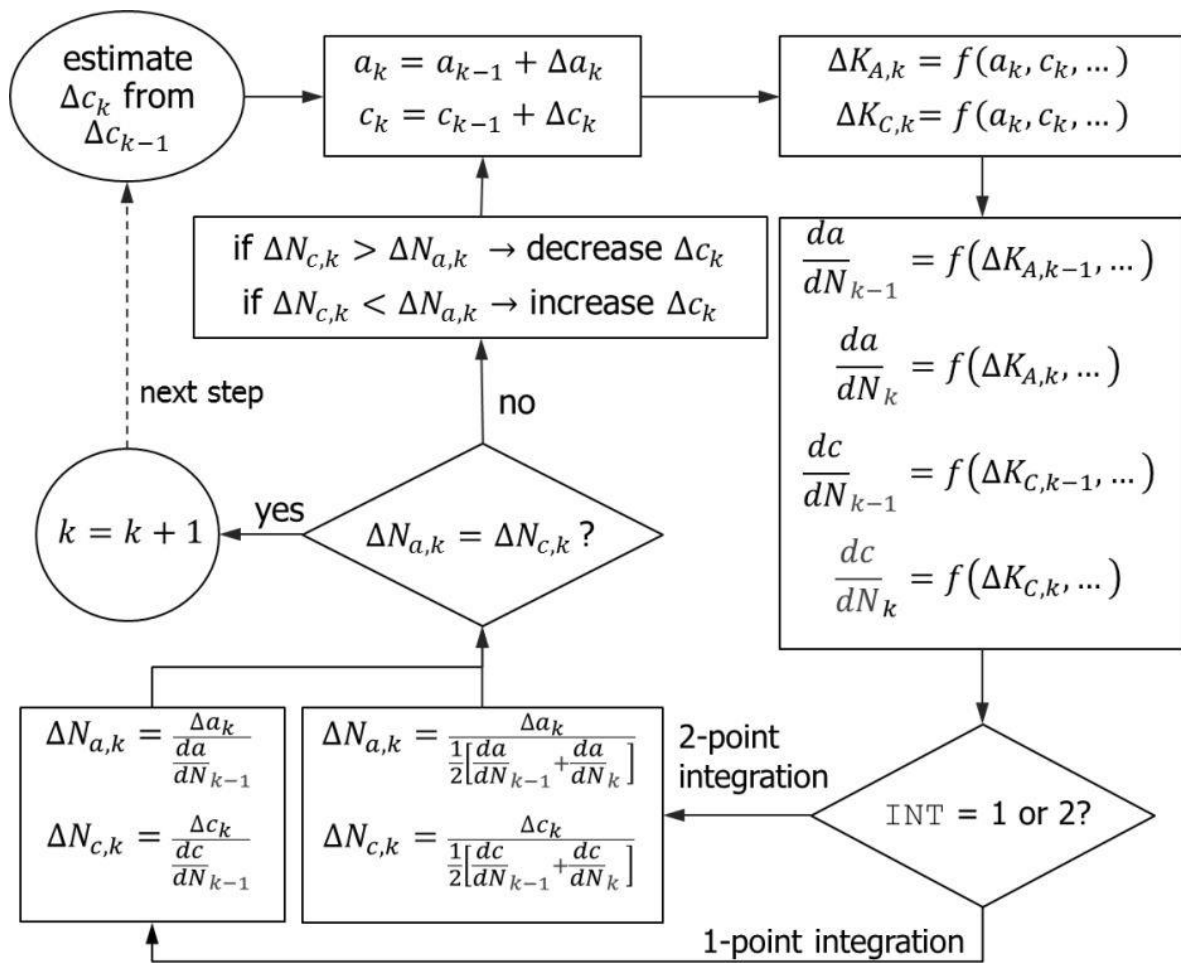
Figure 2-2: Crack growth calculation flowchart

Not shown in the flowchart is that in each calculation step it is checked whether $\Delta K > \Delta K_{th}$, $\Delta K_A < \Delta K_c$ and $\Delta K_C < \Delta K_{Ic}$, with reference to Eq. (2-1).

Step V: Relating the crack size to N_k   After rounding-off each ΔN_k to integers, the cycles are summed and some checks are carried out:

– The difference between N_a and N_c may not exceed 0.1% of the total N,

$$|N_a - N_c| < \max(N_a, N_c) \cdot 10^{-3}$$

– The difference between $\Delta N_{a,k}$ and $\Delta N_{c,k}$ may not exceed 0.1 on average,

$$\left| \frac{\sum_{k=2}^{n_{bb}} \Delta N_{a,k} - \Delta N_{c,k}}{n_{bb}} \right| < 0.1$$

– The minimum number of N is 10 in each calculation step;

– The error due to the rounding to integers in each k may not exceed 0.01 on average,

$$\left| \frac{\sum_{k=2}^{n_{bb}} \Delta N_k - \Delta N_{k,rounded}}{n_{bb}} \right| < 0.01$$

If all conditions are met, the calculation continues to the next phase.

2-4 Phase 3: Re-characterisation of the crack at breakthrough

At breakthrough it is assumed that during a limited number of cycles ($N = 10-100$) the crack suddenly snaps through. If not otherwise specified, the rules of the BS for non-ductile tearing are followed, see Figure 2-3.[3] When experimental measurements indicate that a different c_2^* should be used, a value of a^*/t in accordance with the measurement is used.
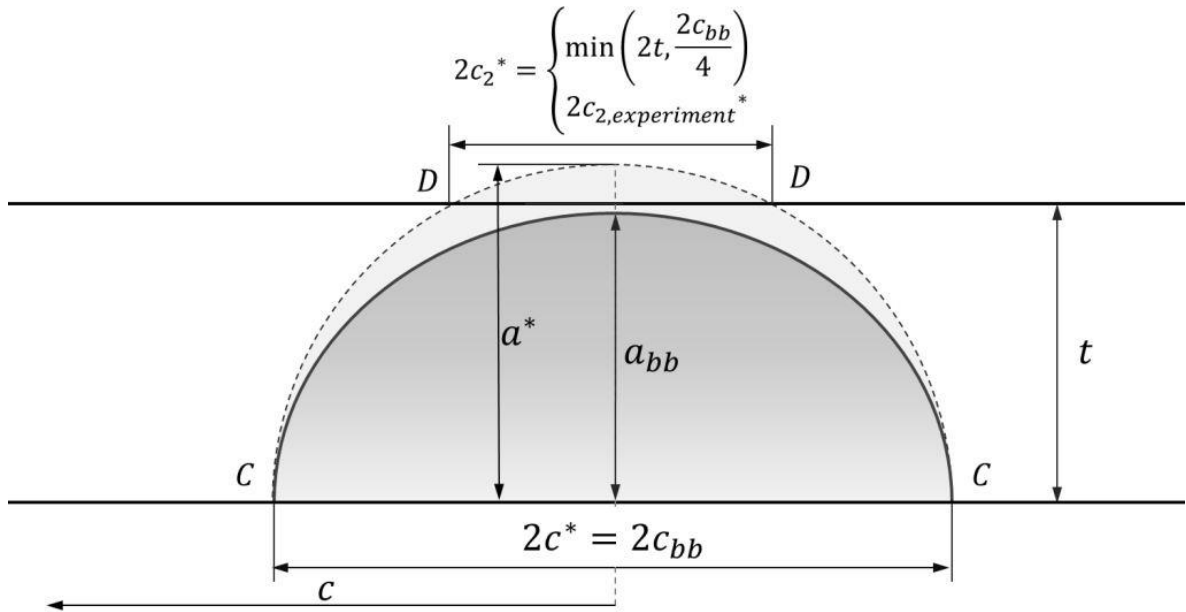
Figure 2-3: Re-characterisation of the crack at breakthrough

---

[3]The BS recommends the use of a different re-characterisation for ductile tearing situations, that occur when the load during the stable crack growth stage is very large compared to the yield load.

2-5 Phase 4: Crack propagation after breakthrough

After breakthrough, the length of $\Delta c_{2,k}$ is the unknown variable and Δc_k is now fixed. Length $c_c - c^*$ is known as the difference between the critical crack length c_c (Eq. (1-2)) and the length at breakthrough. Optionally, a different value for c_{max} can be used to cut-off the calculation before c_c. For most loading conditions, a linear spacing of Δc_k is recommended.

Step I: Relating the crack size and geometry to the SIF   After breakthrough, three options can be used for the SIF estimate. The first is to use the approximative equation of Ando, Fujibayashi, Nam, Takahashi and Ogura (AFNTO), the authors of the first paper with this solution [23]. Their solution is hereafter referred to as the AFNTO solution. Alternatively one can use the 'fixed a^*/c^* model' or the equation that is found by FE modelling for this research. This FEM based equation will be treated in Section 3-3.

Step II - V: Relating the SIF and crack length to the crack to the propagation rate, obtaining $\Delta \mathrm{N_k}$ and summation   The Paris relation Eq. (2-2) is again used to estimate crack propagation. The steps for crack propagation after breakthrough are similar to those of crack growth. An initial ΔN_c^* should be selected for the first step after breakthrough, usually it is in the order of $80 \sim 400$.

The same procedure as shown in Figure 2-2 is followed, but $\{a, \Delta a, \Delta K_A, \Delta N_a\}$ are now replaced by respectively $\{c_2, \Delta c_2, \Delta K_D, \Delta N_{c_2}\}$, with reference to Figure 2-3. The checks are identical to the ones for the crack growth phase.

Chapter 3

Modelling cracks with finite elements

As mentioned in Chapter 2, crack growth can be estimated with an empirical formula that relates the SIF range to the crack growth rate. The SIF, and subsequently the SIF range in this relation, can be obtained through an FE analysis.

Three models that are relevant for crack growth modelling will be introduced in the next sections. The first model shows, by comparison with an analytical solution, that the FE method and software package are indeed suitable to accurately approximate the SIF. The second model of a semi-elliptical surface crack compares the FEM results of the SIF to predicted SIF values by the formulae of NR and Wang. Thirdly, in order to derive a 'handbook' solution, a set of FEM of semi-elliptical through-thickness cracks are build and used to derive a approximative solution. This solution is then compared to the AFNTO formula, which is only an assembly of other FE-derived handbook solutions.

All FE analyses are carried out with ANSYS, release 16.1. The models use three-dimensional isoparametric solid elements with reduced integration to increase the computation speed, and are linear-elastic.

3-1 Validation of the finite element method and software

A validation model serves two purposes: (1) it validates the FE method and software package ANSYS and (2) it shows which mesh and/or element types can give the most accurate solution in comparison with an analytical solution. As said, only a few analytical solutions exists and all analytical solution are derived for a geometry with one or multiple boundaries at an infinite distance from the crack. The first issue that arises is that the FE method can only model (anti-) symmetry boundaries. The analytical solution of infinite row of collinear cracks (Figure 3-1) limits the problem of modelling infinity to only one boundary: the infinite height H at which the nominal stress acts. This geometry is therefore selected to validate the FE software and model. H in the FEM is selected as $H = W$ in order to study the effects of the finite height.
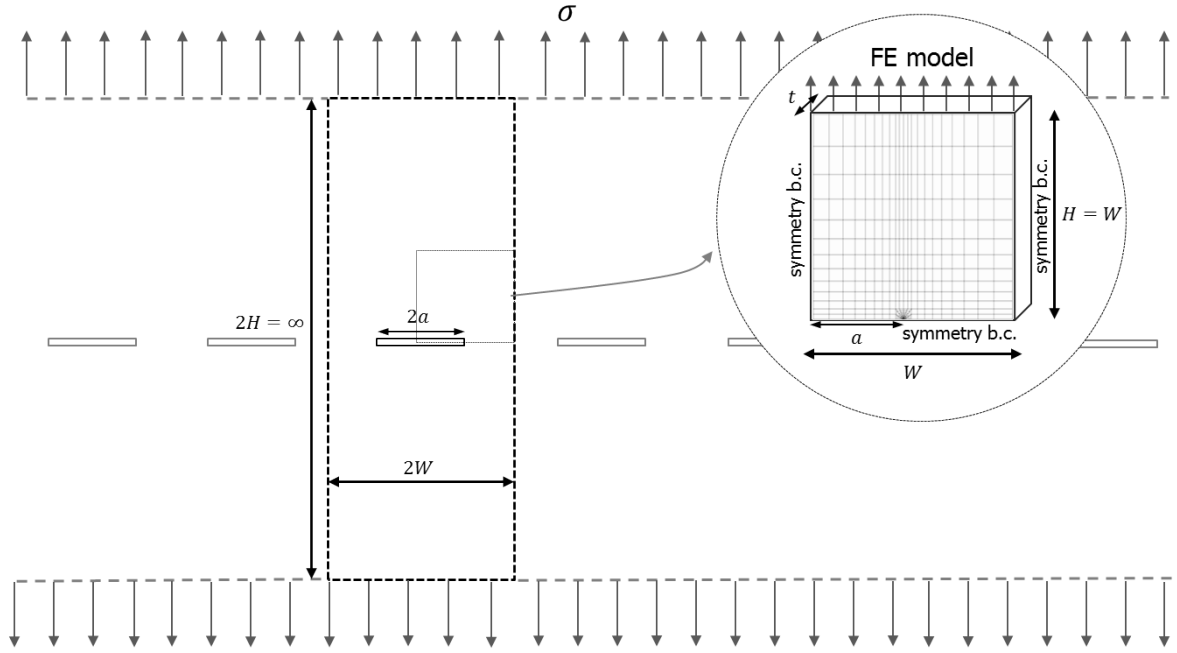
Figure 3-1: Infinite sheet with an infinite row of collinear cracks

The SIF of an infinite row of collinear cracks is given by [9, p. 170]

$$K = \sigma\sqrt{\pi a} \cdot \sqrt{\frac{2W}{\pi a} \tan\left(\frac{\pi a}{2W}\right)} \tag{3-1}$$

To investigate the influence of the mesh and element type, three different configurations are modelled, see Figure 3-2 for examples of the meshes. An example ANSYS script of the validation models is given in Appendix C. The mesh densities are chosen such that the result does not improve much further when the mesh is further refined. Between brackets are the element names used in ANSYS; reference is made to its manual for a detailed description of these elements [28, Part I: Element Library]. The three configurations are:

– A structured mesh with 20-noded elements (SOLID 186)

– A structured mesh with 8-noded elements (SOLID 185)

– An irregular mesh with 20-noded elements (SOLID 186)

Four different crack sizes are modelled, $a/W = \{0.05, 0.1, 0.2, 0.4\}$, and W is kept constant. The mesh density is similar the for four models with the same configuration. The SIF data is retrieved from the crack-tip node at mid-thickness. Neither the thickness nor the number of elements in thickness direction affect the SIF solution at this node, as was demonstrated by the simulations.

Two ways to obtain K are compared: directly from the stress field around the crack or through a J-contour integral. These methods are briefly explained in Appendix D. The validation models and the models that will be presented in the next sections, are considered
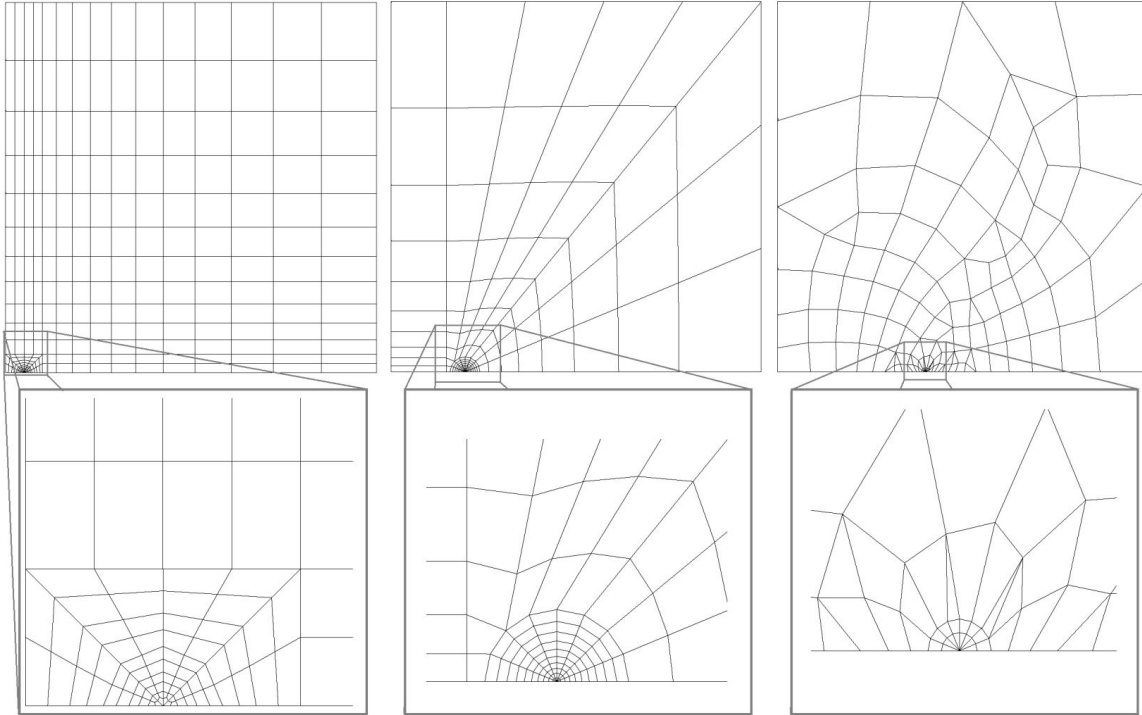
Figure 3-2: Left Structured mesh with 20-noded elements; $a/W = 0.05$
Centre Structured mesh with 8-noded elements; $a/W = 0.2$
Right Irregular mesh with 20-noded elements; $a/W = 0.4$

to be plane strain[1], so when using the J- contour method, K is found through

$$K = \sqrt{\frac{JE}{(1 - \nu)^2}} \tag{3-2}$$

For both the stress field and J-contour integral method, the average of the first three converged contours are used. It is commonly recommended to use only the values of the converged contours, the non-converged ones are considered to be unreliable. The SIF is estimated in FE software by the integration of contours. These contours are formed across a path that connects the nodes surrounding the crack-tip node. For more details on this, reference is made to Appendix D.

In Table 3-1 the ratios between the SIF obtained through FEM by using two different methods and the analytical solution of Eq. (3-1) are given.

The results in Table 3-1 show that FE software package ANSYS can accurately approximate K when compared to an analytical solution. The results of the two smallest cracks, $a/W = \{0.05, 0.1\}$, show that either method and configuration give very accurate results, even when the mesh is irregular or when a lower order element is used. When the crack size increases, both methods increasingly overestimate K which can be explained by the increasing a/H ratio, i.e. the limited height and the larger crack allow the model to deform more than

---

[1]In plane strain conditions, K is somewhat higher than it is under plane stress conditions: $K = \sqrt{JE/(1 - \nu^2)} \approx \sqrt{JE/(1 - 0.3^2)} \approx 1.05\sqrt{JE}$

Table 3-1: Ratios between the SIF from FEM and analytical SIF of an infinite row of collinear cracks for different model configurations and crack sizes.

	a/W	$K_{FEM}/K_{analytical}$	
		K_{FEM} through stress field	K_{FEM} through J-contour integral
20-node structured	0.05	1.001	0.999
"	0.1	1.004	1.003
"	0.2	1.016	1.013
"	0.4	1.046	1.044
8-node structured	0.05	0.994	0.990
"	0.1	1.004	1.003
"	0.2	1.029	1.027
"	0.4	1.047	1.045
8-node irregular	0.05	0.996	0.994
"	0.1	1.005	1.003
"	0.2	1.016	1.016
"	0.4	1.046	1.046

when the height is infinite and this reduced stiffness leads to more crack opening and a SIF that is somewhat higher than the analytical one. This can be avoided by increasing the height to approximately $10a$ or higher, though this consequently increases the number of elements, nodes and computation time. The differences between the three model types are rather small, although using a J-contour integral, 20-noded elements and a structured mesh performs slightly better than the other configurations. This configuration is therefore selected for all FE analyses.

It should be noted that the 20-noded element models require considerably more nodes in comparison with the two other models, so the results do not reflect the accuracy of the models w.r.t. the number of nodes. In hindsight, this would have been a relevant point to consider. However, the decision to use 20-noded elements is not solely based on the results of Table 3-1 but this is also recommended by ANSYS, see [28, 1.2.1.2.].

3-2   FEM of semi-elliptical surface cracks

The FEM of the semi-elliptical surface crack of Figure 1-4 is validated by the analytically derived SIF solution of an embedded ellipse

$$K = \sigma\sqrt{\frac{\pi a}{Q}} \cdot f_\varphi \tag{3-3}$$

where

$$f_\varphi = \left[\left(\frac{a}{c}\right)^2 \cos(\varphi)^2 + \sin(\varphi)^2\right]^{1/4} \tag{3-4}$$

and

$$Q = \int_0^{\pi/2} \sqrt{1 - \left[1 - \left(\frac{a}{c}\right)^2\right] \sin^2 \varphi} \; \mathrm{d}\varphi \tag{3-5}$$

A closed form solution of Q does not exist but a close approximation to Eq. (3-5) is given by

$$Q = 1 + 1.464 \left(\frac{a}{c}\right)^{1.65} \tag{3-6}$$

Figure 3-3 shows both an example mesh of a validation model and a semi-elliptical surface crack. Because of its symmetry, only $1/8^{\text{th}}$ of the geometry of the embedded ellipse and $1/4^{\text{th}}$ of the surface crack needs to be modelled. The mesh of the semi-elliptical surface crack is almost identical to the validation model, except that only the thickness t is modelled. An example ANSYS script file can be found in Appendix E.

The licence type of ANSYS limits the number of nodes of each model to 32,000. This is enough to obtain reasonably accurate results compared to the analytical solution but this limitation forces the user to find a balance between accepting some poorly shaped elements and compromising on the distance of the boundaries that should ideally be at $H/a > 10$, $W/c > 10$ and $t/a > 10$. An element is for instance poorly shaped when the aspect ratio becomes too large (i.e. one of the three dimensions is much smaller or larger than the other two dimensions) or when it is very skewed. To avoid a large number of poorly shaped elements, the distance of the boundaries is less than ideal in each direction. For all models $W = 4c$ and the half height is of the order $H = 2c \sim 4c$. The thickness of the model of an embedded ellipse is $T = 6c + 2a$. W, H and T are selected such that they barely affect the stress field around the crack-tip. Nevertheless, the models still have a less-than-ideal thickness, height and width, and therefore a correction factor for this is applied as well. The following correction factor is originally only used for the NR solution (see Eq. (B-4) or [8]), but is here considered to be a reasonable approximation for an embedded ellipse as well

$$f_w = \left[\cos\left(\frac{\pi c}{2W} \sqrt{\frac{a}{t}}\right)\right]^{-1/2} \tag{3-7}$$

To make a comparison with the plots in [18], $a/c = \{0.2, 0.4\}$. Correcting Eq. (3-3) with f_w of Eq. (3-7), the reference solution for the elliptical validation models becomes[2]

$$K_{ref} = \sigma \sqrt{\frac{\pi a}{Q}} \cdot f_\phi \cdot f_w \tag{3-8}$$

The SIFs of the elliptical validation models are within 1.0% error with respect to K_{ref} for each node along the crack-tip when obtained through the J-contour integral. When K is retrieved through the stress field, K has a maximum 1.2% error with respect to K_{ref} for each node.

---

[2]Inserting $W = 4c; t = T/2 = 3c + a$ and a/c in Eq. (3-7), $f_w = \cos\left(\pi/32\right)^{-1/2} \approx 1.0024$ and $f_w = \cos\{(\pi/8)\sqrt{2/17}\}^{-1/2} \approx 1.0046$ for respectively $a/c = 0.2$ and $a/c = 0.4$, hence the impact of the finite boundaries on the SIF is still rather small and is even smaller if the actual thickness T instead of $T/2$ had been used.
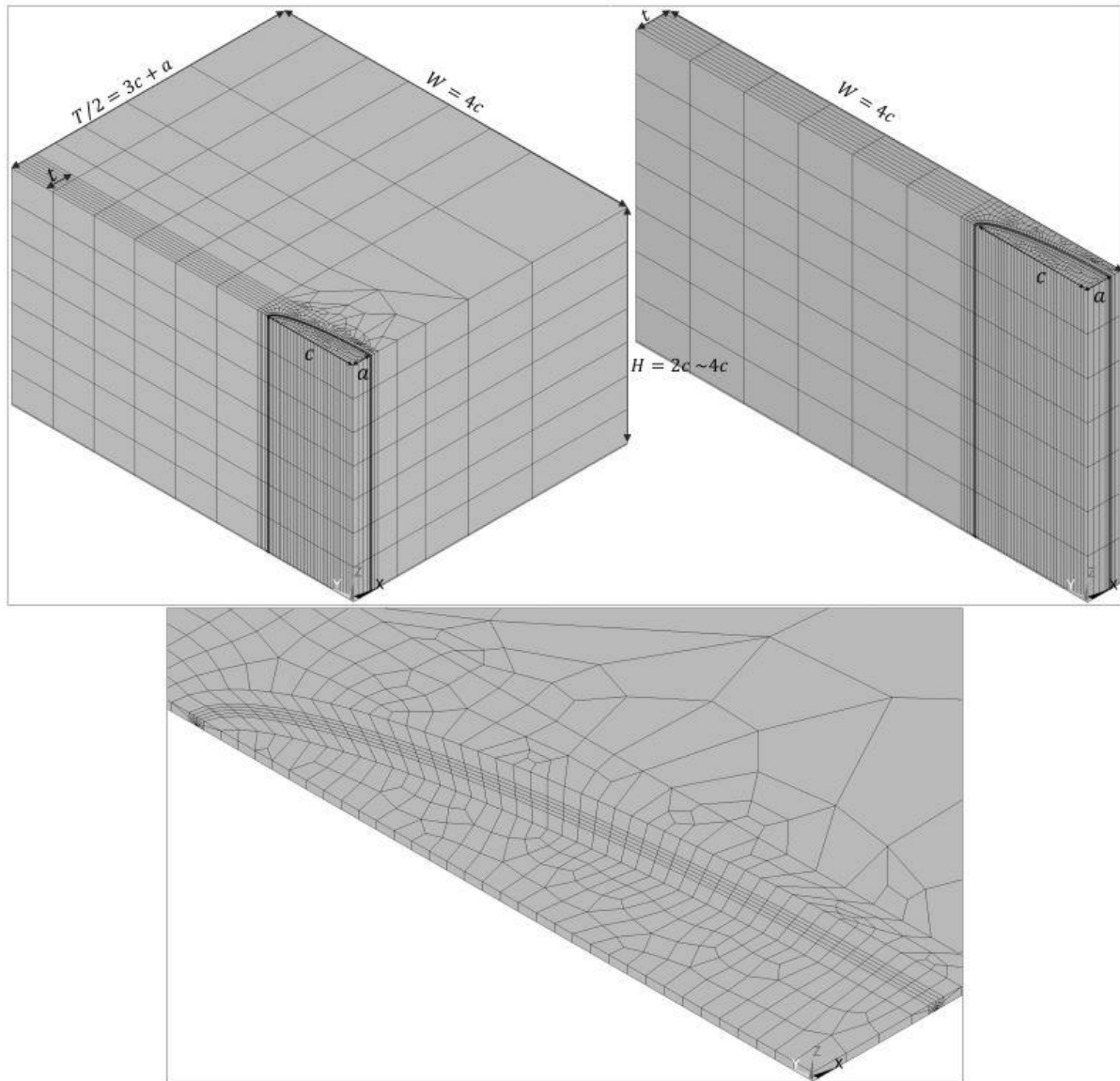
Figure 3-3: Top - Left Embedded ellipse where $a/c = 0.2$ for validation of the semi-elliptical
surface crack with $a/t = 0.7$
Top - Right Semi-elliptical surface crack with $a/c = 0.2$, $a/t = 0.7$
Bottom Close-up of the first layer of elements

The loading, shown in Figure 3-4, is expressed as

$$\sigma(X) = \sigma \left(1 - \frac{X}{a}\right)^n \tag{3-9}$$

A uniform ($n = 0$) and a linear ($n = 1$) stress distribution are considered.

The Boundary Correction Factor (BCF) of present FEM results as well as the NR and the
Wang formula (Section B-2) for $a/c = 0.2$ and $a/c = 0.4$, for both the deepest point A and
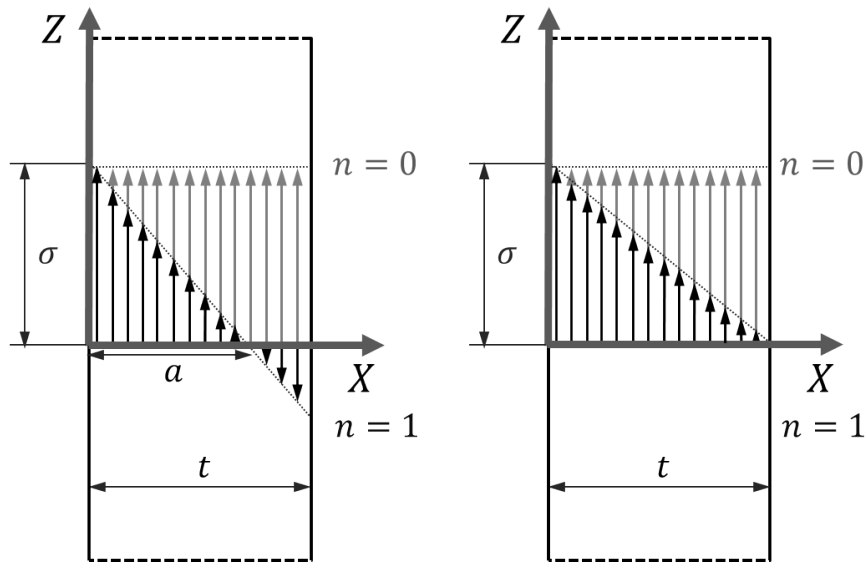
Figure 3-4: Stress distribution $\sigma(X)$ applied to the FEM of a
Left Semi-elliptical surface crack
Right Semi-elliptical through-thickness crack

the surface point C, are plotted in Figures 3-5 and 3-6. The BCF is here defined as

$$Y = \frac{K}{\sigma\sqrt{\pi a/Q}} \tag{3-10}$$

Figures 3-5 and 3-6 also show the FEM results of Wang and Isida *et al.* [16].[3,4] The width correction f_w is divided out of the plotted results so the shown BCF is for a plate with an infinite width.

The FEM results of Wang are likely to be more accurate because these are not only validated by an embedded ellipse but also by a degenerated 2-D model of the crack. This 2-D model result is compared to a handbook solution of a deep edge crack. Furthermore, the Wang FEM are higher and wider and hence better resemble an infinite solid. Despite some minor differences, the Isida *et al.* and present FEM confirm the predictions of the NR solution up to $a/t = 0.8$ but for deeper cracks, the Wang formula predicts the FE results better.

---

[3]The FEM results Isida *et al.* are shown if available, otherwise the BCF found by their FEM derived prediction formula is taken.

[4]In the article of Wang [18], FE results are added in a similar fashion. The source is cited as [16], except that in the Wang article the names of the authors of this source are given as Shiratori, M. , Niyoshi, T. and Tanikawa, K. However, the original source cites the authors as Isida, M. , Noguchi, H. and Yoshida, T. Furthermore, in the Wang article, FE solutions are given for both point A and C but only for the special case of $a/c = 1.0$ solutions for point C are given in [16]. The article of Wang gives the impression that all BCF of 'Shiratori' in Figures 3 - 6 is obtained through FEM but in [16] some FEM results are omitted and approximated by a FEM derived formula instead.
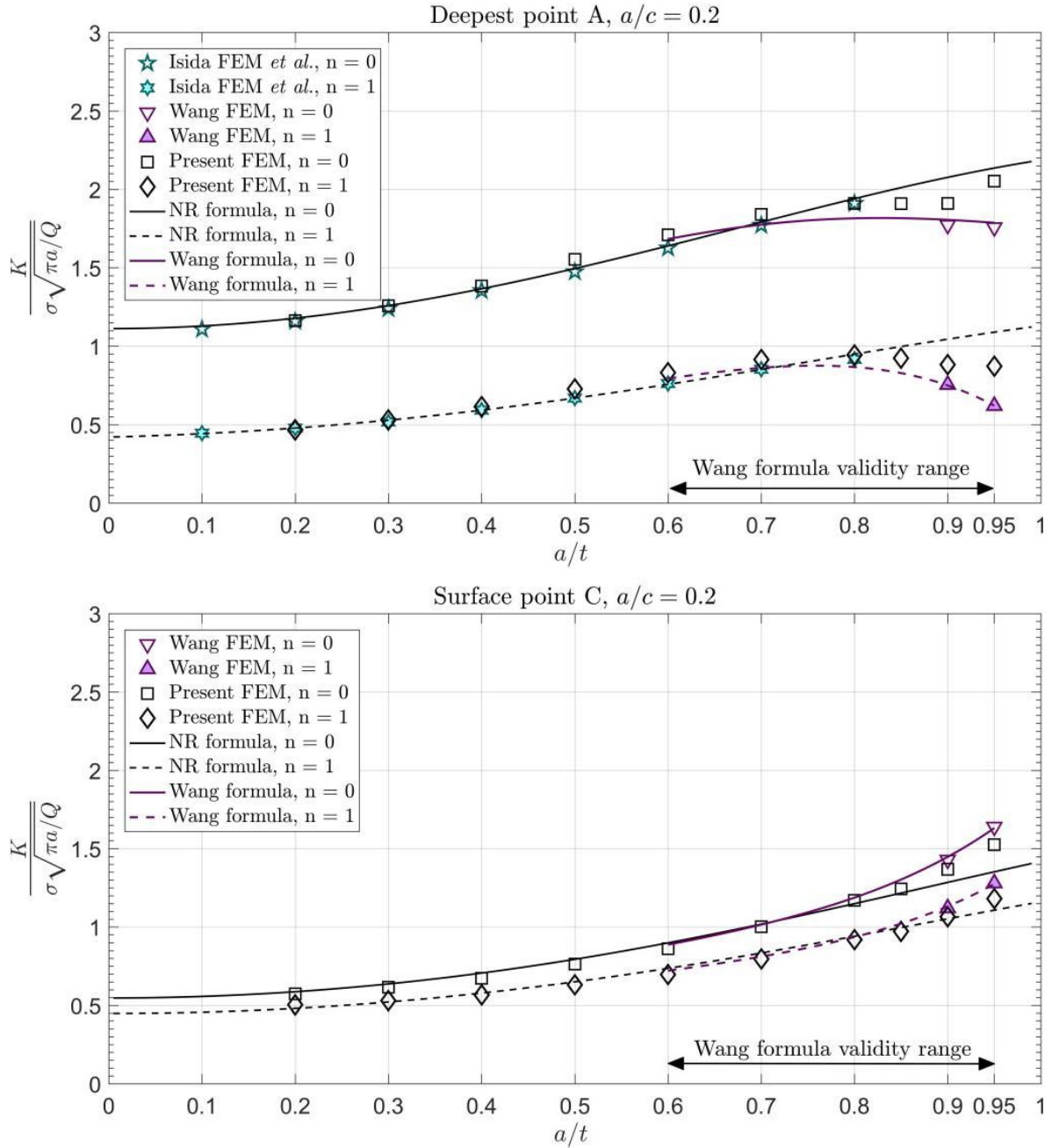
Figure 3-5: Comparison between the BCFs predicted by formulae and by FEM for $a/c = 0.2$
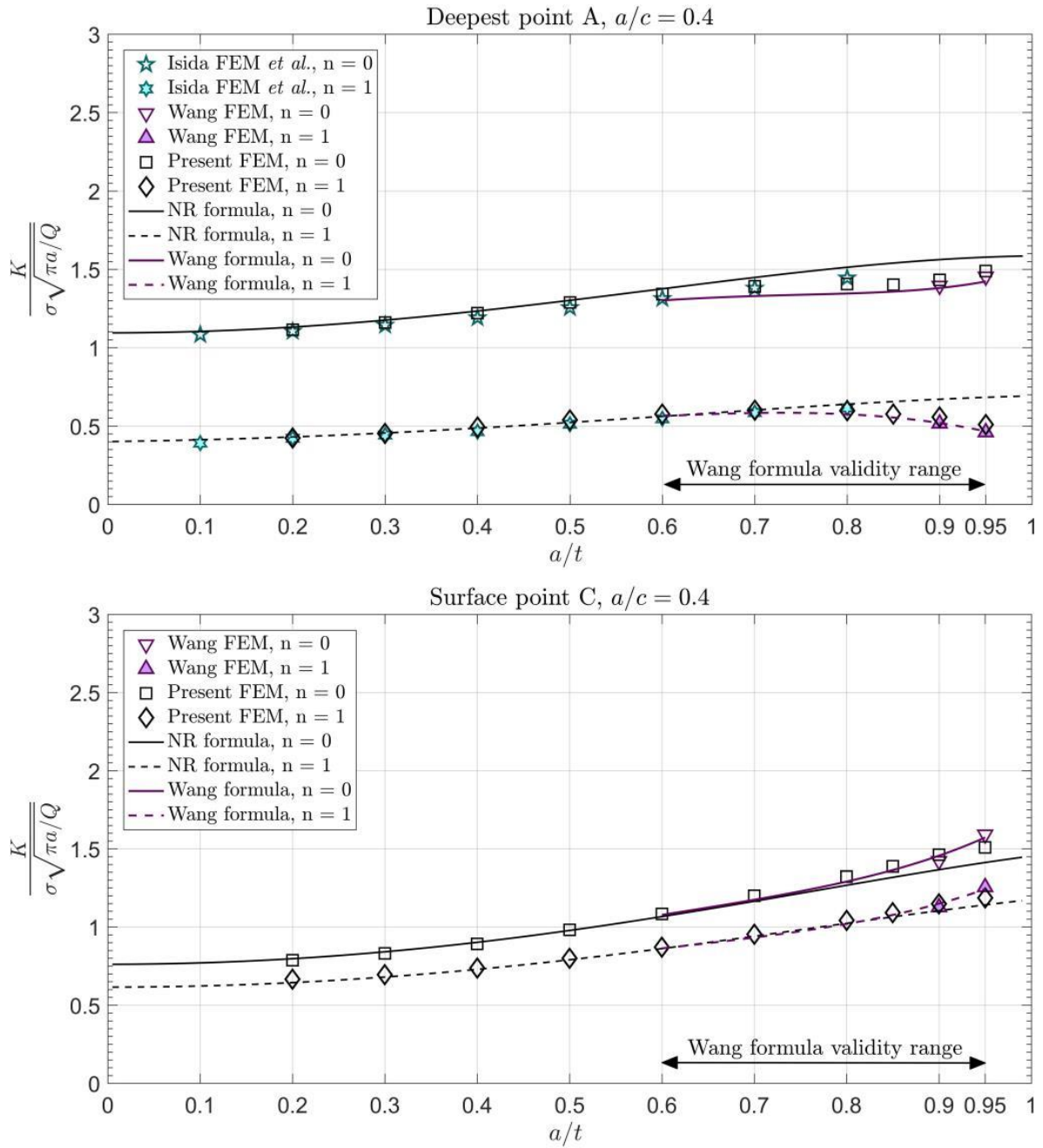
Figure 3-6: Comparison between the BCFs predicted by formulae and by FEM for $a/c = 0.4$

3-3   FE models of semi-elliptical through-thickness cracks and comparison with the AFNTO model

The third set of models aim to estimate the SIF of semi-elliptical through-thickness cracks (Figure 3-7). These estimated K will be fitted into BCF prediction formulae. This set of FE-derived BCF formulae is then compared to AFNTO SIF solution found in the literature (see also Section B-3).
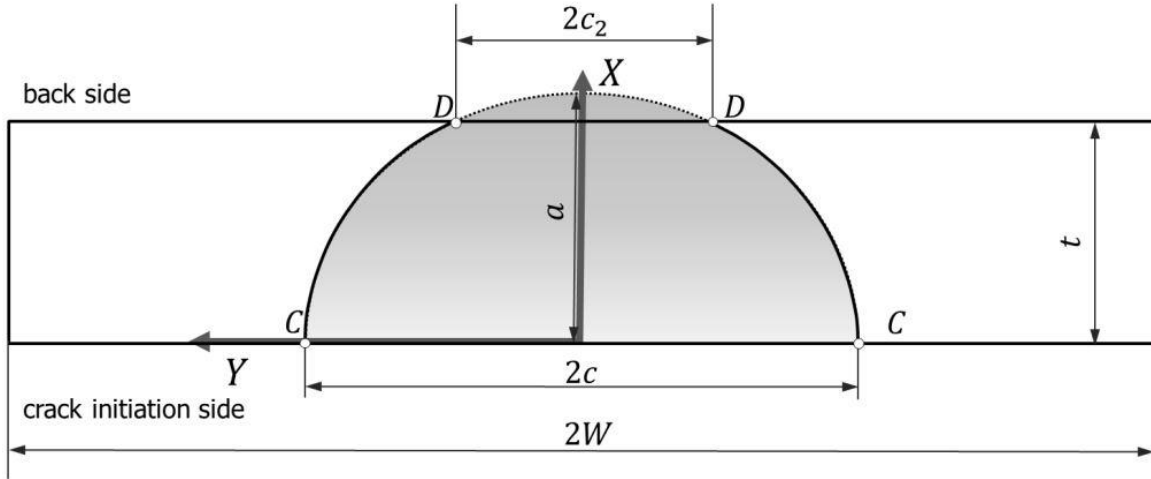
Figure 3-7: Semi-elliptical through-thickness cracks

The stress field applied to the FEM, shown in Figure 3-4, is given by

$$\sigma(X) = \sigma\left(1 - \frac{X}{t}\right)^n \tag{3-11}$$

where $n = 0$ for a uniform, and $n = 1$ for linearly decreasing tensile stress field. To avoid any contact between the crack surfaces, the crack is only loaded by tensile stresses.

Similar to the semi-elliptical surface crack where the growth is solely determined by the SIF at the depth and surface points, it is assumed that the SIF at points C and D only are sufficient to predict shape development of the propagating crack. The shape is assumed to remain semi-elliptical.

The BCF is defined as the Y in Eq. (1-1).[5] It is assumed that the BCF depends on four different input variables: the first is the loading condition ($n = 0$ or $n = 1$), the second is the location (point C or D) and the other two are the ratios a/c and a/t. a/t can be expressed in terms of c_2/c as well

$$\frac{c_2}{c} = \sqrt{1 - \left(\frac{t}{a}\right)} \tag{3-12}$$

---

[5]The BCF, which is the normalised SIF is expressed as in Eq. (3-10) when it is normalised to the analytical solution of a circular crack in an infinite solid. In this case the BCF is normalised to the analytical solution of a straight through-thickness crack in an infinite plate.

The following ratios are analysed: $a/c = \{0.4, 0.6, 0.8, 1.0, 1.25, 1.5, 1.75, 2.0\}$ and $c_2/c = \{0.24, 0.28, ..., 0.92\}$, $c_2/c = \{0.94, 0.95, ..., 0.99\}$ so a total of $8 \times 24 = 192$ models are used for curve fitting a BCF-relation.

The models are validated by the analytical solution for a straight, through-thickness centre crack that is corrected for its finite width, see also Section B-4. The reference solution for the validation model is then given by

$$K_{ref} = \sigma \sqrt{\pi c} \cdot f_w \left(\frac{c}{W} \right) \tag{3-13}$$

where the width correction f_w for a straight centre crack is given by

$$f_w \left(\frac{c}{W} \right) = \left[1 - 0.025 \left(\frac{c}{W} \right)^2 + 0.06 \left(\frac{c}{W} \right)^4 \right] \left[\cos \left(\frac{\pi}{2} \frac{c}{W} \right) \right]^{-1/2} \tag{3-14}$$

All models have a width of $W = 6c$. For the (straight) validation models the correction is therefore constant at $f_w = 1.01683$. Hence, also K_{ref} remains uniform along the thickness. For the semi-elliptical through-thickness models f_w varies along the crack-tip because instead of c in Eq. (3-14), the 'local' c is used, i.e. the respective Y-coordinates of each of the crack-tip nodes.

The SIF values are obtained by the J-contour integral. This method is not suitable to retrieve the SIF value at the nodes where three free surfaces meet (i.e. point C and D), see Appendix D for a brief explanation why this is the case. The SIFs at these points are therefore assumed to have the same value as the first neighbouring crack-tip node.

The through-thickness models cannot be constructed in a similar way as the surface crack models, i.e. by extruding a typical, semi-squared 'spider web' type of mesh from the crack initiation side along (a part of) a semi-elliptical line, as for instance shown in the close-up in Figure 3-3. However, as shown in Figure 3-8, this extrusion heavily distorts the spider-web shape at the back side and is therefore not suitable for sharply curved through-thickness cracks. To avoid this distortion, the elliptical lines at and around the crack-tip are approximated by a reasonably large number of straight lines, see Figure 3-9.

This latter model can be modified into a validation model when the crack-tip mesh is extruded along a straight line perpendicular to the surface and not along the curved 'elliptical' line. In Figure 3-10 an example can be found of the model and its validation mesh. An example ANSYS script file can be found in Appendix F.

This mesh type is by no means the best mesh possible but it does allow for a - at least some sort of - comparison with a validation model. Models similar to that of Figure 3-10 are therefore used for all FEM.
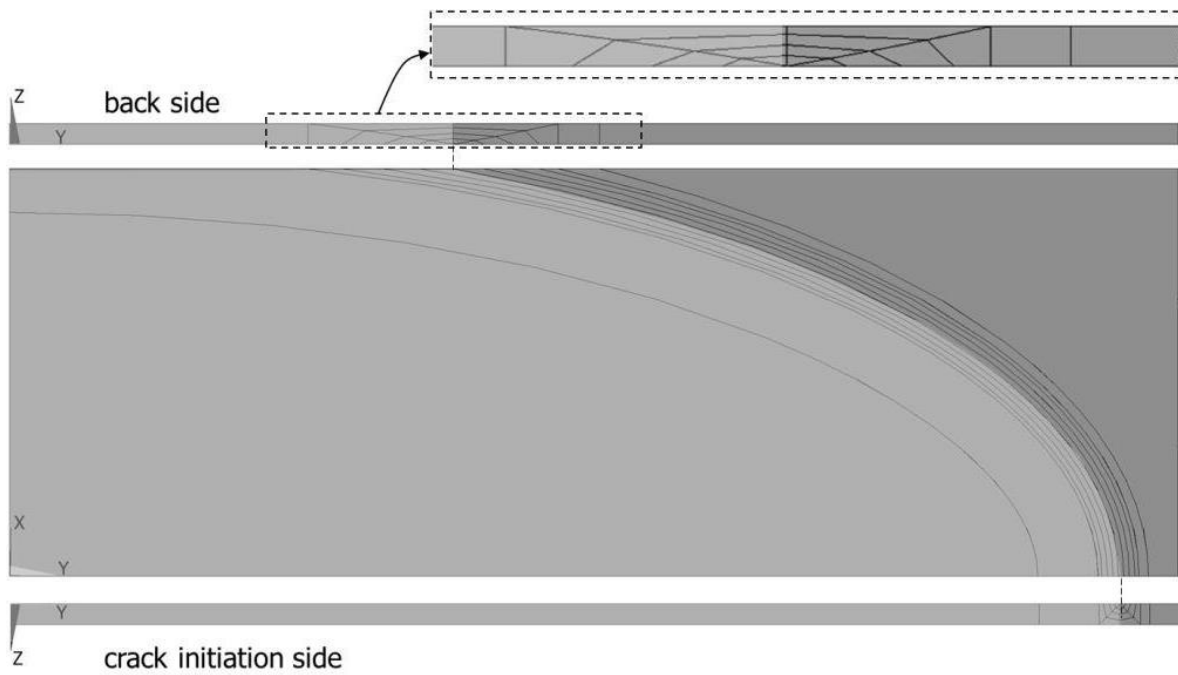
Figure 3-8: Crack volumes (lighter grey) created by extruding a semi-squared spider web mesh from the crack initiation side along a part of a semi-elliptical line. $a/c = c_2/c = 0.4$
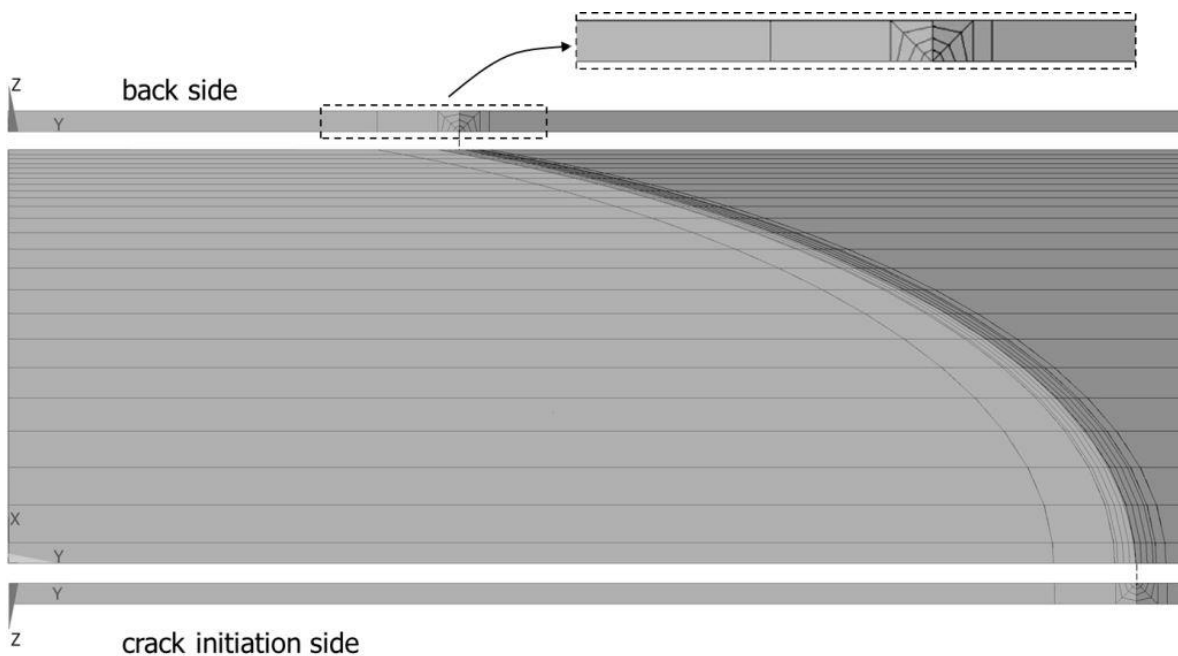
Figure 3-9: Crack volumes (lighter grey) created by extruding a typical, semi-squared 'spider web' mesh from the crack initiation side along straight lines that approximate a part of a semi-elliptical curve. $a/c = c_2/c = 0.4$
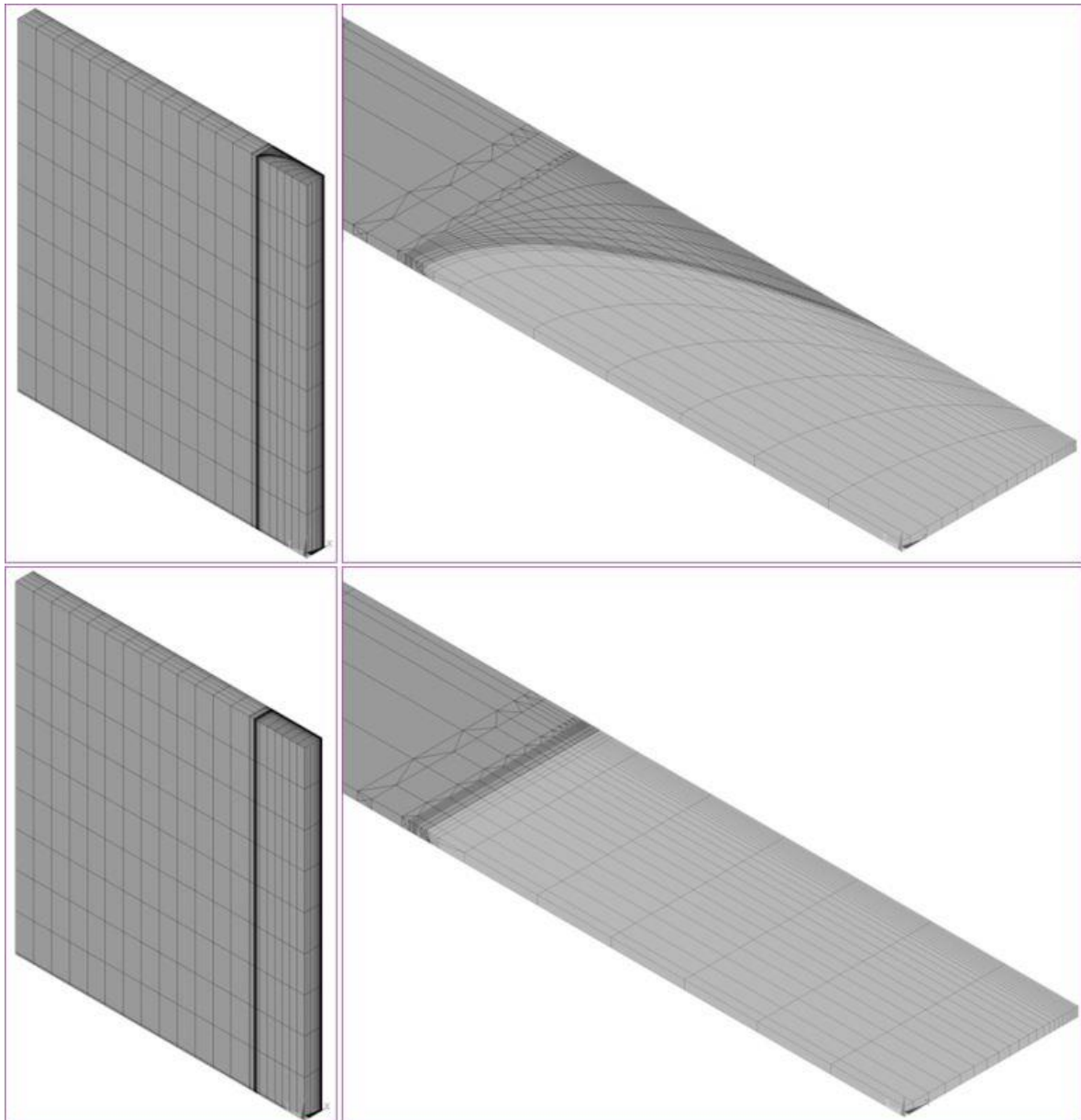
Figure 3-10: Model and validation model for $a/c = c_2/c = 0.4$
Top - **Left** Model of a semi-elliptical through-thickness crack
Top - **Right** Close-up of the first layer of elements
Bottom - **Left** Validation model (straight centre crack)
Bottom - **Right** Close-up of the first layer of elements

The limitation on the number of nodes one can use means that for each of the 192 models there is a trade-off between the following:

A very curved crack front is more accurately modelled by a large number of nodes around the crack front area.

$\Leftrightarrow$

Using a large number of nodes around crack front area implies that less nodes remain for the other parts, leading to poorly shaped elements elsewhere.

Since K at the surface cannot be obtained through a J-integral, it is approximated by using the K of the crack-tip node next to the surface crack-tip node. This neighbouring node should be as close as possible to the surface for a better approximation.

$\Leftrightarrow$

Elements that are small in X-direction require a large number of elements in Y, Z-direction to avoid large aspect ratio elements.

A small radius r for the spider-web shaped crack-tip mesh improves the accuracy and convergence of the J values.

$\Leftrightarrow$

A small r requires a large number of elements in Y, Z-direction to avoid large aspect ratio elements.

The model is as high as possible to approximate an infinite plate

$\Leftrightarrow$

A high model requires a large number of elements in Z-direction to avoid large aspect ratio elements

A close-up of the mesh around the crack-tip is shown in Figure 3-11. The models have no particular units attached to its dimensions, but all have the same thickness t. So to give an idea of the range of used radii, r is expressed in terms of t as is also shown in Figure 3-11.
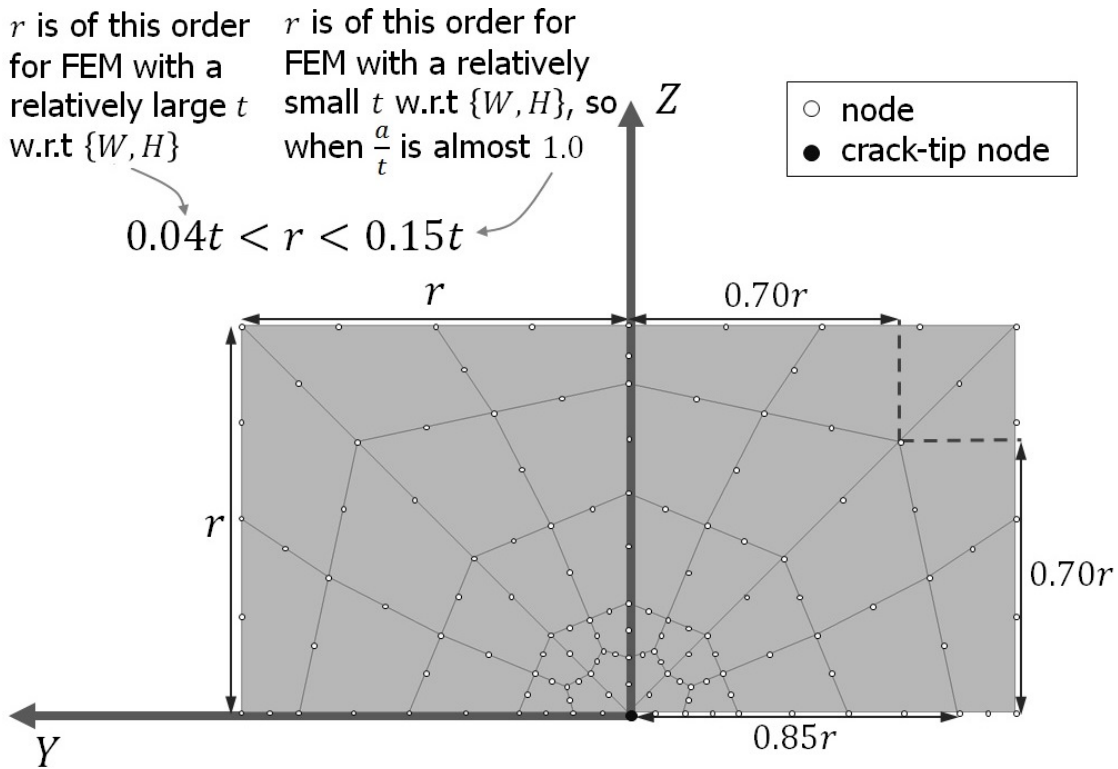
Figure 3-11: Crack-tip mesh used for all FEM

By comparison of the results of the validation model and the reference solution, the extent to which elements with a large aspect ratio can still give accurate solutions can be analysed. In Figure 3-12 the results of the validation model of Figure 3-10 is shown. Only the averaged values of the converged contours - in this example the 3$^\mathrm{rd}$, 4$^\mathrm{th}$ and 5$^\mathrm{th}$ - are used throughout this research. For this particular case, the maximum deviation from the reference solution w.r.t the converged contours is 6.8%, and is below 7.0% for all 192 models.
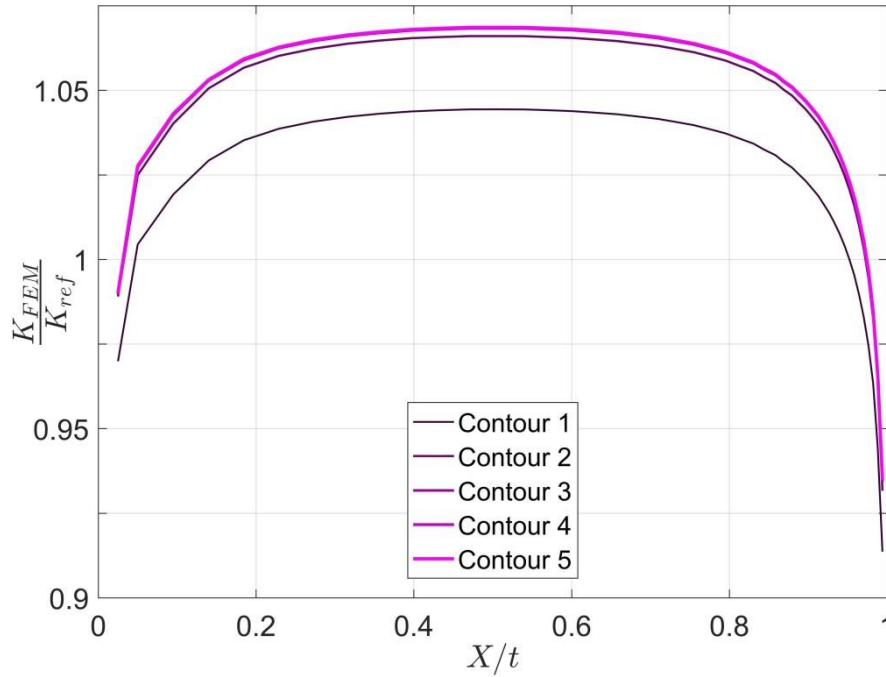
Figure 3-12: Ratio between the FEM obtained K and the reference solution of Eq. (3-13) of five contours around the crack-tip of the validation model of Figure 3-10. Contours 3 and 4 lay on the same curve as contour 5.

Clearly, the SIF is not constant along the thickness. In Figure 3-13 two other validation FEM contour results are shown: for a crack that is respectively small and one that is large in comparison with t. In Figure 3-14 the meshes of these two models are shown.[6]

Similarly, contours can also be retrieved from the semi-elliptical through-thickness cracks, see for some examples Figure 3-15. An intuitive explanation for this variation along the crack-tip of the BCF can be given: a crack tends to grow towards a shape that minimizes the amount of surface energy. In this case, when considering a uniform tensile load, maintaining a curved crack front requires more energy than a straight crack front. The more curvy fronts therefore have a tendency to grow faster and must accordingly have a higher BCF. The less curvy parts have a slightly lower BCF because the crack-front is longer compared to the straight crack

---

[6]Though no clear explanation was found to explain this variation of K_{FEM} along the thickness, it is possible that shear may cause this behaviour. For a crack that is short compared to t, e.g. the one on the left side of Figure 3-14, the crack opening is more constrained by the surrounding material and this results in a that K_{FEM} varies less along the thickness. For a relatively long crack w.r.t t, e.g. Figure 3-14 on the right, the crack opening is constrained to a lesser extent and displays a larger variability of K_{FEM}. It is therefore hypothesised that fluctuations in crack opening displacements along the thickness cause the material to shear in the $X - Z$ plane and that this will affect the value of K_{FEM}.
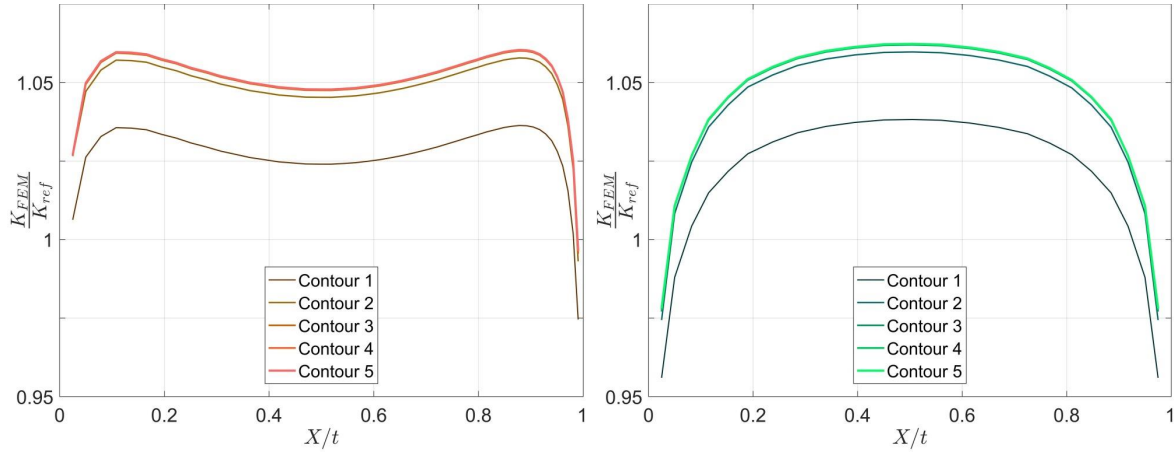
Figure 3-13: K_{FEM}/K_{ref} for five contours of the validation model for
Left $a/c = 2.0$ and $c_2/c = 0.28$
Right $a/c = 0.6$ and $c_2/c = 0.98$

to which it is normalised, hence more fracture energy is needed to create a new surface along this longer front.

For each of the FEM, the SIF is found for point C and D, and for a uniform and linear stress distribution. The SIF values are normalised as

$$Y_{C,0} = \frac{K_{FEM}}{\sigma_m \sqrt{\pi c} \cdot f_w\left(\frac{c}{W}\right)} \tag{3-15a}$$

$$Y_{C,1} = \frac{K_{FEM}}{(\sigma_m + \sigma_b)\sqrt{\pi c} \cdot f_w\left(\frac{c}{W}\right)} \tag{3-15b}$$

$$Y_{D,0} = \frac{K_{FEM}}{\sigma_m \sqrt{\pi c_2} \cdot f_w\left(\frac{c_2}{W}\right)} \tag{3-15c}$$

$$Y_{D,1} = \frac{K_{FEM}}{(\sigma_m + \sigma_b)\sqrt{\pi c_2} \cdot f_w\left(\frac{c_2}{W}\right)} \tag{3-15d}$$

Weight functions   As mentioned in the introduction, FE results of several types of crack geometries can be used to find a weight function with the method of Glinka and Shen [15]. They showed that when the SIF for two different load cases (e.g. uniform and linear stress) is known, a weight function can be approximated by determining the constants in a standard equation, Eq. (1-8). The main assumption when using this equation of Glinka and Shen is that $\sigma(x)$ only varies along the x-coordinate of a general crack size a (Figure 1-6). A modified version of their formula for the semi-elliptical surface crack, Eq. (B-6 and B-7) was based upon the analytical solution for an embedded ellipse, because this still allows for an expression that does only depend on x and crack depth a. However, for the semi-elliptical through-thickness crack the stress distribution is expressed in global coordinates, $\sigma(X)$, and this translates into $\sigma(x, y)$ when using the local coordinates of Figure A-1. Hence, for this type of cracks the standard weight function equation cannot be used and only uniform and linear stresses can be predicted with the current FE results.
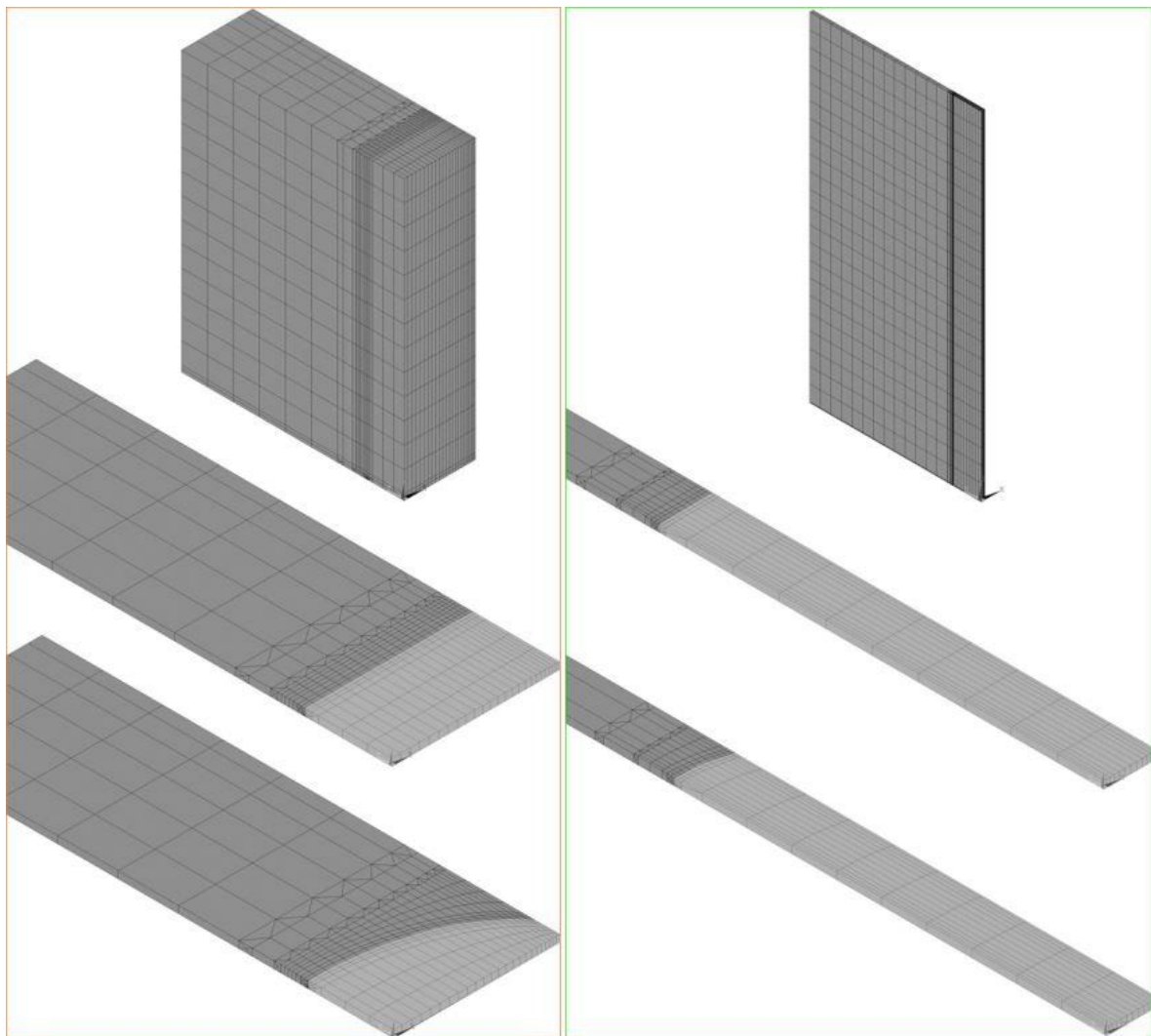
Figure 3-14: (**Top**) Full validation FEM, (**Centre**) close-ups of the first layer of elements of the validation and (**Bottom**) crack model
Left $a/c = 2.0$ and $c_2/c = 0.28$
Right $a/c = 0.6$ and $c_2/c = 0.98$
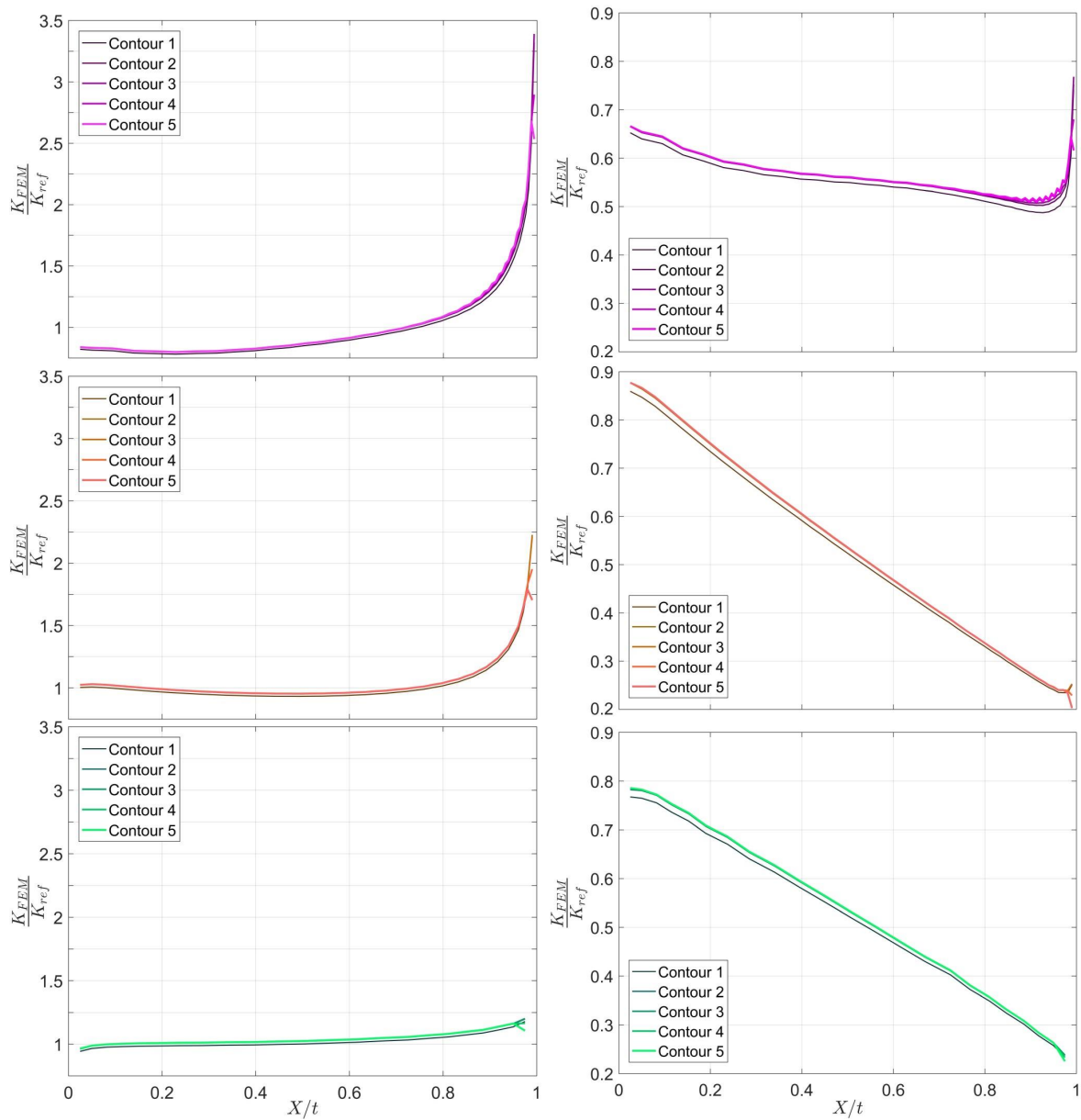
Figure 3-15: K_{FEM}/K_{ref} for five contours of the semi-elliptical through-thickness crack model for a uniform (**Left**) and a linear (**Right**) nominal stress distribution (Eq. (3-11))

Top $a/c = 0.4$ and $c_2/c = 0.4$

Centre $a/c = 2.0$ and $c_2/c = 0.28$

Bottom $a/c = 0.6$ and $c_2/c = 0.98$

The normalised results of Eq. (3-15) are curve-fitted into four formulae. The expression is chosen such that it minimises the number of constants and yet has a minimal error w.r.t the FE results and an adjusted r^2 of at least 0.99. The equations have a maximum error w.r.t the FE results of 6.6%, but much better in most cases. The formulae are

$$Y_{C,0} = 1.50 - 0.536 \left(\frac{a}{t}\right)^{-0.008246} + \left[0.09782 - 0.0882 \left(\frac{a}{c}\right)^{-1.081}\right] \left(\frac{a}{t}\right)^{-1.289} \tag{3-16a}$$

$$Y_{C,1} = 0.77 + 0.2843 \left(\frac{a}{t}\right)^{-0.7473} - 0.2529 \left(\frac{a}{c}\right)^{-0.4966} \left(\frac{a}{t}\right)^{-0.9227} +$$
$$0.0005974 \left(\frac{a}{c}\right)\left(\frac{a}{t}\right) \tag{3-16b}$$

$$Y_{D,0} = 1.271 \left(\frac{a}{t}\right)^{-26.73} + 1.304 \left(\frac{a}{c}\right)^{-0.4908} \left(\frac{a}{t}\right)^{-3.082} + 1.33 \left(\frac{a}{c}\right)^{-0.2891} +$$
$$0.1523 \ln\left(\frac{a}{t}\right)\left(\frac{a}{c}\right) - 0.3052 \ln\left(\frac{a}{t}\right) \tag{3-16c}$$

$$Y_{D,1} = -89.04 \left(\frac{a}{t}\right)^{-3.857} + 89.25 \left(\frac{a}{c}\right)^{-0.003415} [1/(a/t)]^{3.867} +$$
$$0.3383 \left(\frac{a}{c}\right)^{-0.4113} - 0.135 \ln\left(\frac{a}{t}\right) + 0.01466 \left(\frac{a}{c}\right)\left(\frac{a}{t}\right) \tag{3-16d}$$

The validity range of Eq. (3-16) is ($0.4 \leq a/c \leq 2.0$), and ($1.030 \leq a/t \leq 7.089$) or - equivalently - ($0.24 \leq c_2/c \leq 0.99$). In the range ($0.99 < c_2/c < 0.999$), the BCF is assumed to linearly in- or decrease towards the analytical solution for a straight centre crack. As previously stated, a straight centre crack has a BCF of $Y = 1$. For a straight centre crack under pure bending and $t/c \to 0$, the BCF is analytically derived as [29]

$$K^b = \frac{1+\nu}{3+\nu} \cdot \sigma_b \sqrt{\pi c} \tag{3-17}$$

The Poisson's ratio is fixed at $\nu = 0.3$ to get the analytical value where the approximative BCF converges towards. Furthermore, the linear stress distribution of Eq. (3-11) is obtained by setting $\sigma_m = \sigma_b$. Therefore $Y_{C,1}, Y_{D,1}$ converge to

$$\lim_{t/c \to 0} Y_{C,1} = \frac{\sigma_m + \sigma_b(1+0.3)/(3+0.3)}{\sigma_m + \sigma_b} = 0.697$$
$$\lim_{t/c \to 0} Y_{D,1} = \frac{\sigma_m - \sigma_b(1+0.3)/(3+0.3)}{\sigma_m + \sigma_b} = 0.303$$

For $c_2 \geq 0.999$ or $(c_2 - c)/t < 0.01$, i.e. when the average 'slope' of the crack is very small, the crack is assumed to be a straight through thickness crack.

In Figure 3-16 and 3-17 some results of the equations Eq. (3-16) are shown, together with the AFNTO solution. The linear stress field used in both equations is that of Eq. (3-11). The differences between the AFNTO and FEM equations are considerable but both curves do at least follow a similar trend and their values are in the same order. Though no conclusions can

be drawn on the accuracy or reliability of either two models, this similarity does indicate that the model scripts do not contain unacceptably large flaws and that no significant calculation errors have been overlooked.
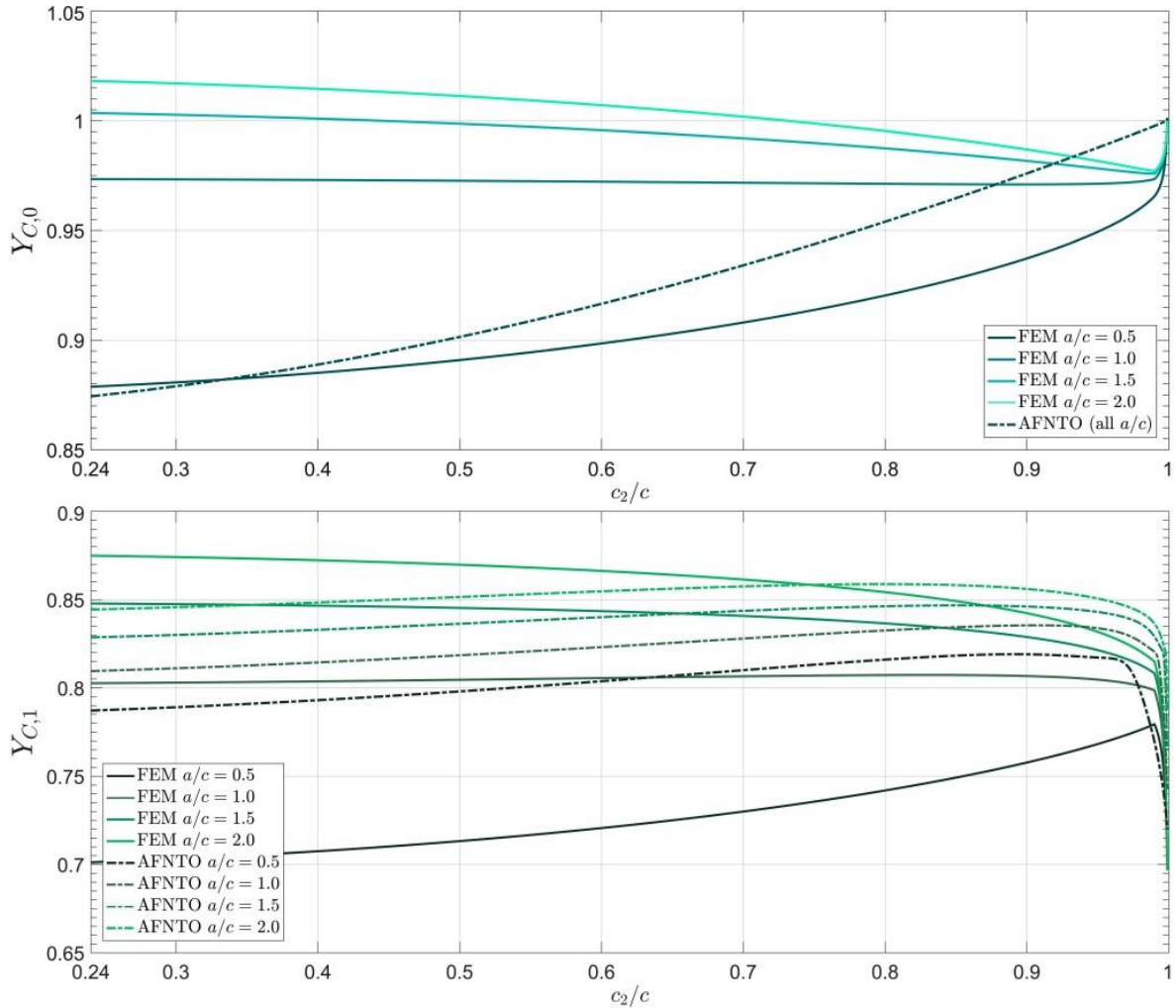
Figure 3-16: Estimated BCF for point C by Eq. (3-16a-b) and AFNTO Eq. (B-8)
        Top Uniform stress distribution
        Bottom Linear stress distribution
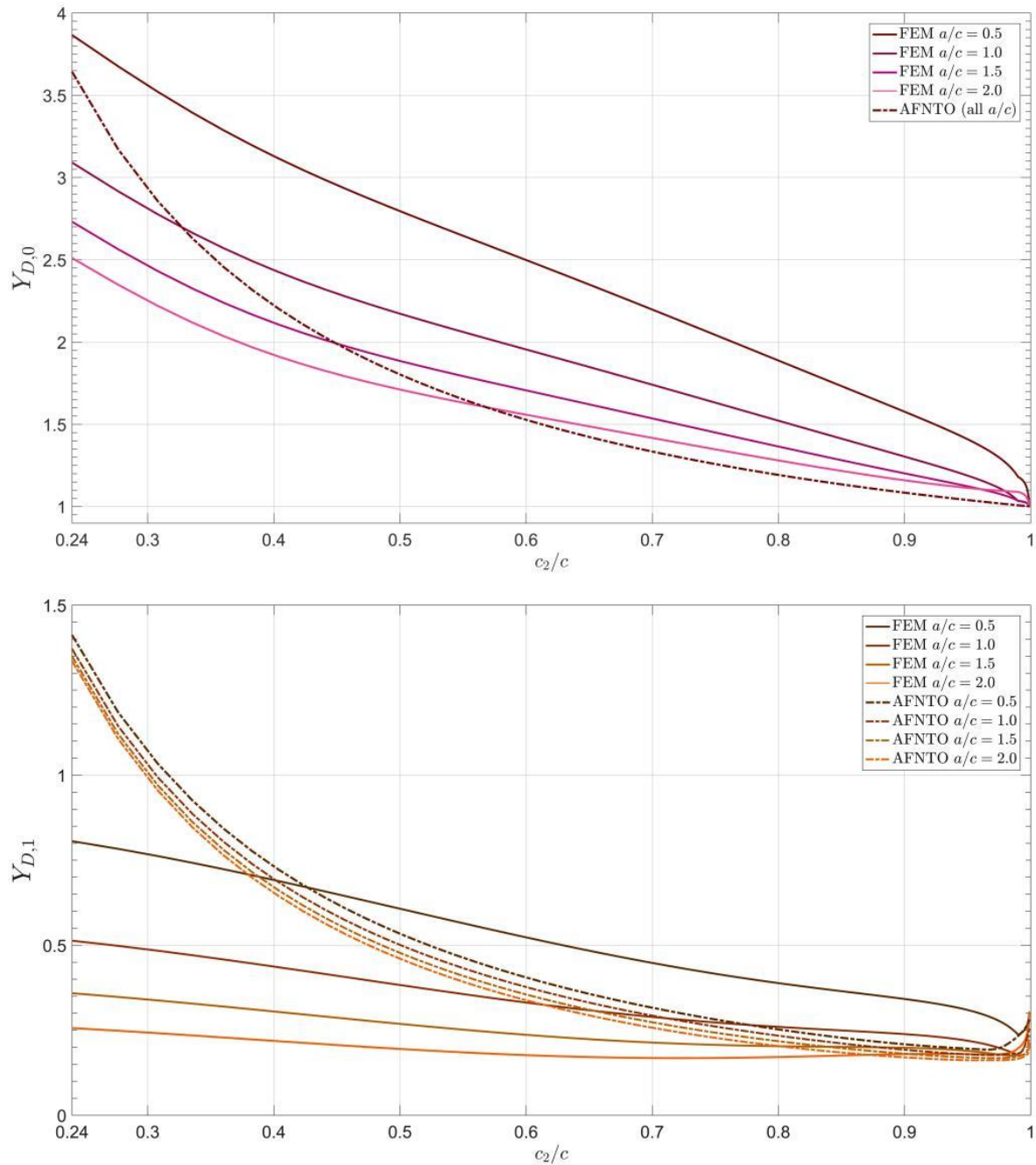
Figure 3-17: Estimated BCF for point D by Eq. (3-16c-d) and AFNTO Eq. (B-8)
    Top Uniform stress distribution
    Bottom Linear stress distribution

Chapter 4

The accuracy of predictive models in comparison with experiments

For an LBB analysis, both the estimation of the number of stress cycles to attain a certain crack shape as well as the prediction of the crack shape at and after breakthrough during the crack development are of primary interest to calculate the leakage rate and the number of cycles before reaching the critical crack size. In this chapter the models to estimate the crack shape at and after breakthrough will be compared to experimental data found in the literature. In Appendix G the input values for all experimental data-sets are given. Not all of these sets were complete in the sense that all information was available to run the numerical model. Educated guesses have been made to fill in missing information so that these experiments could nonetheless be used. The methods used to fill the gaps are further explained in Appendix H.

4-1 Comparison between the estimated breakthrough shape and experiments

Numerical simulations of other research [21, 22] indicated that the breakthrough shape is predominantly affected by the ratio between membrane and bending stresses. The numerical model of [21] has been validated with experimental crack shape development data. The calculation scheme of this previous research is essentially identical to the numerical calculation procedure described in Chapter 2. Calculations of this experimentally validated numerical model indicated that the shape up to and at breakthrough is largely insensitive to the:

- Material constants, like $\hat{C}$ and $\hat{m}$ in Eq. (2-2)
- Initial crack size, as long as $a_1/c_1 > 0.1$
- Initial crack depth, as long as it is not too deep $a_1/t < 0.1$ yet large enough for the SIF and growth models to be applicable.

Table 4-1: Input for the prediction model for the breakthrough shape

Material	$\Delta K_{th}, K_{Ic}, K_c$	$0, 100, 200$	$[\text{MPa}\sqrt{\text{m}}]$
	$\hat{C}_C$	10^{-10}	$[(\text{MPa}\sqrt{\text{m}})^{-3.0} \cdot \text{m}]$
	$\hat{m}$	3.0	$[\,\text{-}\,]$
Geometry	a_1, c_1	$5 \cdot 10^{-3}, 6.25 \cdot 10^{-3}$	$[\text{m}]$
	t, W	$0.050, 10$	$[\text{m}]$
	a_{bb}	$0.995 \cdot t$	$[\text{m}]$
Loading	$\Delta\sigma_t, \Delta\sigma_b$	$\{0 \sim 55\}, \{-5 \sim 50\}$	$[\text{MPa}]$
Calculation	$\Delta N_{a,2}$	$\{600 \sim 1800\}$	$[\text{Cycles}]$
	INT	2-point integration of $\mathrm{d}a/\mathrm{d}N$, $\mathrm{d}c/\mathrm{d}N$	
	TP	at $a = 0.6t$ or no transition	
	PC	No plasticity correction	

In these cases, relative differences stay within 10% error when $\{\Delta K_{th}, K_{Ic}, K_c, \hat{C}, \hat{m}, a_1, c_1, t, W\}$ are varied. Hence, almost regardless of the initial crack dimensions or material properties, predictive models and experimental data on the breakthrough shape can be compared to each other. This allows for a comparison between the predictive value of different configurations of the numerical model that was described in Sections 2-2 and 2-3.

Tough the numerical model is largely insensitive to most of the input values, two variables that do give significant differences are selected to predict the breakthrough shape. The first is a transition from the NR formula to the Wang formula in the range $(0.6 \leq a/t < 0.95)$. The results of Section 3-2 showed that the current FE results are closer to the Wang SIF prediction than to the NR prediction, so a transition to the Wang formula possibly improves the accuracy of the estimates for these breakthrough shapes. The second variable is whether or not to use the Newman-Raju correction (NRC) to the crack growth relation in length direction, Eq. (2-3). So in total four different calculation models are compared to published breakthrough shapes from experiments. The remaining input for the prediction models is given in Table 4-1. The values are more or less arbitrarily selected, though all are within a normal range for engineering applications.

In Figure 4-1 and 4-2 experimental data is plotted together with the estimates. The data-sets of Nam *et al.* [25] for combined bending and tension were tested under a variable amplitude bending stress range, although up to breakthrough $\Delta\sigma_b(c)/\Delta\sigma_m$ was fairly constant. The average of this ratio up to breakthrough is used in Figure 4-1.

The predictive value of the numerical models are evaluated by the coefficient of determination r^2, i.e. the fraction of the variation of the experimental values that can be explained by the prediction model.[1] The results are given in Table 4-2. The model with the best predictive result uses only the NR and no NRC. Slightly worse results were found for the two models that do use this NRC. It should be noted that this outcome is based upon only 17 experiments and that the r^2 outcomes are relatively favourable to data-points that are both well predicted *and* have a high variance. Moreover, though the predictions are largely insensitive to most of

---

[1]Note that r^2 is **not** the squared radius r. $r^2 = 1$ means that the curve perfectly matches the data and $r^2 = 0$ means that none of the variability in the data is explained by the model. For more explanation, reference is made to `http://www.mit.edu/~6.s085/notes/lecture3.pdf`, Section 3.4 *Model Evaluation*.
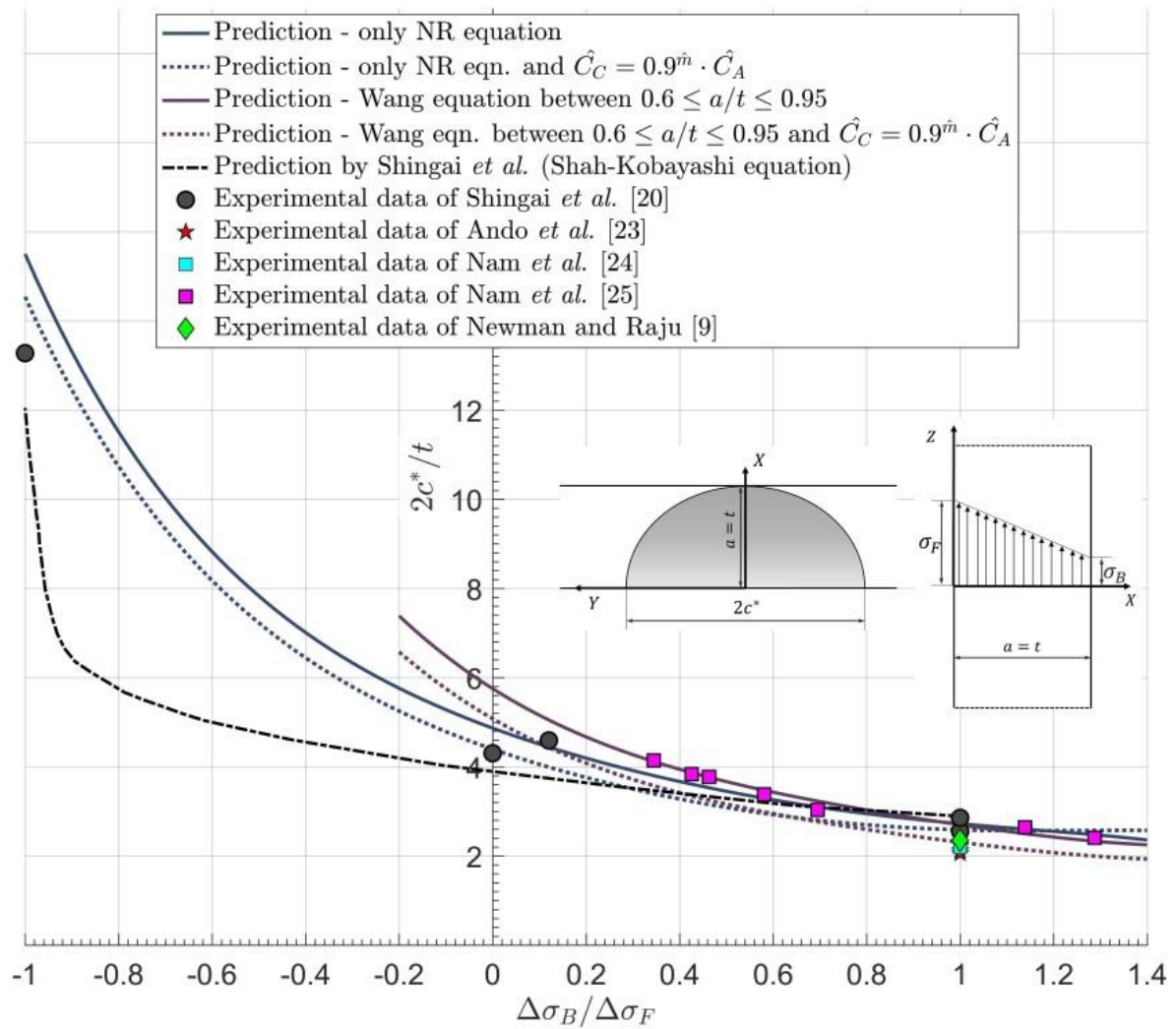
Figure 4-1: Relation between $\Delta\sigma_B/\Delta\sigma_F$ and the shape at breakthrough according to different estimation methods and experimental data

the input values, they can still differ up to 10%, so no firm conclusions should be drawn from this results yet.

Table 4-2: r^2 of the numerical models for crack growth

Model	r^{2*}
Only NR SIF equation and $\hat{C}_A = \hat{C}_C$	0.806
Only NR SIF equation and $\hat{C}_C = 0.9^{\hat{m}} \cdot \hat{C}_A$	0.753
NR + Wang SIF equation between $0.6 \le a/t \le 0.95$	0.655
NR + Wang SIF equation between $0.6 \le a/t \le 0.95$ and $\hat{C}_C = 0.9^{\hat{m}} \cdot \hat{C}_A$	0.782

---

*One result of the breakthrough shape of a crack under a pure bending stress ($\Delta\sigma_B/\Delta\sigma_F = -1.0$) Shingai *et al.* of is left out of the r^2 calculation because the numerical calculation scheme cannot model crack growth with the Wang formula if $\Delta\sigma_B/\Delta\sigma_F < -0.2$. This experiment is therefore left out of all r^2 calculations.
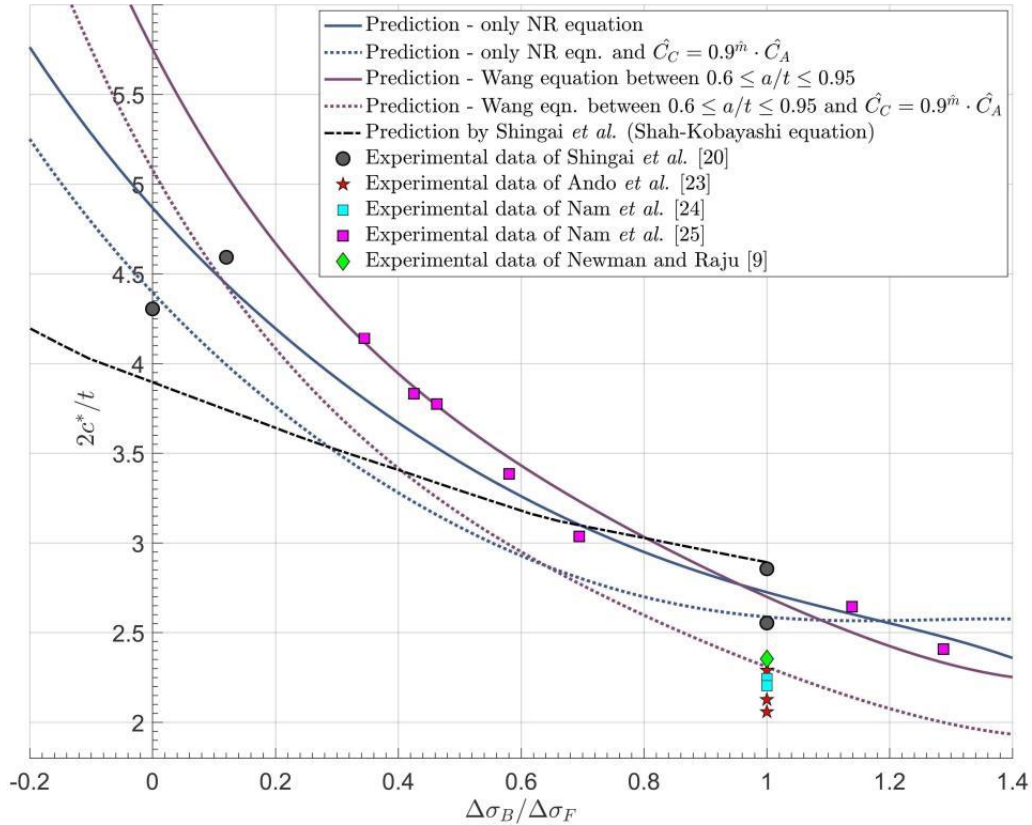
Figure 4-2: Close-up of Figure 4-1

4-2 Comparison between the predicted N and experiments

The same four models of the previous section are also evaluated for their predictive value of the number of cycles up to and directly after breakthrough. Again, it is assumed that the crack grows until reaching a depth of $a_{bb} = 0.995t$ before suddenly breaking through the wall. Right after breakthrough, in accordance with the experimental data, the 'depth' axis of the semi-elliptical through-thickness crack is assumed to have a value in the order of $a^* = 1.005t$, which is roughly $1/10^{\text{th}}$ of the crack length at the non-breakthrough side. See also Figure 2-3. After breakthrough, the AFNTO SIF model is applied to make a comparison of the complete data-set and the experimental results. The results are shown in Figures 4-3 to 4-4. Only data-set TH-3 (Figure 4-3) shows the growth data from crack initiation; for the other three cases the growth was measured after c had grown 1.3 mm.

In most cases, the articles of the data-sets also published some predictive calculations that used the NR SIF solution. For the TB data-sets it is stated that the same crack growth model in length and depth direction has been applied [25]. The articles of two other data-sets, TH and THL, do not explicitly mention whether this NRC is used or not but the predictions of the shape development indicate that this correction was not applied [23, 24]. Because of the limited information on their numerical procedure, their predictions could not be reproduced here.

The models with an NRC are performing better in all cases. Using the Wang equation in the

range $0.6 \leq a/t \leq 0.95$ solution did not improve the prediction.
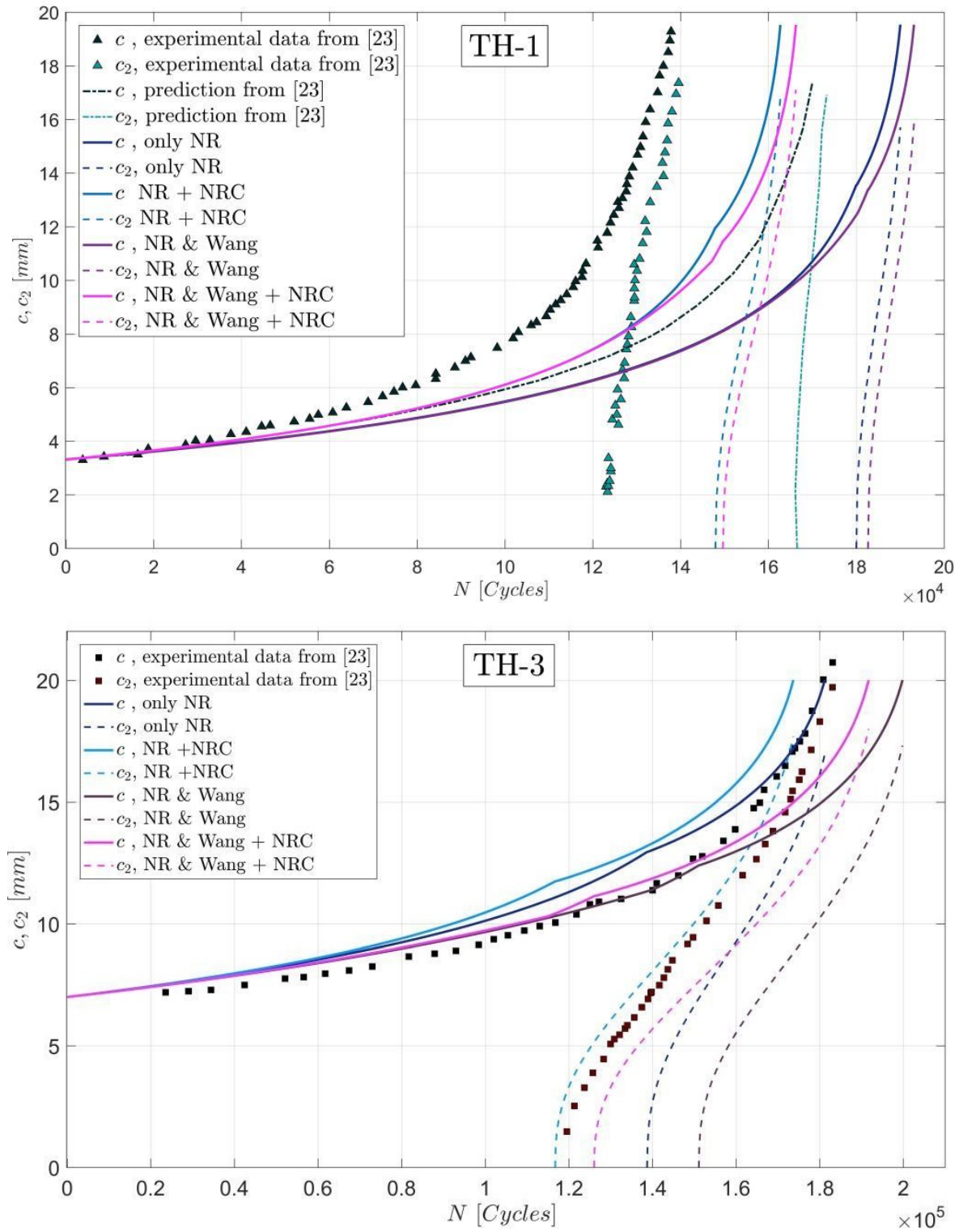
Figure 4-3: Prediction and experimental data of crack growth for data-sets TH-1 and TH-3
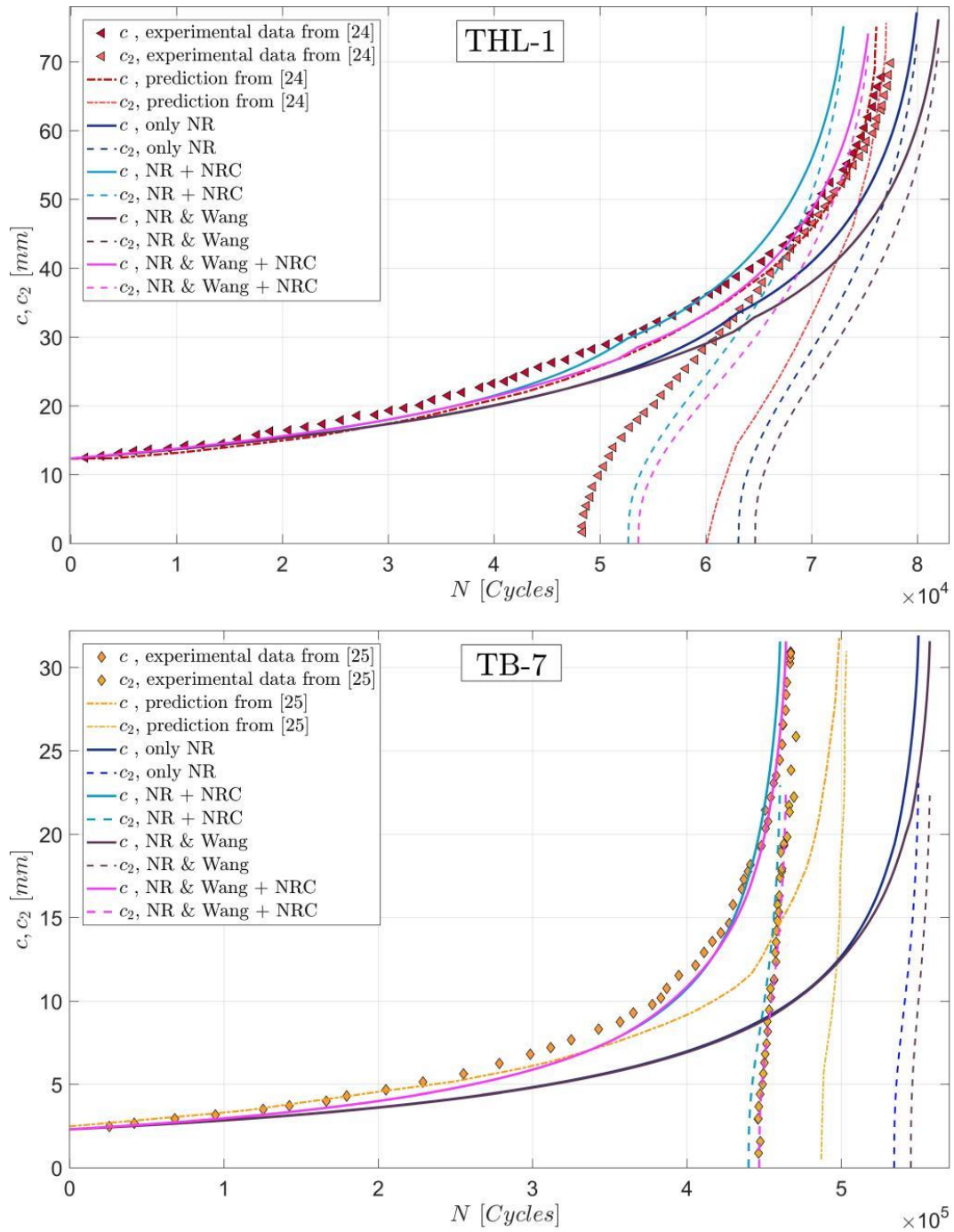
Figure 4-4: Prediction and experimental data of crack growth for data-sets THL-1 and TB-7

4-3   Comparison between the predicted crack propagation and experiments

For crack propagation after breakthrough, three models are compared to experimental data:

   – 'AFNTO', that uses the AFNTO solution to estimate the SIF;

– 'Fixed a/c', that fixes ratio a^*/c^* throughout crack propagation, see Figure 1-8;

– 'FEM', that uses the curve-fitted FEM results of Eq. (3-16) to estimate the SIF;

The characterisation of the crack shape after breakthrough, i.e. the values used for a^*, c^*, was in accordance with the measurements from experiments, usually the depth axis of the ellipse was in the order of $a^* = 1.005t$. The predictive models use these two known values so that the after-breakthrough models are not affected by the numerical procedure up to breakthrough. The AFNTO model is also used for the 'FEM' model when $a/t < 1.030$, the range where the FEM-model is not valid.

The predictive results by the authors of the data source, the researchers who also developed the AFNTO model, could not exactly be reproduced. However, for the specimens under a tensile load, the results of the current numerical scheme in combination with the AFNTO model are convincingly close enough to rule out any large differences in either numerical scheme. The calculated crack growth under tension at the front and the back of the specimen of both the current model and - if given- the prediction of the authors of the experiments is shown in Figure 4-6. The legend for these and all other remaining figures in this chapter is shown in Figure 4-5.

The differences between the current AFNTO model predictions and the AFNTO model predictions in the article with data-sets for specimens loaded by combined bending and tension are larger than the differences for data-sets under tension. This is caused by insufficient information regarding the data-sets, for instance on the applied bending stress range.

The experimental data of the crack length at the breakthrough side c_2, the predictions in the data-articles as well as the results from the current three models for specimens under combined bending and tension are given in Figures 4-7 and 4-8. From these data it is clear that overall the AFNTO model has te best predictive results for combined bending and tension. Using a fixed a/c ratio after breakthrough is in all but one case (TH-3) overestimating the growth rate of the crack, which is to a lesser extent also the case for the FEM curve-fit model. No clear 'winner' can be identified in the case of pure tension (Figure 4-6).

> ▲ c , experimental data from [23,24,25]
> ▲ c_2, experimental data from [23,24,25]
> ---- c , prediction from [23,24,25]
> ------ c_2, prediction from [23,24,25]
> —— c AFNTO
> —— c_2 AFNTO
> ······ c fixed a/c
> ········ c_2 fixed a/c
> – – c FEM
> – – · c_2 FEM
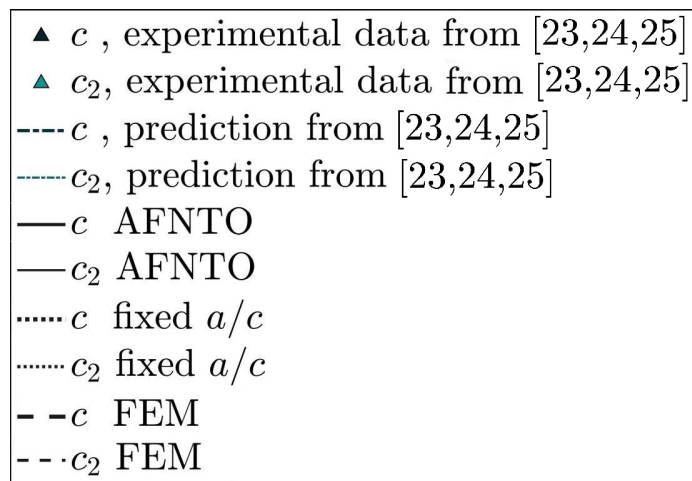
Figure 4-5: Legend for Figures 4-6 to 4-8. Note that the symbol-colour combination for each experimental data-set is unique, and that the 'prediction from [23,24,25] ' line (-.-.-.-.) adopts the colour from the data-set-symbol. Shown is the example of data-set TH-1.
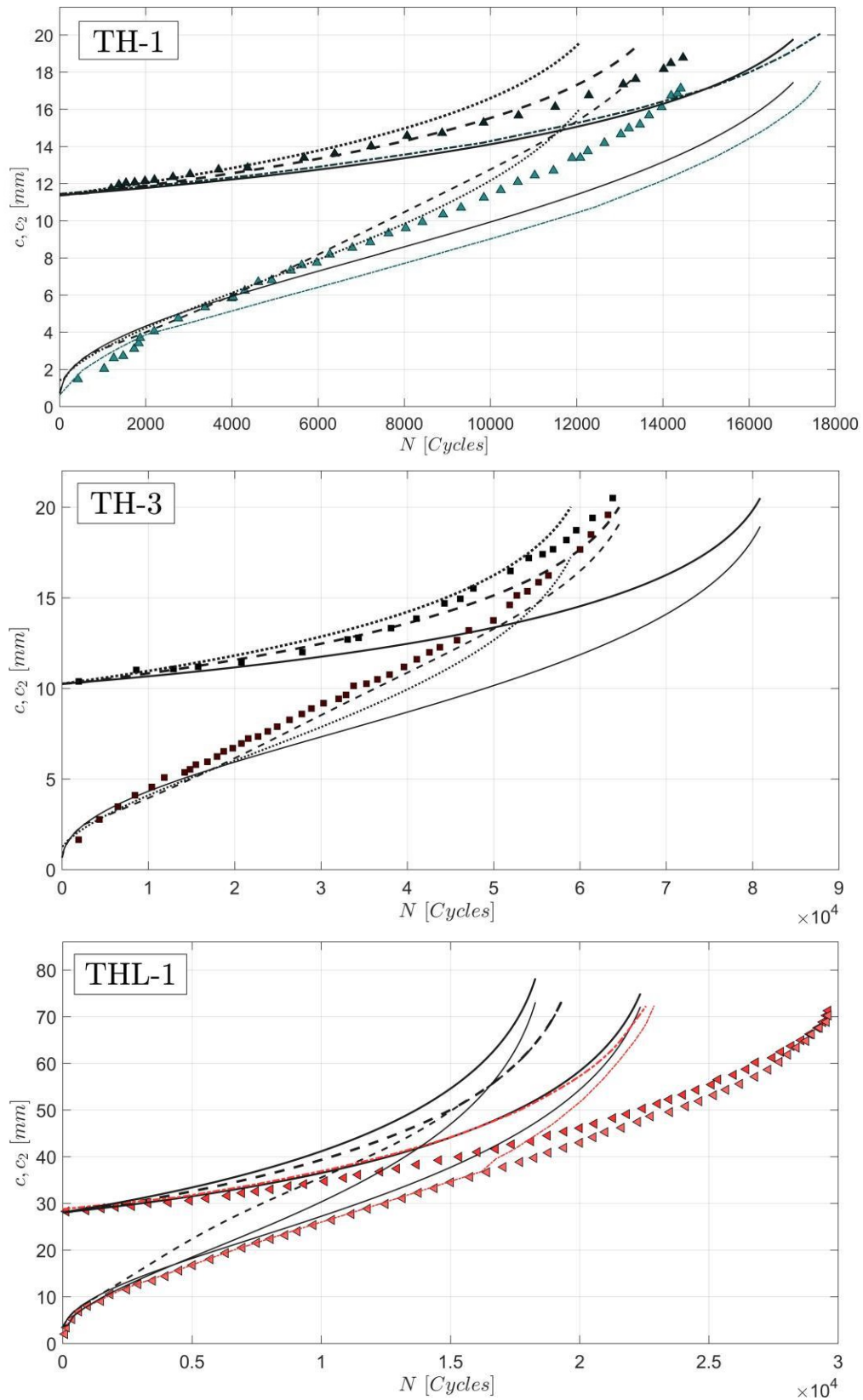
Figure 4-6: Predicted and measured data of crack growth after breakthrough (tension)
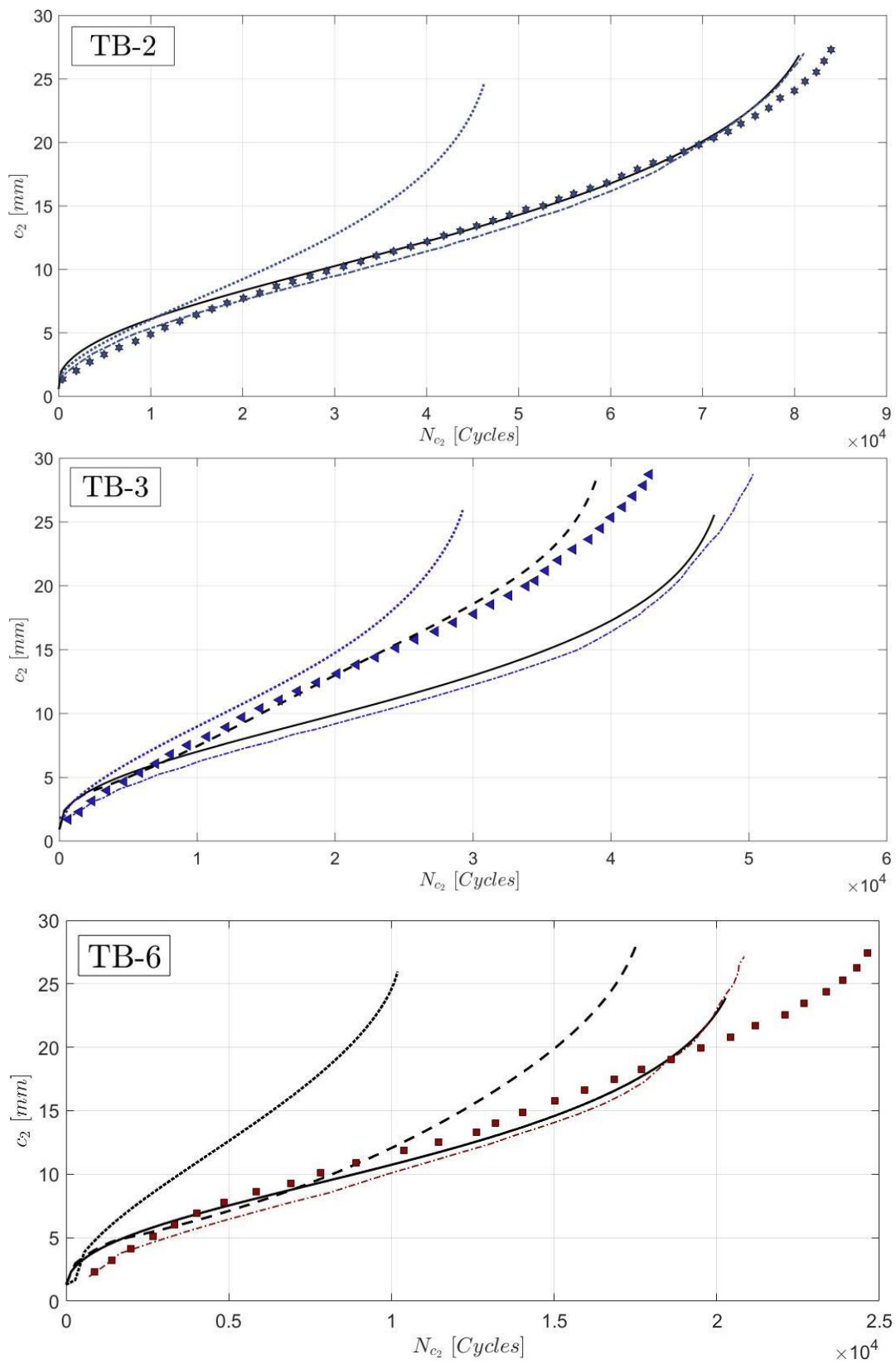
Figure 4-7: Predicted and measured crack growth at the breakthrough side (tension and bending)
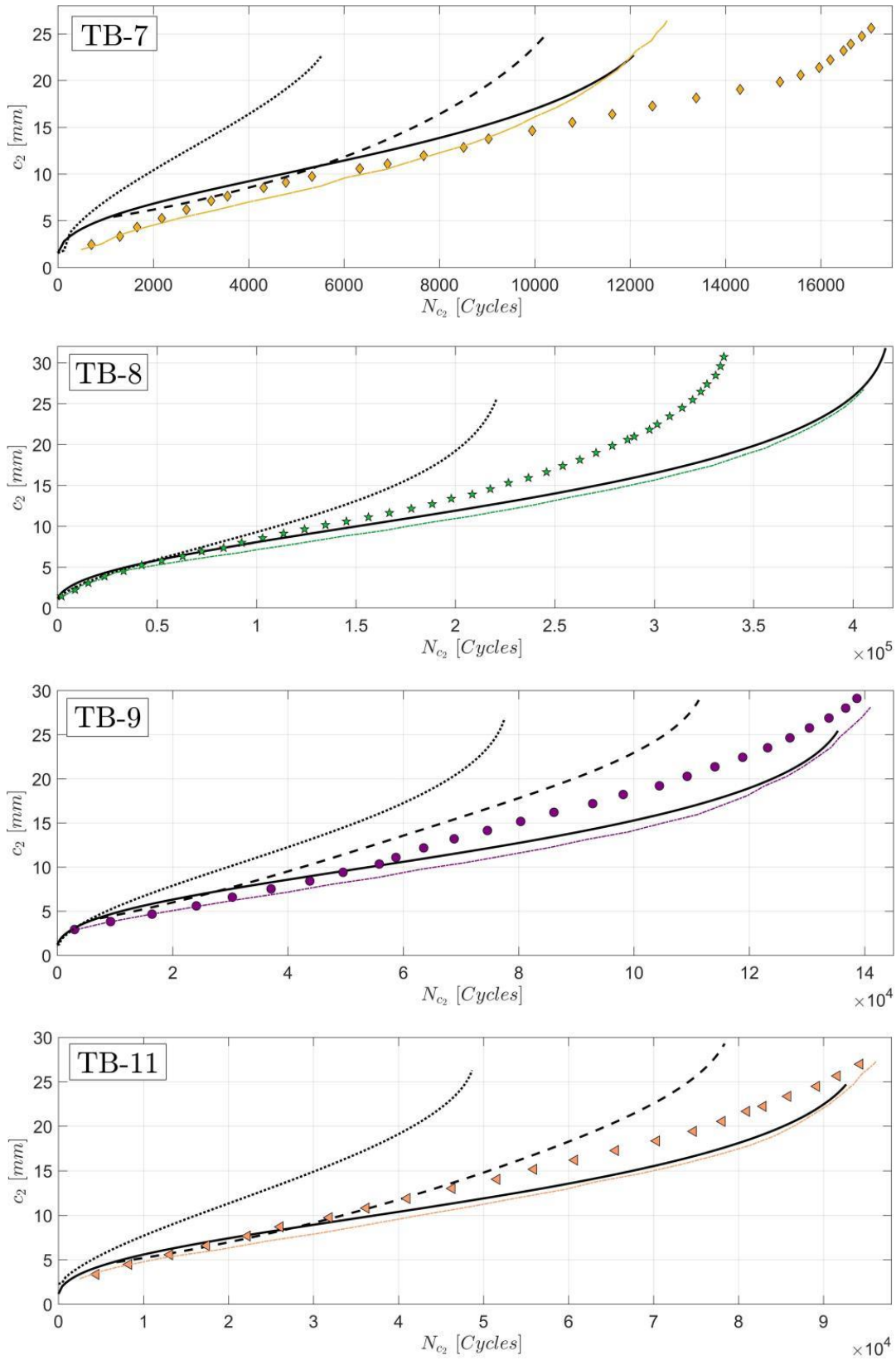
Figure 4-8: Predicted and measured crack growth at the breakthrough side (tension and bending)

Chapter 5

Analysis of the data, conclusions and recommendations

5-1 Analysis of the data taken from external sources

The present thesis relies heavily on three publications from the same group of researchers that also introduced the AFNTO SIF model, these articles will first be reviewed in this chapter. For a brief discussion on a smaller issue related to the AFNTO formula for combined membrane and bending stress, reference is made to Section B-3. Hereafter, the authors of [23, 24, 25] will be referred to as 'the authors', and the research of these articles is referred to as 'their' research or experiments.

Unfortunately, their experiments have a different configuration for each new experiment, thus none of the experiments was repeated. This repeating is necessary to estimate the scatter of the results and to assess the performance of the models when more than one test result is available. As a consequence, the unknown confidence level for the outcomes is a limitation.

As mentioned, crack growth can be estimated by using a crack growth relation. The authors use the commonly applied Paris relation, but their method to find $\hat{C}$ and $\hat{m}$ in Eq. (2-2) is questionable. As pointed out in Section A-4, one cannot simply obtain $\hat{C}$ and $\hat{m}$ from a manufacturer's specification but one has to conduct experiments for each batch of material in order to reliably estimate these. These experiments had been carried out by the authors but in such a way that the values they obtained for $\hat{C}$ and $\hat{m}$ may be unreliable.

Before breakthrough, they use the NR equation to estimate ΔK using their measured crack depth and length. Some criticism can be given to this:

- The NR equation *in itself* has an error margin of 5.0% up to $a/t \leq 0.8$, and, as discussed in Section 3-2, possibly larger error margins beyond this ratio. For other crack shapes ΔK can be found with much higher or even analytical precision.

- The crack depth was determined afterwards from the typical 'beach marks' that fatigue cracks sometimes leave on the crack surface. These marks may be hard to identify or measure precisely.

– Estimating ΔK requires a precise estimate for both a and c, whereas other crack shapes can be characterised by a single crack size, like for instance the centre cracked specimen described in Section B-4.

– The authors did not indicate to what extent the actual crack deviated from the semi-elliptical modelled crack so the applicability of the NR solution is unknown.

– In the article of Newman and Raju, it is recommended to use a corrected value in length direction, $\hat{C}_C = 0.9^{\hat{m}} \cdot \hat{C}_A$. Despite this recommendation, the authors did not use this correction when they curve fitted their results of the crack growth in length direction. One could argue that this type of material is better described without this correction, or perhaps the authors had other reasons to disregard this advice, but they did not discuss this option in their publications.

Two of their articles only derived a relation for $dc/dN = \hat{C}_C(\Delta K_C)^{\hat{m}}$ and applied it to growth in both length and depth direction. Only in the article for combined bending and tension, they plotted not only the growth relation in length direction but also showed the results for $da/dN = \hat{C}_A(\Delta K_A)^{\hat{m}}$. They concluded that the growth relation for the length was indeed applicable to model the growth in depth direction as well.

The applicability of a model is open for interpretation and whether a fit "*[..] agrees relatively well with the results from the surfaces*"[25], is a matter of engineering judgement rather than an exact science. This said, in particular the data-sets with a load ratio $R = 0.5$ do not appear to be in good agreement with the fitted model, see Figure 5-1.[1] More objectively, the goodness-of-fit of the original Paris relations can be assessed by the coefficient of determination r^2, of which the results can be found in Table 5-1. Clearly, both fits of Nam *et al.* have a very low r^2 value, or in other words: they barely describe the trend of the data-points.

Table 5-1: Coefficients of determination r^2 of the fitted relations between the SIF range versus the crack growth rate versus in depth direction loaded by a different load ratio R

Curve fit	R	r^2
Nam *et al.* [25]	0.1	0.35
Current research	0.1	0.87
Nam *et al.* [25]	0.5	0.10
Current research	0.5	0.97

The question that now arises is whether these newly fitted and better matching Paris curves in depth direction will improve the predictions for the crack shape development. Calculations of this development (before breakthrough) is for instance shown in Figure H-2 in which the original, by the authors derived Paris relation constants have been used. Nevertheless, while using a better matching relation should result in a closer approximation to the experimental data, this is not the case but rather the contrary (not shown in the figure). This could indicate

---

[1]No raw data is available, therefore the data-points are retrieved from the pdf-file of the article with software ENGAUGE DIGITIZER 9.5. Thus, the straight lines through the data-points (shown as dashed lines in Figure 5-1) were digitally retrieved as a dozen of points on the graph, and these points were again curve fitted. Is was verified that $\hat{C}$ and $\hat{m}$ could be approximated within the 95% confidence bounds of the fitted Paris curves of the original figures by Nam *et al.* by digitally retrieving data that was subsequently MATLAB curve fitted. In absence of any raw experimental data, this alternative method to approximate the data is considered accurate enough to be used for this research.
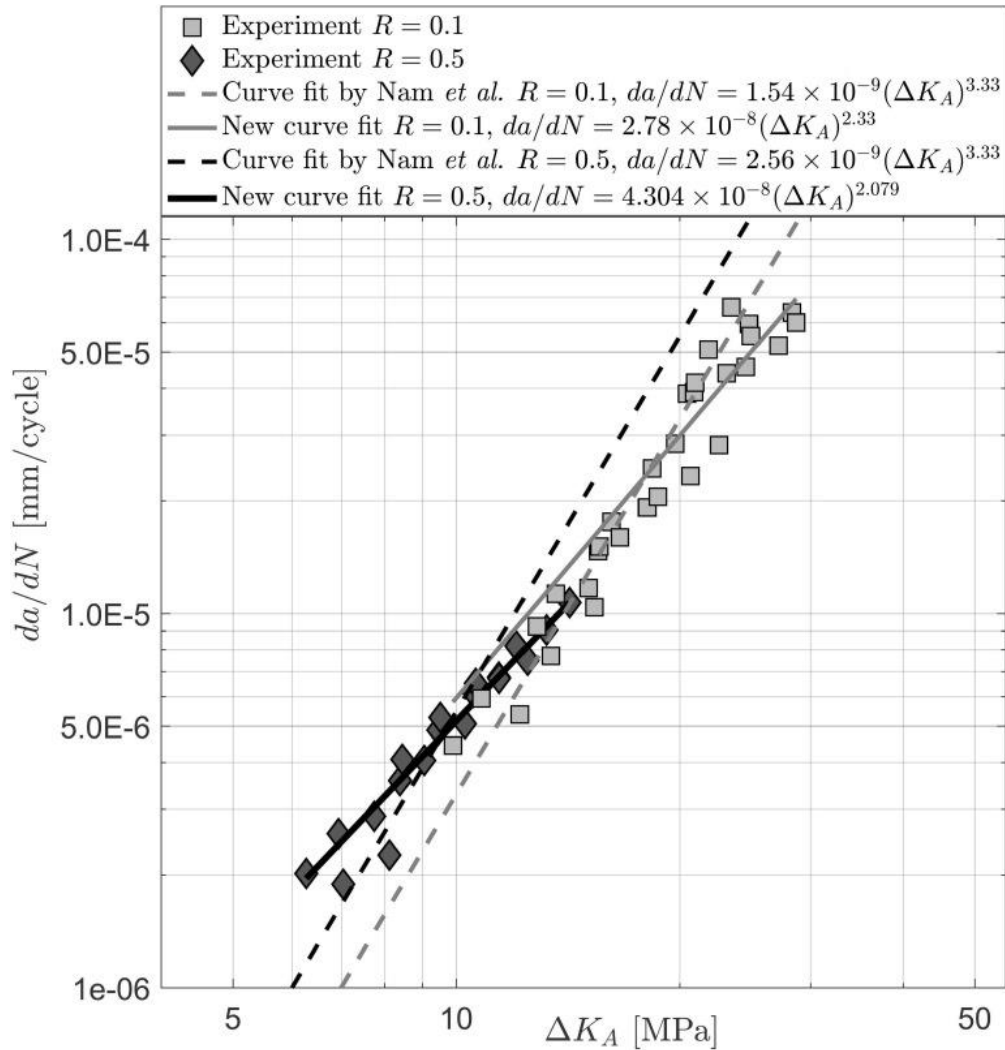
Figure 5-1: Relation between crack growth rate versus SIF range in depth direction as found by [25] and present curve fitting.

that the ΔK_A values that were obtained through measurements of the crack shape and the use of the NR equation, are indeed ill-suited to be used for estimating the Paris relation parameters $\hat{C}$ and $\hat{m}$.

A better testing method that limits the number of variables to a minimum, is to use a standardised test method with a compact tension or centre cracked specimen. For these cracked shapes, ΔK can be estimated with much more precision than with the NR solution and the growth relation can therefore be derived with more reliability. In addition, these standardised specimens can be characterised by only one crack size, which also adds to the reliability of the tests. To sum, other crack shapes than the semi-elliptical surface crack are more suitable for the derivation of a crack growth relation.

Though the followed approach for the estimation of ΔK may be troublesome, one can still argue that the NR equation is well established and that the observed crack shape was such that the NR SIF model was applicable. Assuming that the beach marks were clearly distinguishable

and precisely measured, their method *could*, in this best case scenario, give usable ΔK values.

However, after breakthrough, the authors used their own, non-validated and newly developed SIF formula to estimate $\hat{C}$ and $\hat{m}$. For one of their test materials, SS 41 steel, they actually found a considerably higher value for $\hat{m}$ in the Paris relation after breakthrough but this was "*thought to be attributable to the fact that the [...] sample of the SS 41 steel suffered an overall general yielding prior to penetration of the crack*" [23]. Though this could indeed be an explanation, they did not consider the option that their formula for the SIF might not be a proper one to be used. For the other material used in their experiments, high tension steel, they did fit the data into a single Paris relation and concluded that it was therefore appropriate to predict crack growth and propagation with their new formula. Because the calculated and measured results agreed fairly well, they also concluded that "*[...] the behaviour of fatigue cracks after through-thickness can be evaluated quantitatively using the stress intensity factor assessment method proposed in this report.*" [23].

Their conclusion is highly questionable: fitting a line through data-points does *not* prove that their SIF model is correct, it merely shows that the parameters of a fitted curve can be adjusted in such a way that the data-points on a graph can be reasonably well approximated by a single line. In other words, $\hat{C}$ and $\hat{m}$ are *chosen* such that the NR and AFNTO model accurately predict crack growth and propagation. The growth rate from actual measurements ($\Delta c/\Delta N$) is attached to a value ΔK from the NR or AFNTO SIF, which in its turn is later used to estimate this growth or propagation. It is therefore no surprise that the AFNTO model performs well for crack propagation estimations but this could equally well be caused by the chosen values for $\hat{C}$ and $\hat{m}$. It does not yet say anything about the validity of the AFNTO SIF model.

5-2   Conclusions I: Estimating surface crack growth and breakthrough shape

The first aim of this research, developing a numerical calculation scheme to predict surface crack growth more accurately compared to existing numerical methods, can now be assessed by answering the following questions:

1-a) To what extent does the numerical calculation scheme developed in this research solves *perceived* shortcomings of other methods?

1-b) How does this numerical calculation scheme perform in comparison with experimentally determined results of the breakthrough shape?

1-c) What is the influence on the accuracy of the estimations for crack shape and growth when the SIF is not only estimated by the NR solution, but also by the Wang solution in the range of $(0.6 \leq a/t < 0.95)$?

1-a   The 'other methods' in 1-a, refer to numerical calculation schemes that were briefly mentioned in the Chapter 1, i.e. Chapter 8 of [6] and [8, 7, 22, 25]. Because these methods are only described in a broad outline, the real limitations or inaccuracies remain unidentified, hence the wording '*perceived* shortcomings' is preferred.

The numerical scheme of Chapter 2 solves the issue of selecting values for the 'knowns' to solve the 'unknowns' in two dimensional crack growth models. Experimental results of [19] indicate that in most practical cases the crack can grow up to almost 100% of the thickness. With this information, it is convenient to divide the remaining cross section in depth direction $a_{bb} - a_1$ into a large number of increments Δa_k to serve as a known to solve the unknowns Δc_k and ΔN_k. To solve both unknowns, an extra requirement is necessary: $\Delta N_{a,k} = \Delta N_{c,k}$. One of the shortcomings of the other methods is that they require that ΔN_k is known in advance as well, but this number of cycles is difficult to estimate beforehand. Selecting a small ΔN_k may result in a large number of calculation steps. On the other hand, a large ΔN_k results in large increments $\Delta a_k, \Delta c_k$ and this weakens the assumption that the increment is small enough to assume that $\Delta K_{A,k}$ and $\Delta K_{C,k}$ remain constant. The current numerical scheme limits the selection of knowns and the build-in checks verify that the selected input results in an outcome that is within pre-set limits for errors.

Besides this assistance with the selection of input values, the current numerical model offers some other benefits. One of the options is the 2-point integration. This option does not only averages between the growth rates at the beginning and end of the increment, but also iteratively finds new values for $\Delta K_{A,k}, \Delta K_{C,k}$ that are consistent with the new values of a_k, c_k. Other options include a logarithmically in- or decreasing spacing of Δa_k or the use of a small scale plasticity correction factor.

1-b The accuracy of the prediction depends on much more than just the numerical scheme. Selecting an appropriate crack growth relation and determining the material constants in these empirical relations make the difference between a reliable prediction or an entirely inadequate estimate of the number of load cycles up to breakthrough.

On the other hand, it was found that the predictions of the crack shape at breakthrough is in most cases not much affected by the growth relation or material constants. In comparison with the breakthrough shapes from experiments that were reported in the literature, the predictions of the numerical models were reasonably accurate. The best estimates are found for the model with only the NR SIF equation and the same material constants in respectively length and depth direction. The difference with two other models that use the NRC is small. The number of experiments is limited so no firm conclusions should be drawn from these results yet. It does show, however, that the numerical calculation model can be used to roughly estimate the shape at breakthrough.

As said, the growth model and material parameters do affect the prediction of load cycles and the growth during and up to breakthrough to a large extent. The material values $\hat{C}, \hat{m}$ and the used crack growth model were taken from the literature and used as an input in the numerical model. As highlighted in the previous section, the reliability of these values is open to doubts, but presuming they were correct, it is found that using a different value for the growth rate in length direction, i.e. the NRC, improved the accuracy of the estimated number of load cycles versus crack length. The use of the Wang SIF equation did not improve the results, but this could equally well be attributed to the applied method to obtain $\hat{C}, \hat{m}$.

It is known that the rolling direction of the material and other inhomogeneities affect the growth rate of the crack. An interesting question would be if the results could be further enhanced by using different growth models in length and depth direction that are based on actual measurements instead of the empirical NRC. The NRC is only a roughly estimated

correction from crack growth data of a broad range of materials. In absence of these tests, it is recommended to use the NRC.

1-c No evidence is found that the Wang formula is more accurate than the sole use of the NR SIF equation, despite the finding that the SIFs from current FE analysis are closer to the SIF values obtained by the FEM of Wang and Isida *et al.*. The effect was negligible when considering the estimated number of load cycles versus crack growth. Although again an explanation can be sought in the applied method to obtain the material values, neither the largely $\hat{C}, \hat{m}$ independent breakthrough shape predictions did improve with the Wang solution. Only the combination with an NRC gave reasonable results. Overall, considering the experimental data of this research, no clear advantages of using the Wang equation for deep surface cracks have been found.

5-3 Conclusions II: Estimating crack propagation after wall penetration

2) How do the newly FE-derived SIF solution and two existing methods that consider a crack after wall penetration perform in comparison with experimentally obtained data?

Unfortunately, due to the used methods to obtain $\hat{C}, \hat{m}$, no firm statements or conclusions can be drawn. As said, the values of $\hat{C}, \hat{m}$ are such that, regardless of the actual accuracy of the model, the results will be biased towards the AFNTO SIF model. A slight modification of $\hat{C}, \hat{m}$ affects the results considerably. This means that these reported material values are neither suitable as provisional, educated guesses. Because of this, neither model can be recommended or rejected at this point. Instead of a comparison with experimental data, which would have been much more relevant when making recommendations for a LBB assessment, all that remains is therefore a comparison on how the models perform relative to each other.

The fixed a/c model predicts the highest crack growth rate at the front and back side of the specimens. It predicts that the crack reaches criticality within much less cycles than the AFNTO and FEM solutions. Presuming that the reported $\hat{C}, \hat{m}$ are more or less realistic, it would also mean that the growth rate is overestimated by a factor two or more in most cases. When taking into account that the *mean* material values are used in the current predictions whereas for LBB calculations often design values will be used, this will lead to an unnecessary cautious estimate that is perhaps not viable from an economical perspective. For leakage rate predictions, which depend on the crack length at the back side, it is the other way around: the crack is not leaking as much as estimated and will likely get detected later than predicted. Similar conclusions can be drawn for the FEM model, though to a lesser extent. The AFNTO SIF equations tend to estimate c_2 the best. To emphasise: this is *only* true if the crack growth constants happen to be accurate.

In absence of any official recommendations regarding crack shape propagation, it is probably safe - not to say very safe - to use the fixed a/c model for the determination of crack propagation and herewith for estimations of the number of cycles before the crack reaches criticality. It is furthermore advised to use the AFNTO SIF model for leakage rate predictions, as this model is likely to give a safer estimate for the crack opening area at the back of the wall.

5-4   Recommendations for further research

It is highly recommended to carry out new experiments in a different test set-up so that these three solutions can be evaluated for their performance on crack propagation estimates. It appears that the fixed a/c model overestimates the actual growth rate. New experiments can provide a reliable crack propagation rate estimate, which in its turn can identify a model that predicts crack propagation both safe and economically viable.

It is recommended that these new experiments are carried out with large, rectangular, Moss tank-aluminium test samples under a temperature that is -163 °C so that it resembles the actual environment. The crack growth relation should be obtained with a standardised test sample and testing procedure, preferably with different test samples that correspond with the depth and length direction of the crack, for any likely orientation a crack may have in a spherical tank. It is furthermore recommended that both tensile and bending stresses are applied and that the amplitude of the stress range remains constant during the test. The same test configuration must be repeated at least a couple of times to determine the variability of the experiments. With this experimental data it can then be assessed which - if any - of the three suggested models give a reasonable estimate. Once this is known, other influencing factors such as multi-axial loading, the presence of welds or the curvature of the plates can be further researched and added to the models.

Fracture mechanics

A material fractures when the work applied to it is high enough to overcome the attractive forces between the atomic bonds. When this atomic bond force is exceeded, the fracture energy is converted into energy to create two new surfaces. When predicting the fracture forces at atomic bond level, all sorts of micro and macro flaws act as stress raisers, therefore global stresses in a material are ill-suited to predict when a material will break. An important part of fracture calculations is therefore the analysis of flaws and local stresses.

A-1   Stress intensities

Figure A-1 shows an arbitrarily shaped the crack surface with its local coordinate system around the crack-tip. Global coordinates are indicated by $\{X, Y, Z\}$. Very close to the crack front the curvature of the crack is negligible and the three-dimensional crack front may be approximated by a two-dimensional coordinate system. The stresses around the crack-tip are expressed in polar coordinates $\{r, \theta\}$ and a stress intensity factor K accounting for the geometry of the crack and cracked body. The stress field depends on the fracture mode. Three fracture modes (Figure A-2) can be distinguished: an opening Mode I where the crack opens orthogonal to the crack face, a sliding Mode II where the crack faces slide in opposite x-direction and a tearing Mode III, where the crack faces slide relative from each other in y-direction. For Mode I, the stress fields are given below, where the higher terms are omitted

$$\sigma_x = \frac{K_I}{\sqrt{2\pi r}} \left[\cos\frac{\theta}{2} \left(1 - \sin\frac{\theta}{2} \sin\frac{3\theta}{2} \right) \right] \tag{A-1a}$$

$$\sigma_y = 0 \quad \text{(plane stress)} \quad ; \quad \nu(\sigma_x + \sigma_z) \quad \text{(plane strain)} \tag{A-1b}$$

$$\sigma_z = \frac{K_I}{\sqrt{2\pi r}} \left[\cos\frac{\theta}{2} \left(1 + \sin\frac{\theta}{2} \sin\frac{3\theta}{2} \right) \right] \tag{A-1c}$$

$$\sigma_{xz} = \frac{K_I}{\sqrt{2\pi r}} \cos\frac{\theta}{2} \sin\frac{\theta}{2} \cos\frac{3\theta}{2} \tag{A-1d}$$
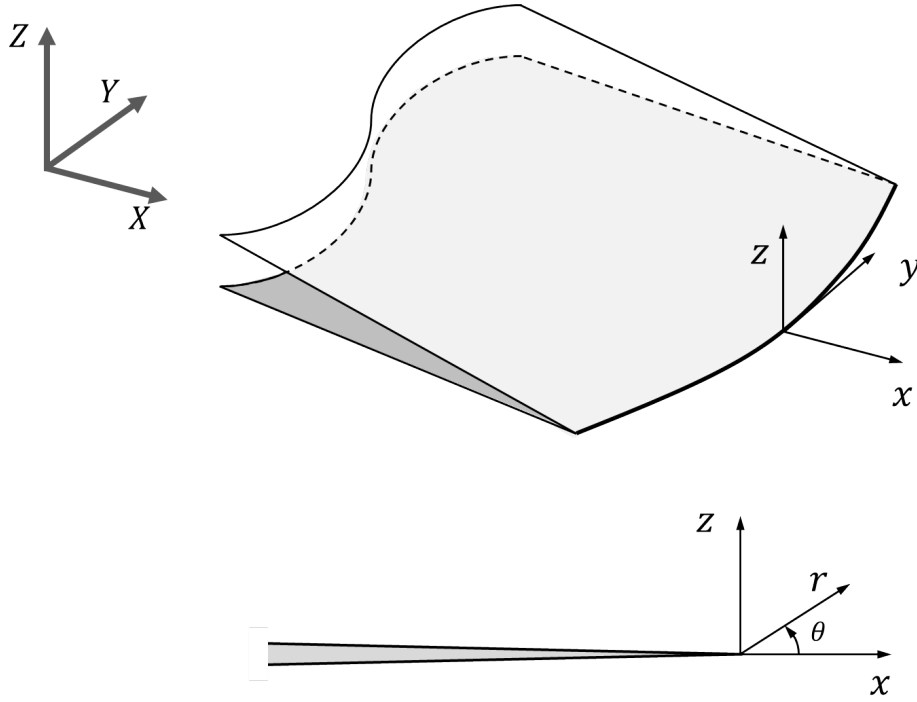
Figure A-1: Local $\{x, y, z\}$ and global $\{X, Y, Z\}$ coordinate system for an arbitrary crack face **(top)** in three dimensions, **(bottom)** in two dimensions

The displacements u are given by

$$u_x = \frac{K_I}{2\mu}\sqrt{\frac{r}{2\pi}}\left[\cos\frac{\theta}{2}\left(\kappa - 1 + 2\sin^2\frac{\theta}{2}\right)\right] \tag{A-2a}$$

$$u_z = \frac{K_I}{2\mu}\sqrt{\frac{r}{2\pi}}\left[\sin\frac{\theta}{2}\left(\kappa + 1 - 2\cos^2\frac{\theta}{2}\right)\right] \tag{A-2b}$$

where

$$\mu = \frac{E}{2(1+\nu)}$$
$$\kappa = \frac{3-\nu}{1+\nu} \qquad \text{(plane stress)}$$
$$\kappa = 3 - 4\nu \qquad \text{(plane strain)}$$

μ is the shear modulus, ν Poisson's ratio and κ a parameter introduced to simplify the equations. The derivation of Eq. (A-1) can be found in several works on Fracture Mechanics, see for instance [30, 31].

Only Mode I is considered in this research. Not only is this mode is the most damaging of all three modes, but also is the structure under consideration, a spherical LNG tank, primarily loaded by stresses normal to the crack face. The commonly used subscripts for the SIF K_I, K_{II}, K_{III} to indicate the fracture mode are therefore omitted and all K refer to K_I.
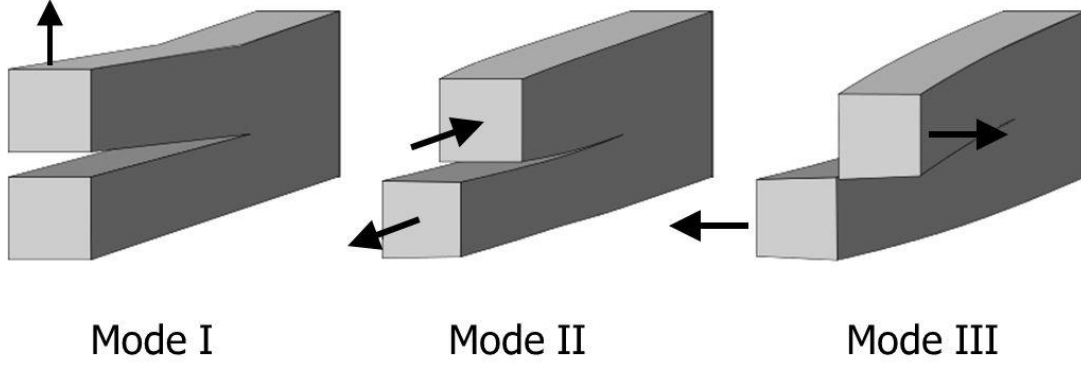
Figure A-2: Mode I, II and III

A-2 Energy release rate and the J integral

As previously mentioned, fracture of materials can be explained from an energy perspective. A useful concept for engineering problems is to express the energy available for incrementing a crack as the *energy release rate* that is defined as

$$\mathcal{G} = -\frac{d\Pi}{d\mathcal{A}} \tag{A-3}$$

where $d\Pi$ is the change in potential energy with respect to the increase of crack area $\mathcal{A}$. Ignoring dissipation and kinetic energy, the potential energy Π is defined as

$$\Pi = \mathcal{U} - \mathcal{F} \tag{A-4}$$

where $\mathcal{U}$ is the elastic strain energy and $\mathcal{F}$ is the work done by external forces. To illustrate the use of $\mathcal{G}$, consider the loaded, cracked plate of Figure A-3, where $a \ll W$. First assume that the plate is loaded by a fixed load P. The change in potential energy in this plate is

$$d\Pi = d\mathcal{U} - d\mathcal{F} = \frac{1}{2}Pdu - Pdu = -\frac{1}{2}Pdu \tag{A-5}$$

The crack area $\mathcal{A} = at$ and assuming that t is constant, inserting Eq. (A-5) in Eq. (A-3) gives

$$\mathcal{G} = -\frac{1}{t}\left(\frac{d\Pi}{da}\right)_{P_{fixed}} = \frac{P}{2t}\left(\frac{du}{da}\right)_{P_{fixed}} \tag{A-6}$$

Next, it is assumed that the displacement is fixed

$$d\Pi = d\mathcal{U} - d\mathcal{F} = \frac{1}{2}udP - 0 = \frac{1}{2}udP \tag{A-7}$$

Inserting Eq. (A-7) in Eq. (A-3) results in

$$\mathcal{G} = -\frac{1}{t}\left(\frac{d\Pi}{da}\right)_{u_{fixed}} = -\frac{u}{2t}\left(\frac{dP}{da}\right)_{u_{fixed}} \tag{A-8}$$
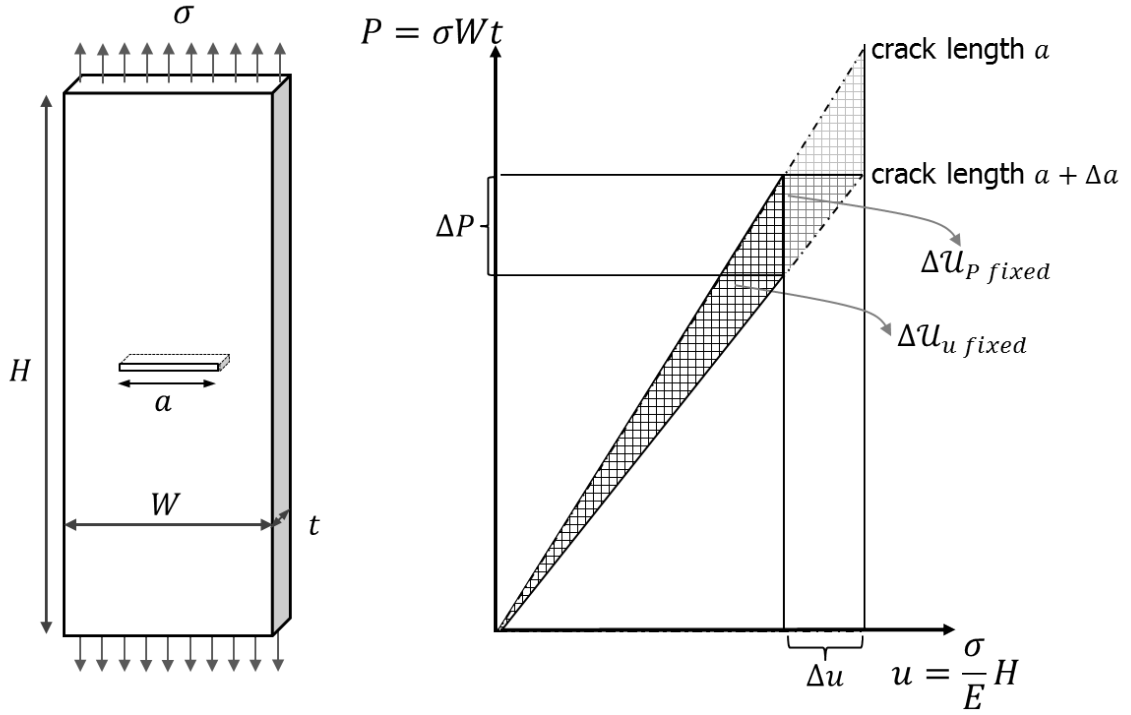
Figure A-3: Relation between load P and elongation u for a linear elastic materials for a plate with a crack

When rewriting Eq. (A-6) and Eq. (A-8) in terms of the compliance $\mathcal{C} = u/P$, it is clear that both expressions are equal and can be expressed as

$$\mathcal{G} = \frac{P^2}{2t}\left(\frac{\mathrm{d}\mathcal{C}}{\mathrm{d}a}\right) \tag{A-9}$$

By using Eq. (A-1) for the stresses and displacements around the crack-tip, it can be shown (e.g. [30, 32]) that $\mathcal{G}$ is related to K by

$$\mathcal{G} = \frac{K^2}{E'} \tag{A-10}$$

with $E'=E$ for plane stress and $E' = E/(1 - \nu^2)$ for plane strain conditions. For non-linear elastic materials the same relation holds but $\mathcal{G}$ is then replaced by J in Eq. (A-10)

$$J = \frac{K^2}{E'} \tag{A-11}$$

For (non)-linear elastic-plastic materials J may be used as well. The energy release rate is then expressed in the form of a *J-contour integral*, here presented in two-dimensions as shown in Figure A-4

$$J = \int_\Gamma \left(\mathcal{W}n_x - T_i\frac{\partial u_i}{\partial x}\right)\mathrm{d}\Gamma \tag{A-12}$$

where u_i are the displacements in x, z-direction. The strain energy density $\mathcal{W}$ and the components of the traction vector T_i are defined as

$$\mathcal{W} = \int_0^{\epsilon_{ij}} \sigma_{ij} \mathrm{d}\epsilon_{ij}$$
$$T_i = \sigma_{ij} n_j$$

where i, j refer to the components in x, z-direction, ϵ to the strain and n_i are the normal vector components in x, z-direction.

The J-integral is contour independent which means that the solution is not affected by the distance of Γ from the crack-tip, which makes this definition of the strain energy release rate well-suited to be used within finite element models.
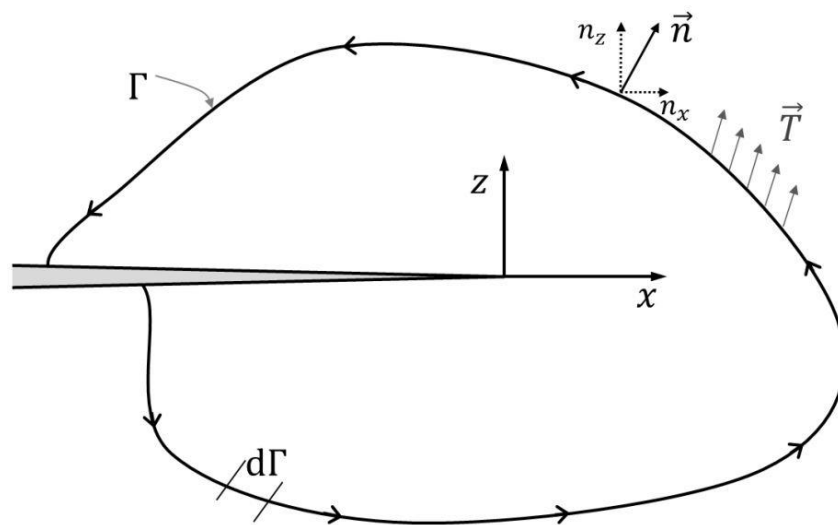
Figure A-4: Arbitrary contour around a crack-tip

A-3 Linear and non-linear fracture mechanics

Although fracture mechanics can be used for non-linear and/or elasto-plastic material models, the calculations simplify considerably when a LEFM model is applied. However, a simple solution to incorporate some sort of plasticity effects can be used within an LEFM model.

Small scale plasticity correction For very sharp cracks, i.e. $r \to 0$ in Eq. (A-1), the stresses become infinite around the crack-tip. In reality, materials are never fully linear-elastic and a small plastic zone around the crack-tip limits the maximum stress to σ_y, see Figure A-5. For the high strength steel used in the experiments, the radius of the plastic zone r_p is in the order of 0.1 mm or smaller, much smaller than a, c, indicating that a linear-elastic calculation is a reasonable assumption. Only the first couple of cycles immediately after breakthrough, when c_2^* is still very small and the ligament around the crack-tip very thin, r_p is large compared to the crack length. Since this only occurs during a few cycles, all stages of crack development are modelled by LEFM.
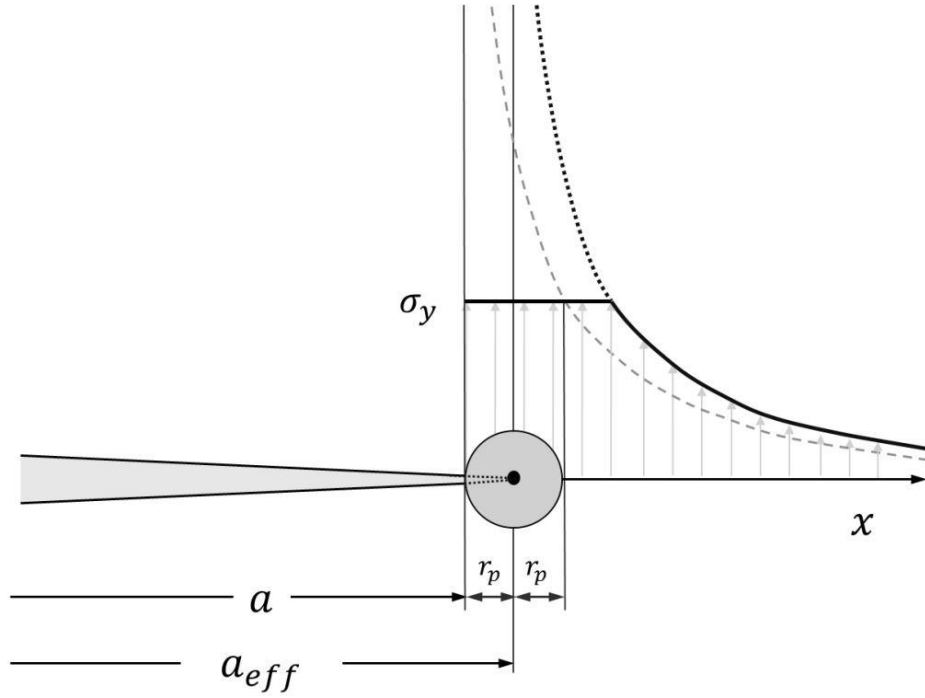
Figure A-5: Small scale plasticity correction

This small plastic zone around the crack-tip acts as a stress raiser. This raised stress level can be incorporated into LEFM calculations by using K_{eff} by virtually extending the crack-tip to the centre of the plastic zone $a_{eff} = a + r_p$. Eq. (1-1) then becomes

$$K_{eff} = Y\,(a_{eff})\sigma\sqrt{\pi a_{eff}} \tag{A-13}$$

For most geometries, finding K_{eff} involves an iterative calculation but for two geometries a closed-form solution is available: the embedded elliptical flaw and the straight centre crack in an infinite sheet. As an assumption, the plasticity correction of the embedded elliptical flaw is used for the semi-elliptical surface crack as well. K_{eff} is then obtained by substituting Q (Eq. (3-6)) in either the NR or Wang solution by

$$Q_{PC} = Q - 0.212\left(\frac{\sigma}{\sigma_y}\right) \tag{A-14}$$

For the crack after breakthrough, K_{eff} is calculated with the closed-form solution of a straight centre crack in an infinite sheet

$$K_{eff} = \frac{K}{\sqrt{1 - \frac{1}{2}(\sigma/\sigma_y)^2}} \tag{A-15}$$

A-4   Relation between the SIF and crack growth

Crack growth and/or propagation rates (hereafter: 'crack growth rates') depend on both a general crack size a and the applied stress range $\Delta\sigma$. It was observed by Paris *et al.*

(cited in [6]) that crack growth rates of specimens loaded by different ranges of cyclic stresses exhibited similar growth rates, but these overlapping growth rates occurred at different crack lengths. Paris *et al.* introduced the idea of relating ΔK to the growth rate. It was found that specimens with the same ΔK had a similar $\mathrm{d}a/\mathrm{d}N$. Growth rates depend on both the severity of the stress distribution around a crack-tip and the difference between σ_{min} and σ_{max}, so it was found that crack growth can be conveniently expressed as a relation between $\mathrm{d}a/\mathrm{d}N = f\left(K_{max}, K_{min}\right)$. This relation can also be expressed in terms of $\mathrm{d}a/\mathrm{d}N = f\left(\Delta K, R\right)$ because $\Delta K = K_{max} - K_{min}$ and $R = K_{min}/K_{max}$. Because R is not always explicitly used as a variable in crack growth relations but the *function* does depend on R, the general form of the crack growth relation is expressed as

$$\frac{\mathrm{d}a}{\mathrm{d}N} = f_R(\Delta K) \tag{A-16}$$

Three regions, shown in Figure A-6, can be distinguished: a threshold region, a Paris region and a stable tearing crack growth region. For stress intensities approaching the ΔK_{th} value, the crack growth becomes increasingly small, and for $\Delta K < \Delta K_{th}$ it is assumed that a macro crack, i.e. a crack having a size of at least 1 mm, does not propagate any further. This ΔK_{th} is an experimentally determined value, depending on the material as well as the load ratio. Because this threshold value is determined by an obviously time restricted test, in reality 'non-propagating' corresponds with a very small growth rate of the order of 10^{-10} m/cycle. A threshold value only applies to macro cracks. On a micro-scale, cracks can grow even below ΔK_{th} as discussed in chapter 8 of [6]. By extrapolation of the Paris curve below the threshold region a conservative estimation can be obtained.

The interval where the growth is approximately proportional to a power function is referred to as the Paris region, after the relation described by Paris and Erdogan [27]

$$\frac{\mathrm{d}a}{\mathrm{d}N} = \hat{C}(\Delta K)^{\hat{m}} \qquad (\Delta K_{th} \ll \Delta K \ll K_{Ic}) \tag{A-17}$$

where $\hat{C}$ and $\hat{m}$ are constants that depend on R and many other factors. It is important to stress that 'material constants' do not cover the full meaning behind $\hat{C}$ and $\hat{m}$ in the Paris relation. They depend not only on the chemical composition of the material, but on a wide range of influence factors, such as temperature, fabrication process, rolling direction and grain size. Even material with the same properties from the same manufacturer, can still display different fatigue growth properties, as discussed in Chapter 8 of [6].

For values of ΔK in the stable tearing region, the crack grows increasingly fast but still in a stable fashion, up to the point critical stress intensity K_c or K_{Ic} is reached. An alternative crack growth relation that accounts for this asymptotic behaviour towards criticality and also incorporates R is proposed by Forman *et al.* [33] as

$$\frac{\mathrm{d}a}{\mathrm{d}N} = \frac{\hat{C}(\Delta K)^{\hat{m}}}{(1 - R)K_c - \Delta K} \qquad (R \geq 0) \tag{A-18}$$

One should keep in mind that relations like Eq. (A-17) and (A-18) are in fact no more than curve fittings between data points. In order to make a better fit to the data, K_c in Eq. (A-18) is not necessarily the same as a K_c found in fracture toughness experiments. Furthermore, $\hat{C}$ and $\hat{m}$ are found by fitting the data to a specific crack growth relation and may not used
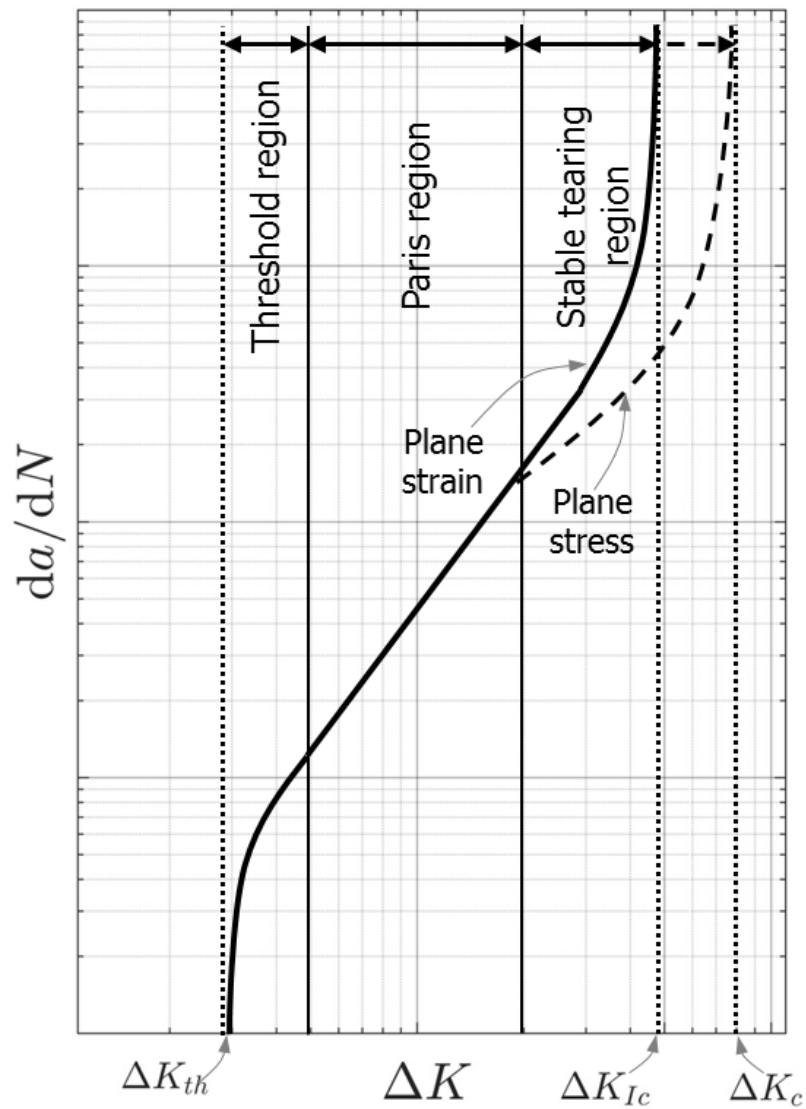
Figure A-6: Crack growth rate as a function of ΔK

in other relations. Given their empirical nature, many variations on Eq. (A-17) and (A-18) exist, see for instance section 8.2.3 of [2] and [34]. Even though none of these relations are justified by a physical laws, they have proven to be useful to estimate crack growth.

<div align="right">

Appendix B

</div>

Stress intensity factor solutions

The nominal stress distribution as shown in Figure B-1 applies to all SIF solutions. The nominal stress is uniform in Y-direction.
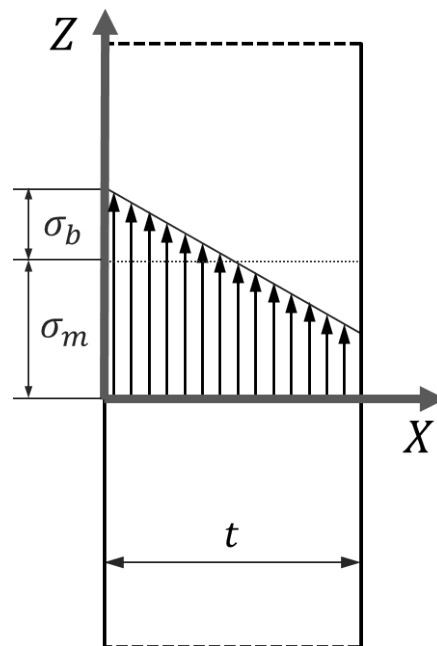
Figure B-1: Nominal stress distribution for all SIF solutions.

B-1   Newman-Raju solution for a semi-elliptical surface crack

Source: [8]
Accuracy: For $(a/t) < 0.8$ and $0 \leq (a/c) \leq 1.0$: better than 5.0 % in comparison with
            FE solutions.

See Figure B-2 and B-3 for the definitions. The SIF is estimated as

$$K = (\sigma_m + H\sigma_b)\sqrt{\frac{\pi a}{Q}} \cdot Y\left(\frac{a}{t}, \frac{a}{c}, \frac{c}{W}, \varphi\right) \tag{B-1}$$

for $0 \leq (a/t) < 1.0$; $(c/W) < 0.5$ and $0 \leq \varphi \leq \pi$. The shape factor Q for an elliptical crack in Eq. (B-1) is approximated by

$$Q = \begin{cases} 1 + 1.464\left(\dfrac{a}{c}\right)^{1.65} & \left(\dfrac{a}{c}\right) \leq 1 \\ \left[1 + 1.464\left(\dfrac{a}{c}\right)^{-1.65}\right]\left(\dfrac{a}{c}\right)^2 & \left(\dfrac{a}{c}\right) > 1 \end{cases} \tag{B-2}$$
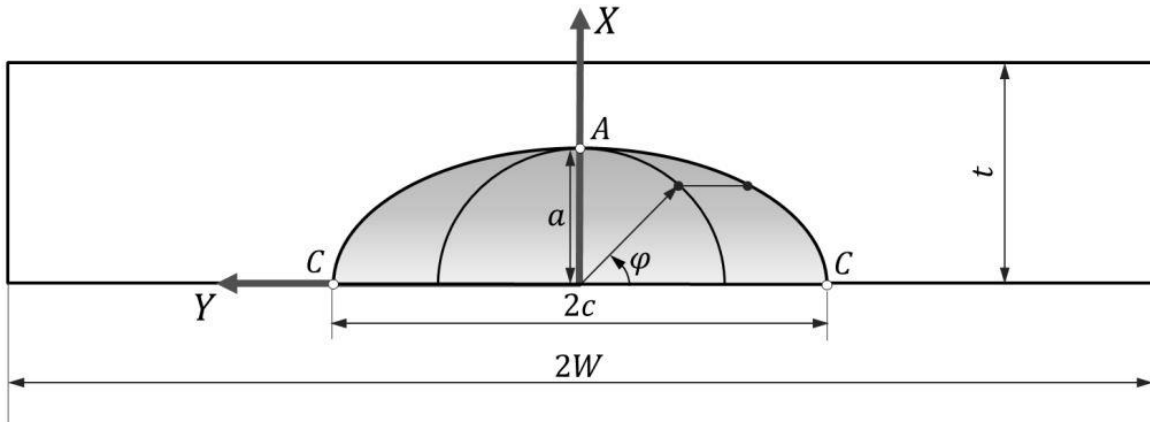
Figure B-2: Semi-elliptical surface crack

Function Y in Eq. (B-1) is given as

$$Y = \left[M_1 + M_2\left(\frac{a}{t}\right)^2 + M_3\left(\frac{a}{t}\right)^4\right] f_\varphi g f_w$$

where

$$M_1 = 1.13 - 0.09\left(\frac{a}{c}\right)$$

$$M_2 = -0.54 + \frac{0.89}{0.2 + (a/c)}$$

$$M_3 = 0.5 - \frac{1.0}{0.65 + (a/c)} + 14\left(1.0 - \frac{a}{c}\right)^{24}$$

$$g = 1 + \left[0.1 + 0.35\left(\frac{a}{t}\right)^2\right](1 - \sin(\varphi))^2$$

where φ is the parametric angle of the ellipse and f_φ is the analytically derived function for an elliptical crack in an infinite solid given as

$$f_\varphi = \left[\left(\frac{a}{c}\right)^2 \cos(\varphi)^2 + \sin(\varphi)^2\right]^{1/4} \tag{B-3}$$
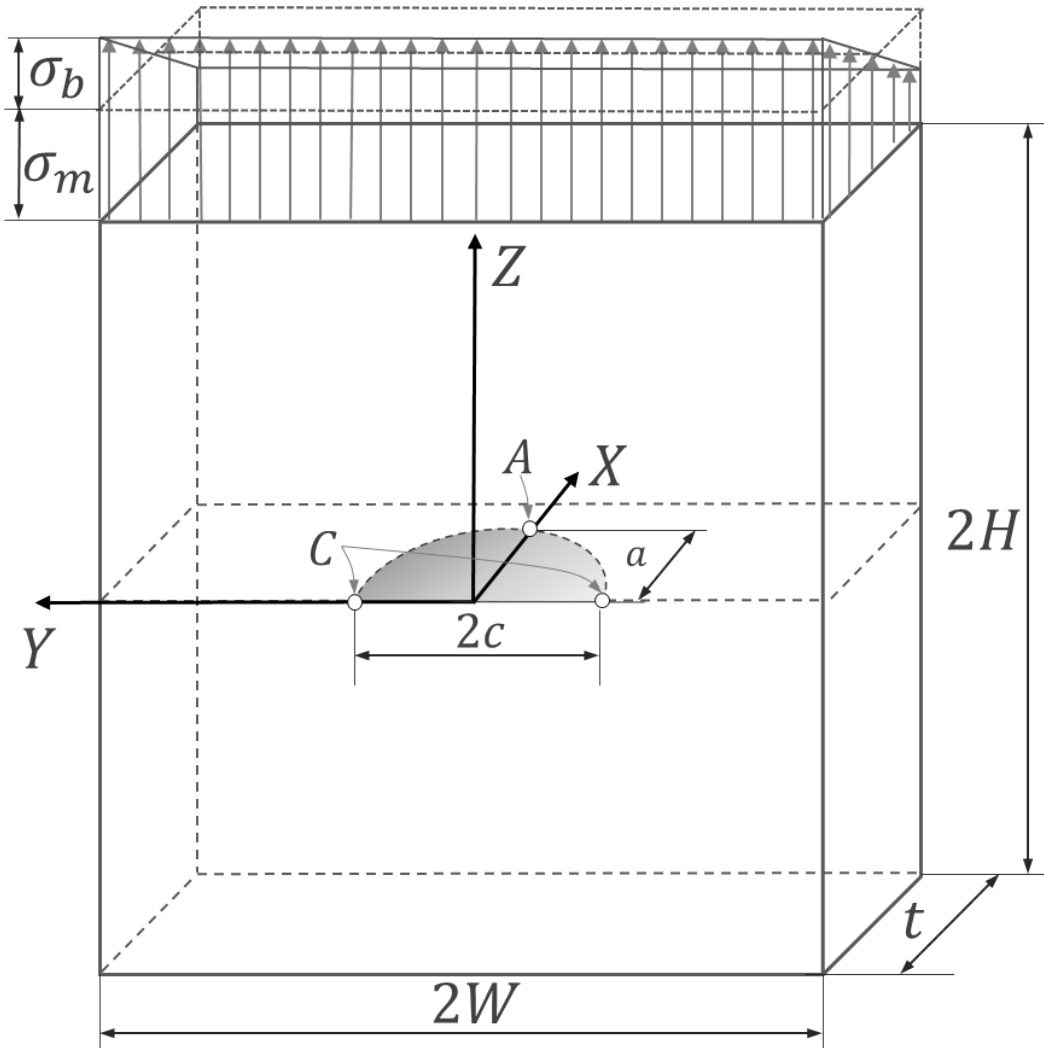
Figure B-3: Definitions for a semi-elliptical surface crack in a finite plate

The correction for a geometry with a finite width is given as

$$f_w = \left[\cos \left(\frac{\pi c}{2W} \sqrt{\frac{a}{t}} \right) \right]^{-1/2} \tag{B-4}$$

Function H in Eq. (B-1) is expressed as

$$H = H_1 + (H_2 - H_1) \sin(\varphi)^p$$

where

$$p = 0.2 + \frac{a}{c} + 0.6 \frac{a}{t}$$

$$H_1 = 1 - 0.34 \left(\frac{a}{t} \right) - 0.11 \frac{a}{c} \left(\frac{a}{t} \right)$$

$$H_2 = 1 + G_1 \left(\frac{a}{t} \right) + G_2 \left(\frac{a}{t} \right)^2$$

with

$$G_1 = -1.22 - 0.12 \left(\frac{a}{c} \right)$$

$$G_2 = 0.55 - 1.05 \left(\frac{a}{c} \right)^{0.75} + 0.47 \left(\frac{a}{c} \right)^{1.5}$$

B-2   Wang solution for a deep semi-elliptical surface crack

Source: [18]

Accuracy: For $0.6 \leq (a/t) \leq 0.95$ and $0.05 \leq (a/c) \leq 2.0$: better than 2.0 % in
comparison with FE solutions.

The SIF can be found through

$$K = \int_0^a \sigma(x) m(x, a) \mathrm{d}x \tag{B-5}$$

in which the expression for a approximate weight function according to Glinka and Shen [15]
for the deepest point of the crack is given as

$$m_A(x, a) = \frac{2}{\sqrt{2\pi(a-x)}} \left[1 + M_{1A} \left(1 - \frac{x}{a} \right)^{1/2} + M_{2A} \left(1 - \frac{x}{a} \right) + M_{3A} \left(1 - \frac{x}{a} \right)^{3/2} \right] \tag{B-6}$$

and for the surface points C it changes to

$$m_C(x, a) = \frac{2}{\sqrt{\pi x}} \left[1 + M_{1C} \left(1 - \frac{x}{a} \right)^{1/2} + M_{2C} \left(1 - \frac{x}{a} \right) + M_{3C} \left(\frac{x}{a} \right)^{3/2} \right] \tag{B-7}$$

Any stress distribution can be inserted in Eq. (B-5). The constants[1] in Eq. (B-6) are deter-
mined as

$$M_{1A} = \frac{\pi}{\sqrt{2Q}} (4Y_0 - 6Y_1) - \frac{24}{5}$$

$$M_{2A} = 3$$

$$M_{3A} = 2 \left(\frac{\pi}{\sqrt{2Q}} Y_0 - M_{1A} - 4 \right)$$

where Q is the same as in B-2. Y_0 and Y_1 are given as

$$Y_0 = B_0 + B_1 \left(\frac{a}{t} \right)^2 + B_2 \left(\frac{a}{t} \right)^4 + B_3 \left(\frac{a}{t} \right)^6$$

$$Y_1 = A_0 + A_1 \left(\frac{a}{t} \right)^2 + A_2 \left(\frac{a}{t} \right)^4 + A_3 \left(\frac{a}{t} \right)^6$$

---

[1]The equations presented here differ from the original paper. The constants as given in [18] do not result
in their plotted figures. The most likely errors are in constants C_1 and A_0. By changing the signs of constants
-0.009223 in A_0 and + 5.0199 in C_1 the K values are in a normal range and the same as plotted in the paper.

where

$$B_0 = 1.0011 - 0.0769 \left(\frac{a}{c}\right) + 0.0009842 \left(\frac{a}{c}\right)^{-1} + 0.0394 \left(\frac{a}{c}\right)^{2} + 0.001157 \left(\frac{a}{c}\right)^{-2}$$

$$B_1 = -10.5675 + 19.155 \left(\frac{a}{c}\right) + 3.2358 \left(\frac{a}{c}\right)^{-1} - 13.2618 \left(\frac{a}{c}\right)^{2} - 0.2772 \left(\frac{a}{c}\right)^{-2} +$$
$$2.9778 \left(\frac{a}{c}\right)^{3} + 0.006956 \left(\frac{a}{c}\right)^{-3}$$

$$B_2 = 22.7713 - 43.4715 \left(\frac{a}{c}\right) - 6.4663 \left(\frac{a}{c}\right)^{-1} + 30.4802 \left(\frac{a}{c}\right)^{2} + 0.6335 \left(\frac{a}{c}\right)^{-2} -$$
$$6.8711 \left(\frac{a}{c}\right)^{3} - 0.01642 \left(\frac{a}{c}\right)^{-3}$$

$$B_3 = -13.4448 + 27.0787 \left(\frac{a}{c}\right) + 3.6922 \left(\frac{a}{c}\right)^{-1} - 19.2574 \left(\frac{a}{c}\right)^{2} - 0.3930 \left(\frac{a}{c}\right)^{-2} +$$
$$4.3610 \left(\frac{a}{c}\right)^{3} + 0.01042 \left(\frac{a}{c}\right)^{-3}$$

$$A_0 = 0.7857 - 0.6852 \left(\frac{a}{c}\right) - 0.0871 \left(\frac{a}{c}\right)^{-1} + 0.3506 \left(\frac{a}{c}\right)^{2} + 0.009223 \left(\frac{a}{c}\right)^{-2} -$$
$$0.07046 \left(\frac{a}{c}\right)^{3} - 0.0002351 \left(\frac{a}{c}\right)^{-3}$$

$$A_1 = -2.0162 + 2.9982 \left(\frac{a}{c}\right) + 0.8834 \left(\frac{a}{c}\right)^{-1} - 2.0495 \left(\frac{a}{c}\right)^{2} - 0.07842 \left(\frac{a}{c}\right)^{-2} +$$
$$0.4547 \left(\frac{a}{c}\right)^{3} + 0.001778 \left(\frac{a}{c}\right)^{-3}$$

$$A_2 = 2.1751 - 3.8937 \left(\frac{a}{c}\right) - 0.8975 \left(\frac{a}{c}\right)^{-1} + 2.9923 \left(\frac{a}{c}\right)^{2} + 0.1326 \left(\frac{a}{c}\right)^{-2} -$$
$$0.6916 \left(\frac{a}{c}\right)^{3} - 0.003140 \left(\frac{a}{c}\right)^{-3}$$

$$A_3 = 0.6706 - 0.5836 \left(\frac{a}{c}\right) - 0.1854 \left(\frac{a}{c}\right)^{-1} - 0.0175 \left(\frac{a}{c}\right)^{2} - 0.03417 \left(\frac{a}{c}\right)^{-2} +$$
$$0.03872 \left(\frac{a}{c}\right)^{3} + 0.0007787 \left(\frac{a}{c}\right)^{-3}$$

For point C, the constants in Eq. (B-7) are as follows

$$M_{1C} = \frac{\pi}{2\sqrt{Q}}(30F_1 - 18F_0) - 8$$
$$M_{2C} = \frac{\pi}{2\sqrt{Q}}(60F_0 - 90F_1) + 15$$
$$M_{3C} = -(1 + M_{1C} + M_{2C})$$

F_0 and F_1 are given as

$$F_0 = \left[C_0 + C_1 \left(\frac{a}{t} \right)^2 + C_2 \left(\frac{a}{t} \right)^4 + C_3 \left(\frac{a}{t} \right)^6 \right] \sqrt{\frac{a}{c}}$$

$$F_1 = \left[D_0 + D_1 \left(\frac{a}{t} \right)^2 + D_2 \left(\frac{a}{t} \right)^4 + D_3 \left(\frac{a}{t} \right)^6 \right] \sqrt{\frac{a}{c}}$$

where

$$C_0 = 2.1439 - 1.9529 \left(\frac{a}{c} \right) - 0.2288 \left(\frac{a}{c} \right)^{-1} + 1.3968 \left(\frac{a}{c} \right)^2 + 0.02022 \left(\frac{a}{c} \right)^{-2} - $$
$$0.3306 \left(\frac{a}{c} \right)^3 - 0.0006248 \left(\frac{a}{c} \right)^{-3}$$

$$C_1 = -5.0199 + 11.7551 \left(\frac{a}{c} \right) + 2.0923 \left(\frac{a}{c} \right)^{-1} - 10.1262 \left(\frac{a}{c} \right)^2 - 0.2000 \left(\frac{a}{c} \right)^{-2} + $$
$$2.6195 \left(\frac{a}{c} \right)^3 + 0.006486 \left(\frac{a}{c} \right)^{-3}$$

$$C_2 = 2.8767 - 10.0641 \left(\frac{a}{c} \right) - 1.4926 \left(\frac{a}{c} \right)^{-1} + 10.7036 \left(\frac{a}{c} \right)^2 + 0.1577 \left(\frac{a}{c} \right)^{-2} - $$
$$3.0476 \left(\frac{a}{c} \right)^3 - 0.006872 \left(\frac{a}{c} \right)^{-3}$$

$$C_3 = 3.7162 - 5.8901 \left(\frac{a}{c} \right) + 0.004638 \left(\frac{a}{c} \right)^{-1} + 2.3415 \left(\frac{a}{c} \right)^2 + 0.004395 \left(\frac{a}{c} \right)^{-2} - $$
$$0.2057 \left(\frac{a}{c} \right)^3 + 0.001692 \left(\frac{a}{c} \right)^{-3}$$

$$D_0 = 2.0778 - 2.0802 \left(\frac{a}{c} \right) - 0.2559 \left(\frac{a}{c} \right)^{-1} + 1.4577 \left(\frac{a}{c} \right)^2 + 0.02443 \left(\frac{a}{c} \right)^{-2} - $$
$$0.3372 \left(\frac{a}{c} \right)^3 - 0.0007403 \left(\frac{a}{c} \right)^{-3}$$

$$D_1 = -6.9548 + 13.4218 \left(\frac{a}{c} \right) + 2.3860 \left(\frac{a}{c} \right)^{-1} - 10.3911 \left(\frac{a}{c} \right)^2 - 0.2266 \left(\frac{a}{c} \right)^{-2} + $$
$$2.5595 \left(\frac{a}{c} \right)^3 + 0.006981 \left(\frac{a}{c} \right)^{-3}$$

$$D_2 = 8.1685 - 15.9579 \left(\frac{a}{c} \right) - 2.7831 \left(\frac{a}{c} \right)^{-1} + 13.0352 \left(\frac{a}{c} \right)^2 + 0.2760 \left(\frac{a}{c} \right)^{-2} - $$
$$3.3388 \left(\frac{a}{c} \right)^3 - 0.009454 \left(\frac{a}{c} \right)^{-3}$$

$$D_3 = -0.7752 + 0.5602 \left(\frac{a}{c} \right) + 1.0412 \left(\frac{a}{c} \right)^{-1} - 1.1856 \left(\frac{a}{c} \right)^2 - 0.09758 \left(\frac{a}{c} \right)^{-2} + $$
$$0.4606 \left(\frac{a}{c} \right)^3 + 0.004009 \left(\frac{a}{c} \right)^{-3}$$

B-3 Ando, Fujibayashi, Nam, Takahashi and Ogura solution for a semi-elliptical through-thickness crack

Source: [25]
Accuracy: Unknown for the assembled solution Eq. (B-8). Eq. (B-12) and Eq. (B-14) are resp. 0.3% and 0.6% or better in comparison with FE solutions for any η.

A solution for a semi-elliptical through-thickness crack under both bending and membrane stresses was developed by Nam, Ando, Ogura and Matui [25], but the first formula for membrane stresses was found by Ando, Fujibayashi, Nam, Takahashi and Ogura [23], hence the abbreviation 'AFNTO'. This solution also appears in [24, 35, 36].

The SIF is given as follows, with reference to Figure B-4

$$K_C = K_C^m + K_C^b \tag{B-8a}$$

$$K_D = K_D^m + K_D^b \tag{B-8b}$$

where the SIF of the membrane stress is given by

$$K_C^m = \frac{\delta(c_e)}{\delta(c)} \cdot f_w(\eta_1) \cdot \sigma_m \sqrt{\pi c} \tag{B-9a}$$

$$K_D^m = \frac{\delta(c_e)}{\delta(c_2)} \cdot f_w(\eta_2) \cdot \sigma_m \sqrt{\pi c_2} \tag{B-9b}$$

and the SIF of the bending stress by

$$K_C^b = f_w(\eta_1) \cdot \Phi(1) \cdot \sigma_b \sqrt{\pi c} \tag{B-10a}$$

$$K_D^b = f_w(\eta_2) \cdot \Phi(1) \cdot \sigma_b \sqrt{\pi c_2} \tag{B-10b}$$

The crack lengths in Eq. (B-9) and (B-10) are

$$c_e = \sqrt{3c^2 + c_2^2}/2 \tag{B-11a}$$

$$c_2 = c\sqrt{1 - (t/a)^2} \tag{B-11b}$$

The finite width correction for a centre cracked plate is taken from [9] as

$$f_w(\eta) = \frac{1 - 0.5\eta + 0.370\eta^2 - 0.044\eta^3}{\sqrt{1 - \eta}} \tag{B-12}$$

where and $f_w(\eta_1), f_w(\eta_2)$ can be found by substituting η_1 or η_2 respectively in Eq. (B-12), which are defined as

$$\eta_e = c_e/W \tag{B-13a}$$

$$\eta_1 = c/W \tag{B-13b}$$

$$\eta_2 = c_2/W \tag{B-13c}$$

The crack opening displacement is approximated by an FE derived expression as well

$$\delta(c_e) = \frac{4\sigma c_e(1 - \nu^2)}{E} \cdot V(\eta) \tag{B-14}$$
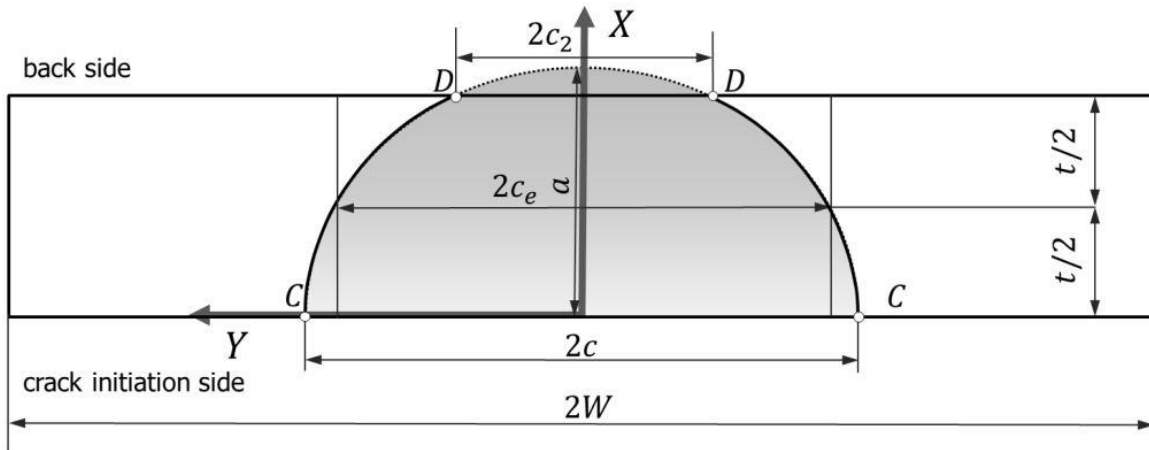
Figure B-4: Definitions for a semi-elliptical through-thickness surface crack

where

$$V(\eta) = -0.071 - 0.535\eta + 0.169\eta^2 + 0.020\eta^3 - 1.071(1/\eta)\ln(1-\eta) \tag{B-15}$$

where $\delta(c), \delta(c_2)$ can be found by substituting $\{c, \eta_1\}$ or $\{c_2, \eta_2\}$ respectively in Eq. (B-14) and (B-15).[2]

The function $\Phi(1)$ in Eq. (B-10) accounts for the influence of the plate thickness. The authors of the AFNTO solution do not specify how they obtained the value of $\Phi(1)$ and only refer to the original source of this function, [29]. Finding the variation of $\Phi(1)$ as a function of the plate thickness is not straightforward as it involves the numerical integration of a Fredholm integral equation of the second kind which can be solved by Liouville - Neumann series. A MATLAB algorithm to solve this type of function can be found online together with the explanation of the algorithm in the accompanying paper [37].[3] However, the kernel of the Fredholm integral consists of a multiplication of two Bessel functions and a third function and attempts to solve this kernel numerically failed because of computation speed issues. The authors of the AFNTO solution did manage to solve this equation somehow, without having access to this algorithm or the computation capacity of a modern day computer. And, somewhat surprisingly given the considerable effort it takes to solve $\Phi(1)$, they made four times the same typo by using $\Phi(I)$ instead of $\Phi(1)$. Nevertheless, to circumvent this elaborate numerical integration process, a curve-fitted approximation of a graph of the normalized thickness versus the bending SIF that is found in [38], is used instead. The approximation is shown in Figure B-5.

B-4   Solution for a centre crack in a finite width-plate

Source: [9, p. 41]
Accuracy: For any c/W: better than 0.1% in comparison with FE solutions.

---

[2]The accuracy is found to be 0.6% or better for a slightly different expression of Eq. (B-15): $V(\eta) = -0.071 - 0.535\eta + 0.169\eta^2 - 0.090\eta^3 + 0.020\eta^4 - 1.071(1/\eta)\ln(1-\eta)$. This variation was published in [9, p.43], the newer third edition of *The stress analysis handbook* than the in the AFNTO articles cited first edition.

[3]http://homepage.divms.uiowa.edu/~atkinson/ftp/Fie.package/
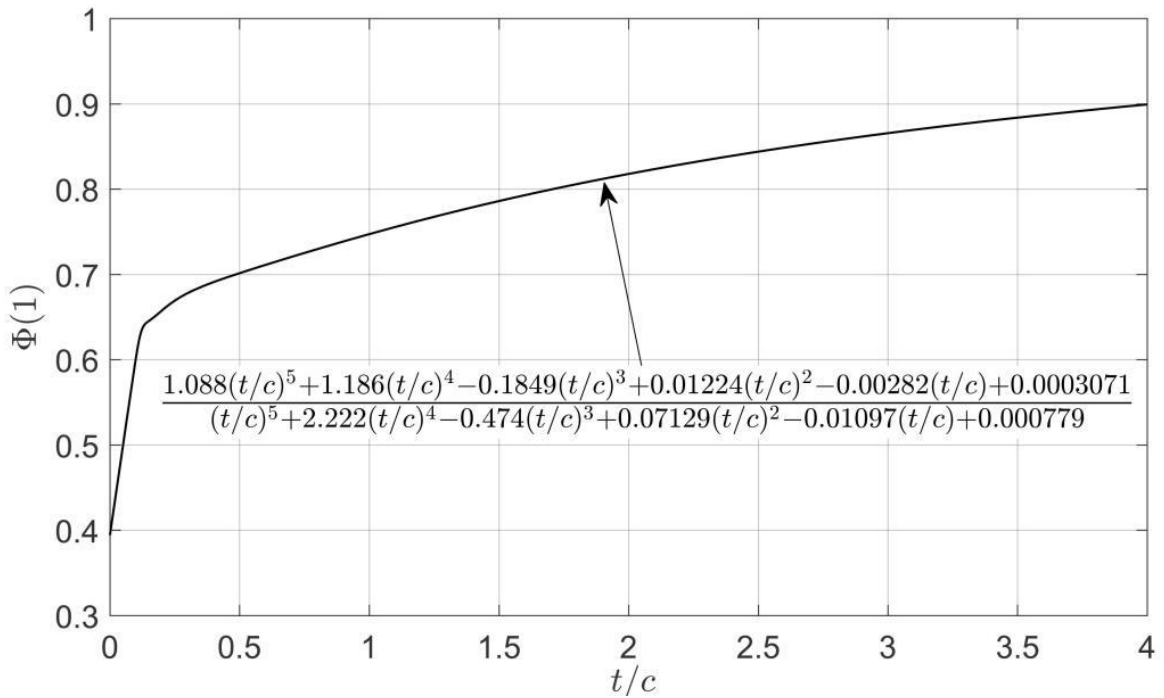
Figure B-5: Approximation of the analytical BCF $\Phi(1)$ for an infinite plate under bending

For a straight centre crack in a finite width-plate (Figure B-6) a solution for f_w, is given by

$$Y = f_w(\eta) = \left(1 - 0.025\eta^2 + 0.06\eta^4\right)\left[\cos\left(\frac{\pi}{2}\eta\right)\right]^{-1/2} \tag{B-16}$$

where $\eta = c/W$.
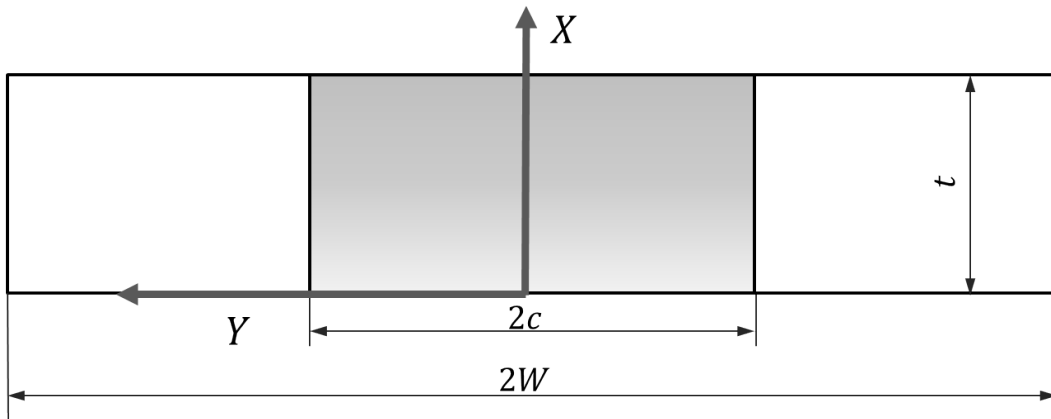
Figure B-6: Definitions for a centre crack in a finite plate

Appendix C

Ansys script for the validation models

Parts of the following code are copied from the verification manual 'VM256' of ANSYS [28]. The example code is for a crack of size $a = 1$.

```
FINISH
/CLEAR
!!!!!!!!!!!!!!!!!!!!!!!!!!!!!!!!!!!!!!!!!!!!!!!!!!!!!!!!!!!!!!!!!!!!
! PLATE WITH COLLINEAR CRACKS, SOLID 186 ELEMENT, Structured mesh
!!!!!!!!!!!!!!!!!!!!!!!!!!!!!!!!!!!!!!!!!!!!!!!!!!!!!!!!!!!!!!!!!!!!
/TITLE, STRESS INTENSITY - WIDE PLATE WITH COLLINEAR CRACKS, A = 1
/PREP7
SMRT,OFF
/COM,*** PLATE WITH COLLINEAR CRACKS IN 3-D USING SOLID186
/COM,
!-------------------
! INPUT VARIABLES
!-------------------
A  = 1          ! HALF CRACK SIZE
W  = 20         ! HALF WIDTH OF THE PLATE
H  = W          ! HALF HEIGHT OF THE PLATE
T  = 0.5        ! PLATE THICKNESS
PI = 3.141592654

EMOD = 30E6     ! YOUNGS MODULUS
NU = 0.3        ! POISSONS RATIO
ET,1,PLANE183   ! PLATE ELEMENT 183 (will be deleted later)
ET,2,186        ! SOLID ELEMENT 186
MP,EX,1,EMOD
MP,NUXY,1,NU

!--------------------
! MODEL GEOMETRY
!--------------------
CSYS,1               ! CYLINDRICAL COORDINATE SYSTEM
K,1,0,0,0
KGEN,6,1,,,,,,10,0 ! 6 x KP AT (0,0,0) NUMBERED 1,11,21,31,41,51
K,6,1
```

```
K,46,1,180
KFILL,6,46,3,16,10 ! FILL LINE BETWEEN NODE 6 AND 46 WITH A NODE AT
                   ! 1/4 OF THE DISTANCE FROM 16 (+10) TO 46
CSYS,0             ! CARTESIAN COORDINATE SYSTEM
KFILL,1,6,4,2,1,3
CSYS,1             ! CYLINDRICAL COORDINATE SYSTEM
KGEN,5,1,5,1,0,180/4,0,10,1,0
CSYS,0             ! CARTESIAN COORDINATE SYSTEM
K,27,0  ,H,0
K,7 ,W-A,0,0
KMODIF,15, 0.82*cos(PI/4),0.82*sin(PI/4),0
KMODIF,35,-0.82*cos(PI/4),0.82*sin(PI/4),0
K,16, A,tan(PI/4),0
K,36,-A,tan(PI/4),0
A,2 ,12, 1,1
A,12,22,11,11
A,22,32,21,21
A,32,42,31,31
A,2 , 3,13,12,
A,12,13,23,22,
A,22,23,33,32,
A,32,33,43,42,
A,3 ,13,14,4,
A,13,23,24,14,
A,23,33,34,24,
A,33,43,44,34,
A,4 ,14,15,5
A,14,24,25,15
A,24,34,35,25
A,34,44,45,35
A,5 ,15,16,6
A,15,25,26,16
A,25,35,36,26
A,35,45,46,36
ASEL,ALL
AGLUE,ALL
L,26,27
L,6,7
LSEL,S,LOC,Y,1
ADRAG,ALL,,,,,,5
ALLSEL,ALL
LSEL,S,LOC,X,A
ADRAG,ALL,,,,,,6
ASEL,ALL
AGLUE,ALL

!---------------------------------------
!  MESH AREAS
!---------------------------------------
NUMMRG, KP,,,,
LSEL,S,LOC,X,A+0.1,W-A-0.1
LESIZE,ALL,,,11,4
LSEL,S,LOC,Y,1.1  ,H-0.1
LSEL,R,LOC,X,-A-0.1,W-A-0.1
LESIZE,ALL,,,11,4
ALLSEL,ALL
LESIZE,53,,,11,1/4
```

```
LESIZE,12,,,2,1
LESIZE,8,,,2,1
LESIZE,41,,,2,1
LESIZE,44,,,2,1
LESIZE,46,,,2,1
LESIZE,48,,,2,1
LESIZE,56,,,2,1
ASEL,ALL
CM,REMOVEAREAS,AREA
MSHKEY,1
AMESH,ALL


!----------------------------------------------
! EXTRUDE TO VOLUME AND MESH
!----------------------------------------------
TYPE,2
ESIZE,,2                 ! Specifies the default number of line divisions
VEXT,all,,,0,0,T         ! Extrude areas to volumes
ALLSEL
ESEL,S,ENAME,,183        ! Select elements of type plane 183
ACLEAR,REMOVEAREAS       ! Delete these elements
ALLSEL


!---------------------------
! DEFINING CRACKTIP
!---------------------------
NSEL,S,LOC,X,0
NSEL,R,LOC,Y,0
CM,CRACKTIP,NODE         ! CRACK TIP NODE COMPONENT


!--------------------------------------------------
! BOUNDARY CONDITIONS
!--------------------------------------------------
ALLSEL,ALL
NSEL,S,LOC,X,-A
DSYM,SYMM,X                     ! SYMMETRY BOUNDARY CONDITIONS
NSEL,S,LOC,X,0,W
NSEL,R,LOC,Y,0
DSYM,SYMM,Y                     ! SYMMETRY BOUNDARY CONDITIONS
NSEL,S,LOC,X,W-A
DSYM,SYMM,X                     ! SYMMETRY BOUNDARY CONDITIONS


!--------------------------------------------------
! LOADS
!--------------------------------------------------
ALLSEL,ALL
D,ALL,UZ,
ALLSEL,ALL
NSEL,S,LOC,Y,H
SF,ALL,PRES,-1/((A*PI)**0.5)        ! SURFACE PRESSURE
ALLSEL,ALL
FINI
/SOLU


!--------------------------------------------------
! SOLVE SYSTEM AND RETRIEVE K AND J-INTEGRAL DATA
!--------------------------------------------------
```

```
AUTOTS,ON
NSUBST,10
OUTRES,ALL,ALL
CINT,NEW,1                         ! CRACK ID
CINT,TYPE,SIFS                     ! DEFINE CRACK TYPE
CINT,CTNC,CRACKTIP,NODE(-1,0,0)    ! DEFINE CRACK TIP COMPONENT
CINT,NCON,6                        ! NO OF CONTOURS
CINT,SYMM,ON                       ! SYMMETRY ON
CINT,NORM,0,2                      ! CRACK PLANE NORMAL
CINT,LIST
CINT,NEW,2                         ! CRACK ID
CINT,TYPE,JINT                     ! DEFINE CRACK TYPE
CINT,CTNC,CRACKTIP,NODE(-1,0,0)    ! DEFINE CRACK TIP COMPONENT
CINT,NCON,6                        ! NO OF CONTOURS
CINT,SYMM,ON                       ! SYMMETRY ON
CINT,NORM,0,2                      ! CRACK PLANE NORMAL
CINT,LIST
ALLSEL,ALL
/NERR,0,,,,
SOLVE
FINI
/POST1
/OUT,
PRCINT,1,NODE(0,0,T/2),K1          ! PRINT K VALUES
PRCINT,2,NODE(0,0,T/2),JINT        ! PRINT J-INTEGRAL VALUES
*GET,K1_3,CINT,1,CTIP,NODE(0,0,T/2),CONTOUR,3,DTYPE,K1
*GET,K1_4,CINT,1,CTIP,NODE(0,0,T/2),CONTOUR,4,DTYPE,K1
*GET,K1_5,CINT,1,CTIP,NODE(0,0,T/2),CONTOUR,5,DTYPE,K1
*GET,J1,CINT,2,CTIP,NODE(0,0,T/2),CONTOUR,1,,
*GET,J3,CINT,2,CTIP,NODE(0,0,T/2),CONTOUR,3,,
*GET,J4,CINT,2,CTIP,NODE(0,0,T/2),CONTOUR,4,,
*GET,J5,CINT,2,CTIP,NODE(0,0,T/2),CONTOUR,5,,
K = (K1_3 + K1_4 + K1_5)/3
*STATUS,K   ! Lists the current parameters and abbreviations
J   = (ABS(J3)+ABS(J4)+ABS(J5))/3
K_J = (J*(EMOD/(1-NU*NU)))**0.5
K_J1 = (ABS(J1)*(EMOD/(1-NU*NU)))**0.5

!------------------------
! WRITE DATA TO TABLE
!------------------------
*STATUS,J
*DIM,LABEL,CHAR,3,
*DIM,VALUE,,3,3
LABEL(1,1) = 'K SIF',
LABEL(2,1) = 'K J-INT'
LABEL(3,1) = 'K J1-INT'
TARGET = (TAN(PI*A/(2*W))/(PI*A/(2*W)))**0.5
*VFILL,VALUE(1,1),DATA,TARGET      ! STRESS INTENSITY FROM REFERENCE
*VFILL,VALUE(1,2),DATA,K
*VFILL,VALUE(1,3),DATA,ABS(K/TARGET)
*VFILL,VALUE(2,1),DATA,TARGET
*VFILL,VALUE(2,2),DATA,K_J
*VFILL,VALUE(2,3),DATA,ABS(K_J/TARGET)
*VFILL,VALUE(3,1),DATA,TARGET
*VFILL,VALUE(3,2),DATA,K_J1
*VFILL,VALUE(3,3),DATA,ABS(K_J1/TARGET)
```

```
SAVE,TABLE_1
!PLCINT,front,2,,,JINT ! Plot J-contours

FINISH
/CLEAR, NOSTART              ! CLEAR DATABASE FOR 2nD SOLUTION
/OUT,

!!!!!!!!!!!!!!!!!!!!!!!!!!!!!!!!!!!!!!!!!!!!!!!!!!!!!!!!!!!!!!!!!!!!!
! PLATE WITH COLLINEAR CRACKS, SOLID 185 ELEMENT,  Structured mesh
!!!!!!!!!!!!!!!!!!!!!!!!!!!!!!!!!!!!!!!!!!!!!!!!!!!!!!!!!!!!!!!!!!!!!
/CLEAR
/TITLE, STRESS INTENSITY  - WIDE PLATE WITH COLLINEAR CRACKS A = 1
/PREP7
SMRT,OFF
/COM, *** PLATE WITH COLLINEAR CRACKS IN 3-DIMENSIONS USING SOLID185
/COM,
!--------------------
! INPUT VARIABLES
!--------------------
A   = 1         ! HALF CRACK SIZE
W   = 20        ! HALF WIDTH OF THE PLATE
H   = W         ! HALF HEIGHT OF THE PLATE
T   = 0.5       ! PLATE THICKNESS
PI = 3.141592654

EMOD = 30E6     ! YOUNGS MODULUS
NU = 0.3        ! POISSONS RATIO
ET,1,SOLID185   ! SOLID 185 ELEMENT
ET,2,SOLID185   ! ELEMENTS AROUND THE CRACK-TIP
MP,EX,1,EMOD
MP,NUXY,1,NU


!--------------------
! MODEL GEOMETRY
!--------------------
CSYS,1     ! CYLINDRICAL COORDINATE SYSTEM
N,1,0,0,0
NGEN,9,20,1 ! Generates additional nodes from a pattern of nodes,
           ! 9 x node at 0,0,0 with numbers 1, 21, 41 , 61 ... ,161
N,11,0.8
N,171,0.8,180
FILL,11,171,7,31,20     ! Fill line between node 11 and 171 with a node
                        ! at 1/7 of the distance, from 31 (+20) to 151
CSYS,0                  ! CARTESIAN COORDINATE SYSTEM
FILL,1,11,9,2,1,9,20,4  ! 4 is last step/first step, unequal spacing
N,19,W-A,0,0
N,79,W-A,H,0
FILL,19,79,2,39,20
N,159,-A,H,0
FILL,79,159,3,99,20
N,172,-A,0
FILL,159,172,9,181,-1,,,.034 ! Increment is -1. decreasing divisions
FILL,11,19,7,,,7,20,15
NGEN,2,200,1,181,,,,T
E,2,22,1,1,202,222,201,201
EGEN,8,20,-1
E,2,3,23,22,202,203,223,222
```

```
EGEN,8,20,-1
EGEN,9,1,-8
EGEN,9,1,73,78
E,171,151,173,172,371,351,373,372   ! 111
E,151,131,174,173,351,331,374,373 ! 112
E,131,132,175,174,331,332,375,374 ! 113
EGEN,7,1,-1
E,138,139,159,181,338,339,359,381
TYPE,2
EMODIF,1                ! MODIFY ELEMENTS 1 TO 8 FROM TYPE 1 TO TYPE 2
*REPEAT,8,1
NUMMRG,NODE            ! MERGE COINCIDENT NODES
ALLSEL,ALL


!--------------------------
! DEFINING CRACKTIP
!--------------------------
NSEL,S,LOC,X,0
NSEL,R,LOC,Y,0
NLIST                 ! node 1 and 201
CM,CRACKTIP,NODE      ! CRACK TIP NODE COMPONENT, name is cracktip


!-----------------------------------------------
! BOUNDARY CONDITIONS
!-----------------------------------------------
ALLSEL,ALL
NSEL,S,LOC,X,-A
DSYM,SYMM,X                      ! SYMMETRY BOUNDARY CONDITIONS
NSEL,S,LOC,X,0,W
NSEL,R,LOC,Y,0
DSYM,SYMM,Y                      ! SYMMETRY BOUNDARY CONDITIONS
NSEL,S,LOC,X,W-A
DSYM,SYMM,X                      ! SYMMETRY BOUNDARY CONDITIONS
ALLSEL,ALL
D,ALL,UZ,0


!-----------------------------------------------
! LOADS
!-----------------------------------------------
ALLSEL,ALL
NSEL,S,LOC,Y,H
SF,ALL,PRES,-1/((A*PI)**0.5)      ! SURFACE PRESSURE
ALLSEL,ALL
FINI


!-----------------------------------------------
! SOLVE SYSTEM AND RETRIEVE K AND J-INTEGRAL DATA
!-----------------------------------------------
/SOLU
AUTOTS,ON     ! Is default, automatic time stepping
NSUBST,10     ! Specifies the number of substeps
OUTRES,ALL,ALL
CINT,NEW,1                        ! CRACK ID
CINT,TYPE,SIFS                    ! DEFINE CRACK TYPE
CINT,CTNC,CRACKTIP,NODE(-1,0,0)   ! DEFINE CRACK-TIP COMPONENT
                                  ! any node on the open side of the crack
CINT,NCON,6                       ! NO OF CONTOURS
```

```
CINT,SYMM,ON                            ! SYMMETRY ON
CINT,NORM,0,2                           ! CRACK PLANE NORMAL
CINT,LIST
CINT,NEW,2                      ! CRACK ID
CINT,TYPE,JINT                 ! DEFINE CRACK TYPE
CINT,CTNC,CRACKTIP,NODE(-1,0,0)   ! DEFINE CRACK-TIP COMPONENT
CINT,NCON,6                    ! NO OF CONTOURS
CINT,SYMM,ON                   ! SYMMETRY ON
CINT,NORM,0,2                  ! CRACK PLANE NORMAL
CINT,LIST
ALLSEL,ALL
SAVE
/NERR,0,,,,! supresses warnings
SOLVE
FINI


/POST1
/OUT,
PRCINT,1,NODE(0,0,T/2),K1                        ! PRINT K VALUES
PRCINT,2,NODE(0,0,T/2),JINT                       ! PRINT J-INTEGRAL
*GET,K1_3,CINT,1,CTIP,NODE(0,0,T/2),CONTOUR,3,DTYPE,K1
*GET,K1_4,CINT,1,CTIP,NODE(0,0,T/2),CONTOUR,4,DTYPE,K1
*GET,K1_5,CINT,1,CTIP,NODE(0,0,T/2),CONTOUR,5,DTYPE,K1
*GET,J1,CINT,2,CTIP,NODE(0,0,T/2),CONTOUR,1,,
*GET,J3,CINT,2,CTIP,NODE(0,0,T/2),CONTOUR,3,,
*GET,J4,CINT,2,CTIP,NODE(0,0,T/2),CONTOUR,4,,
*GET,J5,CINT,2,CTIP,NODE(0,0,T/2),CONTOUR,5,,
K = (K1_3 + K1_4 + K1_5)/3
*STATUS,K        ! Lists the current parameters and abbreviations
J = (ABS(J3)+ABS(J4)+ABS(J5))/3
K_J = (J*(EMOD/(1-NU*NU)))**0.5
K_J1 = (ABS(J1)*(EMOD/(1-NU*NU)))**0.5


!------------------------
! WRITE DATA TO TABLE
!------------------------
*STATUS,J
*DIM,LABEL,CHAR,3,
*DIM,VALUE,,3,3
LABEL(1,1) = 'K SIF',
LABEL(2,1) = 'K J-INT'
LABEL(3,1) = 'K J1-INT'
TARGET = (TAN(PI*A/(2*W))/(PI*A/(2*W)))**0.5
*VFILL,VALUE(1,1),DATA,TARGET    ! STRESS INTENSITY FROM REFERENCE
*VFILL,VALUE(1,2),DATA,K
*VFILL,VALUE(1,3),DATA,ABS(K/TARGET)
*VFILL,VALUE(2,1),DATA,TARGET
*VFILL,VALUE(2,2),DATA,K_J
*VFILL,VALUE(2,3),DATA,ABS(K_J/TARGET)
*VFILL,VALUE(3,1),DATA,TARGET
*VFILL,VALUE(3,2),DATA,K_J1
*VFILL,VALUE(3,3),DATA,ABS(K_J1/TARGET)
SAVE,TABLE_2


FINISH
/CLEAR, NOSTART                 ! CLEAR DATABASE FOR 3RD SOLUTION
/OUT,
```

```
!!!!!!!!!!!!!!!!!!!!!!!!!!!!!!!!!!!!!!!!!!!!!!!!!!!!!!!!!!!!!!!!!!
! PLATE WITH COLLINEAR CRACKS, SOLID 186 ELEMENT, irregular mesh
!!!!!!!!!!!!!!!!!!!!!!!!!!!!!!!!!!!!!!!!!!!!!!!!!!!!!!!!!!!!!!!!!!
/PREP7
SMRT,OFF
/TITLE, STRESS INTENSITY  - PLATE WITH COLLINEAR CRACKS A = 1
/COM,*** PLATE WITH COLLINEAR CRACKS IN 3-D USING SOLID186

!--------------------
! INPUT VARIABLES
!--------------------
A  = 1            ! HALF CRACK SIZE
W  = 20           ! HALF WIDTH OF THE PLATE
H  = W            ! HALF HEIGHT OF THE PLATE
PI = 3.141592654
T  = 0.5          ! PLATE THICKNESS
EMOD = 30E6       ! YOUNGS MODULUS
NU = 0.3          ! POISSONS RATIO
ET,1,PLANE183     ! PLATE ELEMENT 183, WILL BE REMOVED LATER
ET,2,186          ! SOLID ELEMENT 186
MP,EX,1,EMOD
MP,NUXY,1,NU

!--------------------
! MODEL GEOMETRY
!--------------------
K,1,0  ,0,0               ! DEFINE KEYPOINTS AND LINE SEGMENTS
K,2,W-A,0,0
K,3,W-A,H,0
K,4,-A ,H,0
K,5,-A ,0,0
L,1,2
L,2,3
LESIZE,2,,,4
L,3,4
LESIZE,3,,,4
L,4,5,
LESIZE,4,,,6,.2
L,5,1

!----------------------------------------
! MESH AREAS
!----------------------------------------
ESIZE,,5
KSCON,1,.125,0,8  ! DEFINE CRACK-TIP with singular elements
AL,1,2,3,4,5
AMESH,1
TYPE,2
ESIZE,,2          ! Specifies the default number of line divisions
VEXT,1,,,0,0,T
ALLSEL
ESEL,S,ENAME,,183 ! Select elements of type plane 183
ACLEAR,1          ! Delete these elements

!---------------------------
! DEFINING CRACKTIP
!---------------------------
```

```
ALLSEL
NSEL,S,LOC,X,0
NSEL,R,LOC,Y,0
NLIST
CM,CRACKTIP,NODE          ! CRACK-TIP NODE COMPONENT


!-------------------------------------------------
! BOUNDARY CONDITIONS
!-------------------------------------------------
ALLSEL,ALL
NSEL,S,LOC,X,-A
DSYM,SYMM,X              ! SYMMETRY BOUNDARY CONDITIONS
NSEL,S,LOC,X,0,W
NSEL,R,LOC,Y,0
DSYM,SYMM,Y              ! SYMMETRY BOUNDARY CONDITIONS
NSEL,S,LOC,X,W-A
DSYM,SYMM,X              ! SYMMETRY BOUNDARY CONDITIONS
ALLSEL,ALL
D,ALL,UZ,0


!-------------------------------------------------
! LOADS
!-------------------------------------------------
ALLSEL,ALL
NSEL,S,LOC,Y,H
SF,ALL,PRES,-1/((A*PI)**0.5) ! SURFACE PRESSURE
ALLSEL,ALL
FINI


!-------------------------------------------------
! SOLVE SYSTEM AND RETRIEVE K AND J-INTEGRAL DATA
!-------------------------------------------------
/SOLU
AUTOTS,ON
NSUBST,10
OUTRES,ALL,ALL
CINT,NEW,1                        ! CRACK ID
CINT,TYPE,SIFS                    ! DEFINE CRACK TYPE
CINT,CTNC,CRACKTIP,NODE(-1,0,0)   ! DEFINE CRACK TIP COMPONENT
CINT,NCON,6                       ! NO OF CONTOURS
CINT,SYMM,ON                      ! SYMMETRY ON
CINT,NORM,0,2                     ! CRACK PLANE NORMAL
CINT,LIST
CINT,NEW,2                        ! CRACK ID
CINT,TYPE,JINT                    ! DEFINE CRACK TYPE
CINT,CTNC,CRACKTIP,NODE(-1,0,0)   ! DEFINE CRACK TIP COMPONENT
CINT,NCON,6                       ! NO OF CONTOURS
CINT,SYMM,ON                      ! SYMMETRY ON
CINT,NORM,0,2                     ! CRACK PLANE NORMAL
CINT,LIST
ALLSEL,ALL
SAVE
/NERR,0,,,,
SOLVE
FINI
/POST1
PLNSOL, S,INT
```

```
/OUT,
PRCINT,1,NODE(0,0,T/2),K1        ! PRINT K VALUES  ID = 1
PRCINT,2,NODE(0,0,T/2),JINT      ! PRINT J-INTEGRAL VALUES ID = 1
PRCINT,1,NODE(0,0,T/2),K1        ! PRINT K VALUES ID = 2
PRCINT,2,NODE(0,0,T/2),JINT      ! PRINT J-INTEGRAL VALUES ID = 2
*GET,K1_3,CINT,1,CTIP,NODE(0,0,T/2),CONTOUR,3,DTYPE,K1
*GET,K1_4,CINT,1,CTIP,NODE(0,0,T/2),CONTOUR,4,DTYPE,K1
*GET,K1_5,CINT,1,CTIP,NODE(0,0,T/2),CONTOUR,5,DTYPE,K1
*GET,J1,CINT,2,CTIP,NODE(0,0,T/2),CONTOUR,1,,
*GET,J3,CINT,2,CTIP,NODE(0,0,T/2),CONTOUR,3,,
*GET,J4,CINT,2,CTIP,NODE(0,0,T/2),CONTOUR,4,,
*GET,J5,CINT,2,CTIP,NODE(0,0,T/2),CONTOUR,5,,
K = (K1_3 + K1_4 + K1_5)/3
*STATUS,K       ! Lists the current parameters and abbreviations
J = (ABS(J3)+ABS(J4)+ABS(J5))/3
K_J = (J*(EMOD/(1-NU*NU)))**0.5
K_J1 = (ABS(J1)*(EMOD/(1-NU*NU)))**0.5


!------------------------
! WRITE DATA TO TABLE
!------------------------
*STATUS,J
*DIM,LABEL,CHAR,3,
*DIM,VALUE,,3,3
LABEL(1,1) = 'K SIF',
LABEL(2,1) = 'K J-INT'
LABEL(3,1) = 'K J1-INT'
TARGET = (TAN(PI*A/(2*W))/(PI*A/(2*W)))**0.5
*VFILL,VALUE(1,1),DATA,TARGET    ! STRESS INTENSITY FROM REFERENCE
*VFILL,VALUE(1,2),DATA,K
*VFILL,VALUE(1,3),DATA,ABS(K/TARGET)
*VFILL,VALUE(2,1),DATA,TARGET
*VFILL,VALUE(2,2),DATA,K_J
*VFILL,VALUE(2,3),DATA,ABS(K_J/TARGET)
*VFILL,VALUE(3,1),DATA,TARGET
*VFILL,VALUE(3,2),DATA,K_J1
*VFILL,VALUE(3,3),DATA,ABS(K_J1/TARGET)
SAVE,TABLE_3
FINISH
```

```
!------------------------
! WRITE DATA TO .TXT FILE
!------------------------
RESUME,TABLE_1
/COM
/OUT,Results_collinearcrack,txt
/COM,---RESULTS COMPARISON PLATE WITH COLLINEAR CRACKS A = 1 ---
/COM,
/COM,              | TARGET |  Mechanical APDL |   RATIO
/COM,
/COM, *********************************************************
/COM,    USING SOLID 186 ELEMENT - Structured mesh
/COM, *********************************************************
/COM,
*VWRITE,LABEL(1,1),VALUE(1,1),VALUE(1,2),VALUE(1,3)
(1X,A8,'   ',F10.5,' ',F14.5,'   ',F15.4)
/NOPR
RESUME,TABLE_2
/GOPR
/COM,
/COM, *********************************************************
/COM,   USING SOLID 185 ELEMENT - Structured mesh
/COM, *********************************************************
/COM,
*VWRITE,LABEL(1,1),VALUE(1,1),VALUE(1,2),VALUE(1,3)
(1X,A8,'   ',F10.5,' ',F14.5,'   ',F15.4)
/NOPR
RESUME,TABLE_3
/GOPR
/COM,
/COM, *********************************************************
/COM,   USING SOLID 186 ELEMENT - Irregular mesh
/COM, *********************************************************
/COM,
*VWRITE,LABEL(1,1),VALUE(1,1),VALUE(1,2),VALUE(1,3)
(1X,A8,'   ',F10.5,' ',F14.5,'   ',F15.4)
/NOPR
/COM,
/COM,---------------------------------------------------------
/OUT
FINISH
*LIST,Results_collinearcrack,txt
```

Appendix D

The finite element method

For many engineering problems where no analytical solution is available, one has to resort to numerical methods such as the boundary element method or the finite element method to approximate a field quantity, (e.g. stresses, displacements, strain etc.) in a body or region. Both can be used for fracture mechanics but he boundary element method is more suitable for problems with a small surface/volume ratio. For the geometries in this thesis, this is not really the case, hence using the FEM is considered to be more appropriate.

The FEM essentially comes down to the subdivision of a body into a large number of smaller elements. It is assumed that the actual field quantity within these elements can be approximated by expressions that are not very complex such as a constant, linear or quadratic expression. Elements are connected to each other at their points through nodes and this assembly of nodes and elements forms the mesh. If a large gradient of a field quantity is expected, the mesh needs to be more refined in these areas so that the simple expressions within an element can still approximate the field quantity reasonably well. Alternatively, a special element type can be used. For a cracked body, stress, strain and displacement gradients are very high around the crack-tip and therefore special crack-tip elements can be considered for fracture problems.

Three methods to find the SIF will also be briefly discussed here: the virtual crack extension method, the J-integral method and crack-tip field methods.

Element types   The analysis of a curved crack front is a 3-D problem which needs to be modelled with solid elements. Of these, a variety of shapes are available, such as tetrahedra, pyramids, prisms and hexahedra. The first two shapes are not recommended to be used in ANSYS. The predominantly rectangular shape of the model in this thesis is best modelled by brick elements, prismatic elements are only used to connect the fine brick elements with the coarser ones. A lower order brick element is the 8-node solid, which is the 3-D version of the 4-node plane element shown bottom left in Figure D-1. Correspondingly, the 20-node higher order solid is the 3-D equivalent of the 8-node plane element shown at the top-left of Figure D-1. Varieties such as a 27-node element with an extra node mid-plane and mid-body exist but are not widely applied in FE analysis.

Special crack-tip elements   For linear elastic conditions, the stresses in the vicinity of a crack-tip are inversely proportional to $\sqrt{r}$, as can be seen from Eq. (A-1). To describe this singular behaviour for FE as well, special crack-tip elements can be used around the crack-tip. Higher order elements, which are element types that have more nodes than only the ones at the extremes of the element, can be adjusted in a way that they can describe this singular behaviour when $r \to 0$. Some of the extra nodes that would have otherwise be located mid-side are re-positioned closer to the crack-tip the in the ratio 1:3, so at a quarter of the length of the element side. Lower order elements have an extra node collapsed into the crack-tip node. Examples of these special crack-tip elements are shown in Figure D-1 for two-dimensional element types. For a derivation that confirms that the strains at the crack-tip of a higher order element indeed become infinite and share the $1/\sqrt{r}$ singularity of the analytical solution of Eq. (A-1a), reference is made to [30, 11.4.1].
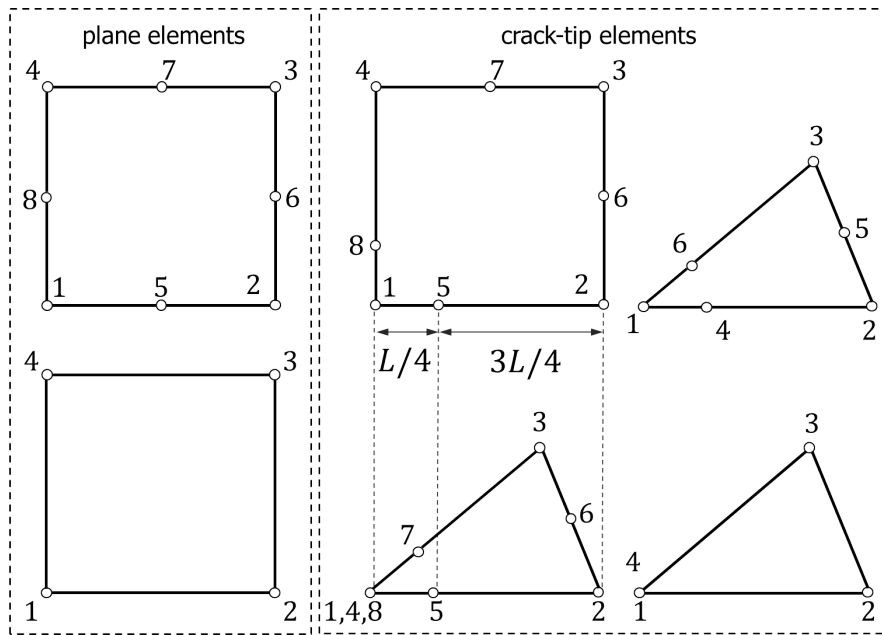
Figure D-1: Examples of quarter point and collapsed elements
            Top - **Left** 8-node plane element
            Top - **Centre** 8-node quarter point element
            Top - **Right** 6-node quarter point element
            Bottom - **Left** 4-node plane element
            Bottom - **Centre** 8-node collapsed quarter point element
            Bottom - **Right** 4-node collapsed element

Virtual crack extension method   This method finds K through the energy release rate and is the numerical equivalent of Eq. (A-3). Reference is also made to Figure A-3. The crack is virtually extended by Δa, and the elongation of the plate is fixed, so $\mathcal{F} = 0$. It is assumed that the stress states around the crack-tip do not significantly change, only the stiffness of the plate is affected by this virtual crack extension. The energy release rate is then approximately

$$\mathcal{G} = -\frac{1}{t}\left(\frac{\mathrm{d}\mathcal{U}}{\mathrm{d}a}\right)_{\delta_{fixed}} \approx -\frac{1}{t}\left(\frac{\mathcal{U}\left(a+\Delta a\right) - \mathcal{U}\left(a\right)}{\Delta a}\right) \tag{D-1}$$

Note that, as the crack grows, elastic strain energy stored in the body decreases, so $\mathcal{G}$ becomes positive. Once $\mathcal{G}$ is known, it can be related to K by Eq. (A-10).

Similarly, to avoid computing the stiffness matrix twice, FE programs often only calculate the differences in stiffness directly around the crack-tip. Because of this, it is important to use crack-tip elements in this area.

J-integral method In Section A-2 the 2-D contour integral is shown. In three dimensions, it essentially comes down to the calculation of a surface integral S, as shown in Figure D-2. When the contours are positioned a bit further away from the crack-tip, it is not necessary to use special crack-tip elements. ANSYS determines the first contour as the first layer of nodes perpendicular to the crack face in its $x - z$ plane, hence in crack growth direction; the second contour as the second layer of nodes etc.
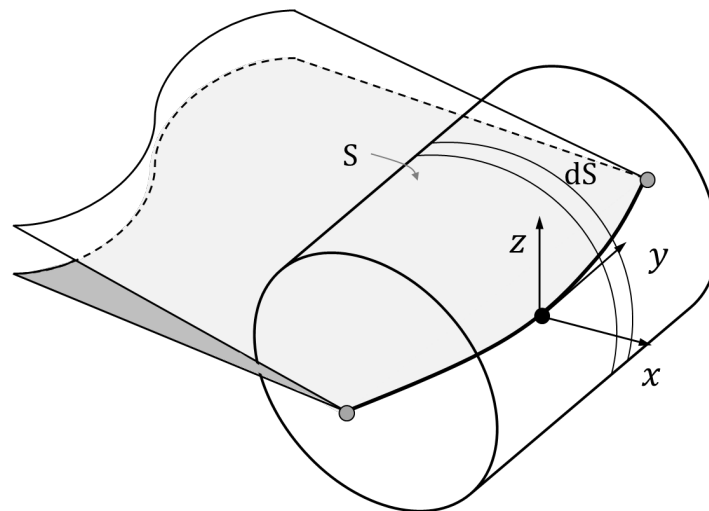
Figure D-2: Surface for computing a J integral in 3-D.

As shown in Figure D-3 and with reference to Figure 3-9 and 3-11,the contour-finding procedure may cause errors for the determination of the J-contour around the crack-tip at the breakthrough side, because the software may not find all node-layers. This problem occurs in particular for very sharp cracks. It can be solved by using a small crack-tip mesh-radius, a very dense element spacing in the vicinity of the breakthrough side and by disregarding the contours further away from the crack-tip.

Only converged J values, typically obtained from contours that are a somewhat further away from the crack-tip, should be used. Close to the crack-tip, the J value is less accurate. As long as the contours are not too close to the crack-tip, it is not needed to use special crack-tip elements. The J values of the nodes at the free surfaces should not be used because the J value for a node is obtained by using the some values of the neighbouring nodes as well. For an explanation how these neighbouring nodes affect the J value, reference is made to [12].

It should furthermore be noted that the J-integral in this thesis is in fact a $\mathcal{G}$-integral because no plasticity or non-linearities are included in the models, as explained in Section A-2. It is nevertheless referred to as a J-(contour) integral, since ANSYS does not distinguish between $\mathcal{G}$ and J, as only the general case of the J-integral method can be selected in the program.
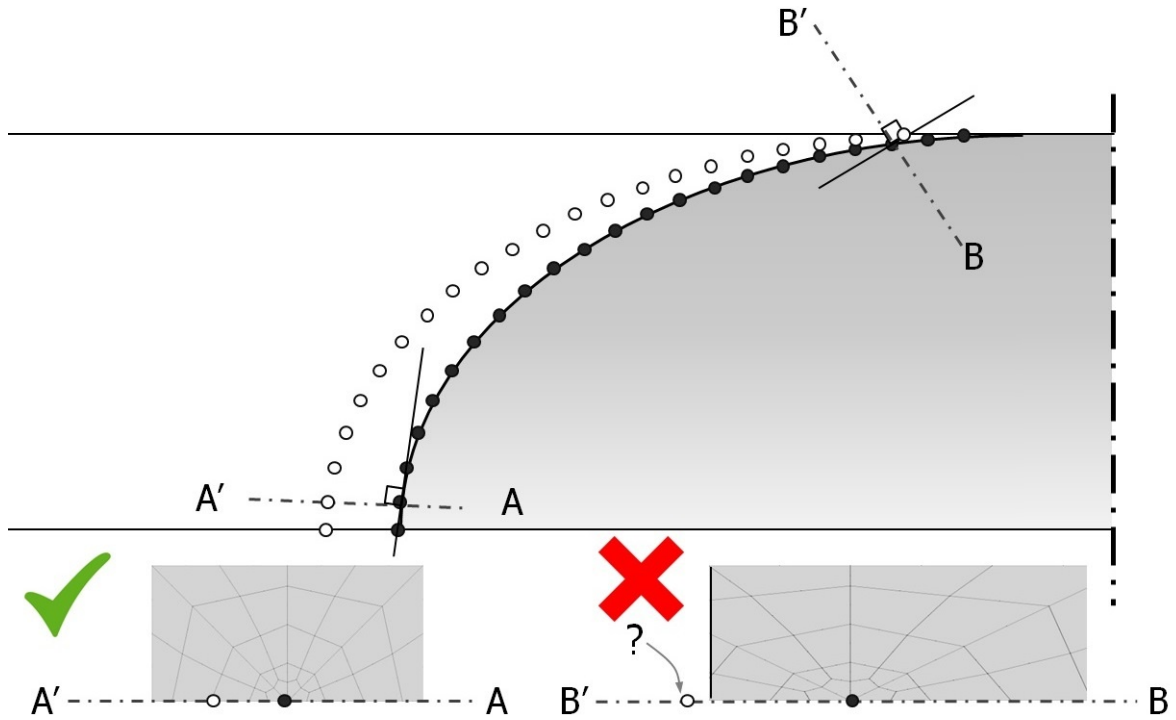
Figure D-3: Illustration of an issue with the J integral at the breakthrough side

Crack-tip field methods   Two variations are available in ANSYS: the displacement extrapolation method that is illustrated in Figure D-4 and the interaction integral method. [1] The latter applies volume integration in a similar fashion as the J-contour does for 3-D problems. It is contour independent as well, but has a slightly different formulation as the J-integral. This formulation is used in this thesis as well, because no special crack-tip elements are required.
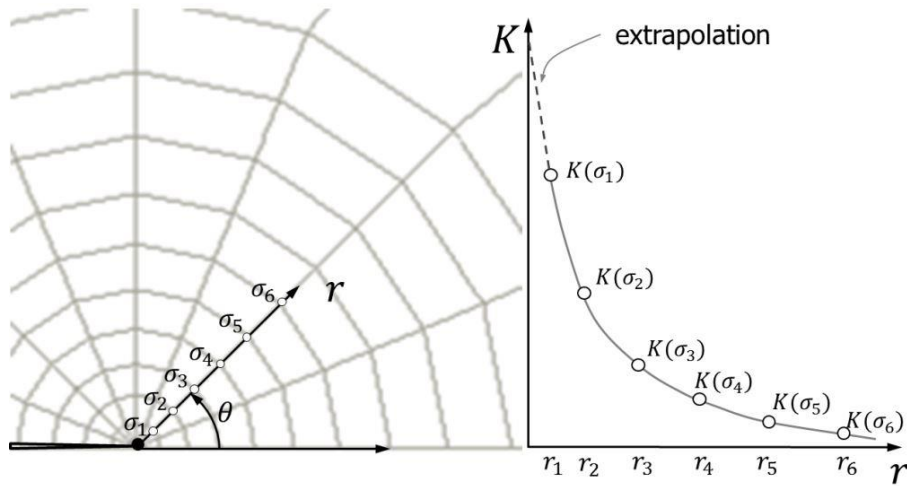
Figure D-4: Stress field extrapolation

---

[1] Operated in ANSYS through respectively the `KCALC` and `CINT` command.

Ansys script for a semi-elliptical surface crack

```
FINISH
/CLEAR
!!!!!!!!!!!!!!!!!!!!!!!!!!!!!!!!!!!!!!!!!!!!!!!!!!!!!!!!!!!!!!
!   SEMI - ELLIPTICAL CRACK MODELLED WITH SOLID 186 ELEMENT
!!!!!!!!!!!!!!!!!!!!!!!!!!!!!!!!!!!!!!!!!!!!!!!!!!!!!!!!!!!!!!
/TITLE, A/C = 0.2  ;  A/T = 0.7
/PREP7
/UIS, MSGPOP,3
/COM,
/VIEW,,-1,-1,1
/VUP,,Z
BTOL,3E-4        ! TOLERANCE FOR GLUE COMMANDS
BOPTN,NWARN,1   ! SUPPRESS WARNING IF GLUE OPERATION FAILS


!--------------------
! INPUT VARIABLES
!--------------------
EMB = 1     ! SEMI-ELLIPSE (0) OR EMBEDDED ELLIPSE (1)
N = 0       ! FOR TENSION: N = 0  ; FOR BENDING N = 1
A = 35      ! HALF AXIS OF THE ELLIPS - SHORT
C = 175     ! HALF AXIS OF THE ELLIPS - LONG
W = 4*C     ! HALF WIDTH OF THE SOLID (in Y-direction)
H = 2.4*C   ! HEIGHT OF THE BLOCK
T = 50      ! THICKNESS OF THE PLATE (in X-direction)
R = 2.2     ! RADIUS AROUND CRACKTIP
R2 = 7.2    ! OUTER RADIUS > R
R3 = 6.8    ! INNER RADIUS > R
SIGMA = 100 ! STRESS
DIV = 46    ! NUMBER OF ELEMENTS ALONG THE CRACK LINE
*IF,EMB,EQ,0,THEN
  /COM,     ****** SEMI-ELLIPTICAL CRACK IN A FINITE WIDTH PLATE
*ELSEIF,EMB,EQ,1
  /COM,     ****** EMBEDDED ELLIPTICAL CRACK IN A LARGE SOLID
  T2 = 3*C + A  ! THICKNESS OF THE SOLID (IN X-DIRECTION)
```

```
*ENDIF
PI = 3.141592654
ET,1,186        ! SOLID ELEMENT 186 - 20 NODE HEXAGONAL
EMOD = 207E3    ! YOUNGS MODULUS
NU = 0.3        ! POISSONS RATIO
MP,EX,1,EMOD
MP,NUXY,1,NU


!--------------------
! MODELLING GEOMETRY
!--------------------
WPOFFS, 0, C, 0
WPROTA,-90,90,0    ! ROTATE THE WORKING PLAN
CSWPLA,11,1         ! DEFINE LOCAL COORDINATE SYSTEM 11
K,1,0,0,0
KGEN,5,1,,,,,,10,0 ! 5 x KP AT (0,0,0) NUMBERED 1,11,21,31,...

K,4,R*0.8,0,0
K,44,R*0.8,180,0
KFILL,4,44,3,14,10 ! FILL THE 'LINE' BETWEEN NODE 4 AND 44 WITH A NODE
                   ! AT 1/4 OF THE DISTANCE NUMBERED FROM 14 (+10) TO 44
KFILL,1,4,2,2,1,1.0
KGEN,5,1,4,1,0,180/4,0,10,1,0

CSWPLA,12,0         ! DEFINE LOCAL COORDINATE SYSTEM 12, CARTHESIAN
K, 5,  R,0,0
K, 6, R3,0,0
K,15,  R,R,0
K,16, R3,R,0
K,25,  0,R,0
K,35, -R,R,0
K,45, -R,0,0
K,46,-R2,0,0
KMODIF,14, R*0.62,R*0.62,0
KMODIF,34,-R*0.62,R*0.62,0
A, 2,12, 1, 1      !
A,12,22,11,11
A,22,32,21,21
A,32,42,31,31
A, 2, 3,13,12,     !
A,12,13,23,22,
A,22,23,33,32,
A,32,33,43,42,
A, 3,13,14, 4,     !
A,13,23,24,14,
A,23,33,34,24,
A,33,43,44,34,
A, 4,14,15, 5      !
A,14,24,25,15
A,24,34,35,25
A,34,44,45,35
A, 5,  6,16,15     !

K,36,-R2,R,0
A,45, 46,36,35

ASEL,ALL
```

```
AGLUE,ALL

WPSTYL,DEFA
WPSTYL, , , , , , 0, 0, 0,
CSYS,0
K,  7,0,0,0
K,100,A,0,0

LOCAL,13,1,0,0,0,,,,C/A ! ELLIPTICAL COORDINATE SYSTEM
L,1,100

CSYS,0
ASEL,ALL
VDRAG,ALL,,,,,,5          ! EXTRUDE AREAS TO VOLUMES
LDELE,5                   ! REMOVE LINE

L, 6,7
L,49,7
NUMMRG,KP, , , ,
AL,5,99,111
VDRAG,79,,,,,,41,
VGLUE,14,19              ! GLUE VOLUMES

BLOCK, 0, T, 0, C+3*R2, 0, R
VSEL,S,VOLU,,19
CM,BOTTOMVOLUME1,VOLU

BLOCK, 0, T, C+3*R2,W , 0, R
VSEL,D,VOLU,,21
CM,BOTTOMVOLUME2,VOLU

ALLSEL,ALL
VSEL,U,VOLU,,BOTTOMVOLUME1,
VSEL,U,VOLU,,BOTTOMVOLUME2,
CM,SUBTRACTVOLUME,VOLU

VSEL,ALL             ! SUBTRACT VOLUMES FROM VOLUMES
VSBV,BOTTOMVOLUME1,SUBTRACTVOLUME,,DELETE,KEEP
CMDELE,SUBTRACTVOLUME

VSEL,S,VOLU,,20
CM,CORNERVOLUME,VOLU
VSEL,S,VOLU,,14
CM,INNERRAD,VOLU
VSEL,S,VOLU,,15
CM,OUTERRAD,VOLU
VSEL,S,VOLU,,22
CM,BOTTOMVOLUME1,VOLU
VSEL,S,VOLU,,21
CM,BOTTOMVOLUME2,VOLU

*IF,EMB,EQ,0,THEN
  VSEL,ALL
  VGLUE,ALL
  ALLSEL,ALL
  NUMMRG,kp, , , ,
*ELSEIF,EMB,EQ,1
```

```
  BLOCK, T, T2,      0,C+3*R2,0,R
  BLOCK, T, T2,C+3*R2,     W,0,R
  VSEL,ALL
  VGLUE,ALL
  ALLSEL,ALL
  NUMMRG,KP, ,
  VSEL,S,VOLU,,19
  CM,BOTTOMVOLUME3,VOLU
  VSEL,S,VOLU,,23
  CM,BOTTOMVOLUME4,VOLU
*ENDIF

!----------------------------
! MESH CRACK AREA
!----------------------------
LSEL,S,LOC,X,0.1,A+R
LSEL,R,LOC,Y,0.1,C+R
LESIZE,ALL,,,DIV,1.0    ! DIVIDE CRACK TIP LINE
ESIZE,,1
VSEL,ALL
VSEL,U,VOLU,,CORNERVOLUME
VSEL,U,VOLU,,INNERRAD
VSEL,U,VOLU,,OUTERRAD
VSEL,U,VOLU,,BOTTOMVOLUME1
VSEL,U,VOLU,,BOTTOMVOLUME2
*IF,EMB,EQ,1,THEN
  VSEL,U,VOLU,,BOTTOMVOLUME3
  VSEL,U,VOLU,,BOTTOMVOLUME4
*ENDIF
MSHKEY,1                ! MAPPED MESHING
VMESH,ALL

ALLSEL,ALL
KSEL,S,KP,,1
LSLK,S,0
LSEL,R,LOC,X,0.01,A+R  ! SELECT LINE AT CRACK TIP
NSLL,S,1
CM,CRACKTIP,NODE        ! DEFINE COMPONENT FOR CRACK TIP
ALLSEL

!----------------------------
! MESH THE OTHER VOLUMES
!----------------------------
SMRT,OFF
LSEL,S,LOC,X,0
LSEL,R,LOC,Y,C+R2
LESIZE,ALL,,,1
LSEL,S,LOC,X,0
LSEL,R,LOC,Y,C+R+0.1,C+R2-0.1
LSEL,R,LOC,Z,0,R
LESIZE,ALL,,,1,
VSWEEP,OUTERRAD        ! MESH OUTER RADIUS

LSEL,S,LOC,X,0
LSEL,R,LOC,Y,C-R3
LESIZE,ALL,,,1
LSEL,S,LOC,X,0
```

```
LSEL,R,LOC,Y,C-R3+0.1,C-R-0.1
LSEL,R,LOC,Z,0,R
LESIZE,ALL,,,1,
VSWEEP,INNERRAD       ! MESH INNER RADIUS

SMRT,10
LSEL,S,LOC,Y,0.1,C-R-0.1
LSEL,R,LOC,X,0
LESIZE,ALL,,,DIV-13,1.1,,,,0
LSEL,S,LOC,X,0.1,A-R3-0.1
LSEL,R,LOC,Y,0
LESIZE,ALL,,,3,1.0,,,,0
VSWEEP,CORNERVOLUME   ! MESH VOLUMES ABOVE THE CRACK

LSEL,S,LOC,X,0.1,T-0.1
LSEL,R,LOC,Y,C+3*R2,
LESIZE,ALL,,,8
LSEL,S,LOC,X,T
LSEL,R,LOC,Y,0.1,C+R2-0.1
LESIZE,ALL,,,24,,,,,0
VSWEEP,BOTTOMVOLUME1  ! MESH VOLUMES IN LENGTH DIRECTION

ESIZE,,1
LSEL,S,LOC,X,0
LSEL,A,LOC,X,T
LSEL,R,LOC,Y,C+3*R2+0.1, W-0.1,
LESIZE,ALL,,,6,
ALLSEL, ALL
VSWEEP,BOTTOMVOLUME2 ! MESH VOLUMES IN DEPTH DIRECTION

*IF,EMB,EQ,1,THEN
  LSEL,S,LOC,X,T+0.1,T2-0.1
  LSEL,R,LOC,Y,0,
  LESIZE,ALL,,,5,5,,,,0
  LSEL,S,LOC,X,T+0.1,T2-0.1
  LSEL,R,LOC,Y,C+3*R2,W
  LESIZE,ALL,,,5,1/5,,,,0
  LSEL,S,LOC,X,T2       ! LONG SIDE, AWAY FROM CRACK
  LSEL,R,LOC,Y,0.1,C+3*R2-0.1
  LESIZE,ALL,,,1,,,,,0
  VSWEEP,BOTTOMVOLUME3
  VSWEEP,BOTTOMVOLUME4 ! MESH REMAINING VOLUMES IN DEPTH DIRECTION
*ENDIF

!---------------------------------------------
! EXTRUDE TO FULL HEIGHT AND MESH OTHER AREAS
!---------------------------------------------
ALLSEL,ALL
ESIZE,,7
ALLSEL,ALL
ASEL,S,LOC,Z,R
VEXT,ALL, , , , ,H-R
ALLSEL,ALL
VSEL,S,LOC,Z,R,H
VSWEEP,ALL
ALLSEL,ALL
```

```
!--------------------------------
! BOUNDARY CONDITIONS
!--------------------------------
*IF,EMB,EQ,0,THEN
  *IF,N,EQ,0,THEN
    NSEL,S,LOC,X,T/2-1,T/2+0.1
    NSEL,R,LOC,Z,H
    D,ALL,UX,0
  *ELSEIF,N,EQ,1
    NSEL,S,LOC,X,A
    NSEL,R,LOC,z,H
    NSEL,R,LOC,Y,0
    D,ALL,UX,0          ! CONSTRAIN UX DOF
  *ENDIF
*ELSEIF,EMB,EQ,1
  NSEL,S,LOC,X,0
  D,ALL,UX,0          ! CONSTRAIN UX DOF
*ENDIF

ALLSEL
NSEL,S,LOC,Y,0
D,ALL,UY,0            ! CONSTRAIN UY DOF
ALLSEL

KSEL,S,KP,,42,46      ! CONSTRAIN AREAS THAT ARE NOT PART OF THE CRACK
LSLK,S,0
LSEL,R,LOC,Z,0
ASLL,S,0
ASEL,A,LOC,Y,C+R,W

*IF,EMB,EQ,0,THEN
  ASEL,A,LOC,X,A+R,T
*ELSEIF,EMB,EQ,1
  ASEL,A,LOC,X,A+R,T2
*ENDIF

ASEL,R,LOC,Z,0
CM,CONSTRAINAREAS,AREA
CMSEL,S,CONSTRAINAREAS,AREA
NSLA,S,1
D,ALL,UZ,0                    ! CONSTRAIN UZ DOF

!-------------------------------------------------
! LOADS
!-------------------------------------------------
*IF,N,EQ,0,THEN                  ! TENSION
  ALLSEL
  NSEL,S,LOC,Z,H
  SF,ALL,PRES,-SIGMA           ! SURFACE PRESSURE LOADING
*ELSEIF,N,EQ,1
  P = (SIGMA+SIGMA*(T-A)/A)/T ! BENDING
  ALLSEL
  SFGRAD,PRES,0,X,A,P          ! PRESSURE LOAD GRADIENT
  NSEL,S,LOC,Z,H
  SF,ALL,PRES,0                ! SURFACE PRESSURE LOADING
*ENDIF
ALLSEL
```

```
FINISH

!------------------------------------------------
! SOLVE SYSTEM AND RETRIEVE K AND J-INTEGRAL DATA
!------------------------------------------------
/SOLU
AUTOTS,ON
NSUBST,10
OUTRES,ALL,ALL
CINT,NEW,1                       ! CRACK ID
CINT,TYPE,SIFS                   ! DEFINE CRACK TYPE
CINT,CTNC,CRACKTIP,NODE(0,0,0),0 ! DEFINE CRACK-TIP COMPONENT
CINT,NORM,0,3                    ! CRACK PLANE NORMAL - Z
CINT,NCON,5                      ! NO. OF CONTOURS
CINT,SYMM,ON                     ! SYMMETRY ON
CINT,LIST
CINT,NEW,2                       ! CRACK ID
CINT,TYPE,JINT                   ! DEFINE CRACK TYPE
CINT,CTNC,CRACKTIP,NODE(0,0,0),0 ! DEFINE CRACK TIP COMPONENT
CINT,NORM,0,3                    ! CRACK PLANE NORMAL - Z
CINT,NCON,5                      ! NO. OF CONTOURS
CINT,SYMM,ON                     ! SYMMETRY ON
CINT,LIST
ALLSEL,ALL

SAVE
/NERR,0,,,,
SOLVE
FINI

/POST1
EPLOT
!PLCINT,FRONT,1,,,K1

SET,LAST,LAST
CMSEL,S,CRACKTIP,NODE
*GET,NNUM,NODE,0,COUNT
*GET,NMIN,NODE,0,NUM,MIN
*DIM,VALUE,ARRAY,NNUM,4
I = 1

*DO,I,1,NNUM
  NCUR = NMIN
  *GET,X_COOR,NODE,NCUR,LOC,X
  VALUE(I,1) = X_COOR
  *GET,Y_COOR,NODE,NCUR,LOC,y
  VALUE(I,2) = Y_COOR
  *GET,K2,CINT,1,CTIP,NCUR,,2,,K1
  *GET,K3,CINT,1,CTIP,NCUR,,3,,K1
  *GET,K4,CINT,1,CTIP,NCUR,,4,,K1
  K = ABS(K2+K3+K4)/3
  VALUE(I,3) = K
  *GET,J2,CINT,2,CTIP,NCUR,,2,,JINT
  *GET,J3,CINT,2,CTIP,NCUR,,3,,JINT
  *GET,J4,CINT,2,CTIP,NCUR,,4,,JINT
  J = ABS(J2+J3+J4)/3
  KJ = (J*EMOD/(1-NU*NU))**0.5
```

```
  VALUE(I,4) = KJ
  I = I+1
  *GET,NMIN,NODE,NCUR,NXTH
*ENDDO

!----------------------------
! WRITE K VALUES TO .TXT FILE
!----------------------------
*CFOPEN,X_Y_K_KJ,TXT                        ! CREATE FILE
*VWRITE,VALUE(1,1),VALUE(1,2),VALUE(1,3),VALUE(1,4) ! WRITE ARRAY TO FILE
(f10.6,3x,f10.6,3x,f10.5,3x,f10.5)          ! FORMAT 3X (3X A BLANK SPACE)
*CFCLOSE                                     ! CLOSE FILE

NSEL,ALL
ESEL,ALL

FINISH
```

Ansys script for a semi-elliptical through-thickness crack

```
FINISH
/CLEAR
!!!!!!!!!!!!!!!!!!!!!!!!!!!!!!!!!!!!!!!!!!!!!!!!!!!!!!!!!!!!!!!!
!         VERY FINE - 24 ELEMENTS IN X-DIRECTION
!!!!!!!!!!!!!!!!!!!!!!!!!!!!!!!!!!!!!!!!!!!!!!!!!!!!!!!!!!!!!!!!
/TITLE, A/C = 0.4 ; C2 = 0.40*C
/PREP7
/UIS, MSGPOP,3
/COM,
/VIEW,,-1,-1,1
/VUP,,Z
!-------------------
!   INPUT VARIABLES
!-------------------
CENTRE = 1      ! BREAKTHROUGH (0) OR CENTRE (1) CRACK
N = 0           ! TENSION: N = 0 ; BENDING N = 1
A = 109.1089451 ! HALF AXIS OF THE ELLIPS - SHORT
C = A/0.4       ! HALF AXIS OF THE ELLIPS - LONG
W = 6*C         ! HALF WIDTH OF THE SOLID (IN Y-DIRECTION)
H = 7.3*C       ! HEIGHT OF THE PLATE
T = 100         ! THICKNESS OF THE PLATE
R = 5.00        ! RADIUS AROUND CRACKTIP
RO = 1.45*R     ! OUTER RADIUS > R
ROO = 2.18*RO   ! TRANSITION TO COARSER MESH > RO
RT = 1.50*ROO   ! TRANSITION TO COARSER MESH II
RI = A/5.55     ! INNER RADIUS > R (towards crack area)
SIGMA = 10      ! STRESS
ET,1,186        ! SOLID ELEMENT 186 - 20 NODE HEXAGONAL
EMOD = 207E3    ! YOUNGS MODULUS
NU = 0.3        ! POISSONS RATIO
MP,EX,1,EMOD
MP,NUXY,1,NU

!-------------------
```

```
!    MODEL GEOMETRY
!--------------------
WPOFFS, 0, C, 0
WPROTA,-90,90,0      ! ROTATE THE WORKING PLANE
CSWPLA,11,1          ! DEFINE LOCAL COORDINATE SYSTEM 11
KGEN,5,1,,,,,,10,0   ! 4 x KP AT (0,0,0) NUMBERED 1,11,21,31,...
K,1,0,0,0
K,4,R*0.85,0,0
K,44,R*0.85,180,0
KFILL,4,44,3,14,10   ! FILLS THE 'LINE'BETWEEN NODE 4 AND 44
KFILL,1,4,2,2,1,1.0
KGEN,5,1,4,1,0,180/4,0,10,1,0
CSWPLA,12,0              ! DEFINE LOCAL COORDINATE SYSTEM 12, CARTHESIAN
K, 5,  R,0,0
K, 6, RI,0,0
K,15,  R,R,0
K,16, RI,R,0
K,25,  0,R,0
K,35, -R,R,0
K,36,-RO,R,0
K,45, -R,0,0
K,46,-RO,0,0
KMODIF,14, R*0.70,R*0.70,0
KMODIF,34,-R*0.70,R*0.70,0
A, 2,12, 1, 1 !
A,12,22,11,11
A,22,32,21,21
A,32,42,31,31
A, 2, 3,13,12,!
A,12,13,23,22,
A,22,23,33,32,
A,32,33,43,42,
A, 3,13,14, 4,!
A,13,23,24,14,
A,23,33,34,24,
A,33,43,44,34,
A, 4,14,15, 5 !
A,14,24,25,15
A,24,34,35,25
A,34,44,45,35
A, 5, 6,16,15  !
A,45,46,36,35
ASEL,ALL
AGLUE,ALL
WPSTYL,DEFA
WPSTYL,,,,,,0,0,0,
CSYS,0
*IF,CENTRE,EQ,0,THEN
  K,100,A,0,0
  K,101,T,0,0
  K,102,T,C,0
  LOCAL,13,1,0,0,0,,,,C/A  ! ELLIPTICAL COORDINATE SYSTEM
  L,1,100
  CSYS,0
  L,101,102
  LPTN,5,6
  LDELE,11,12
```

```
  LDELE, 8,9              ! TO GET THE SAME NUMBERING AS FOR A CENTRE CRACK
  LOCAL,13,1,0,0,0,,,,C/A ! ELLIPTICAL COORDINATE SYSTEM
  L,1,7
  KDELE,100,102
*ELSEIF,CENTRE,EQ,1
  K,7,T,C,0
  L,1,7
*ENDIF
WPROTA,,,90           ! ROTATE THE WORKING PLANE
WPOFFS,,,0.050*T      ! DIVIDE THE LINE
LSBW,5, ,             ! the divisions are different for almost all models
WPOFFS,,,0.090*T
LSBW,8, ,
WPOFFS,,,0.089*T
LSBW,5, ,
WPOFFS,,,0.088*T
LSBW,8, ,
WPOFFS,,,0.080*T
LSBW,5, ,
WPOFFS,,,0.074*T
LSBW,8, ,
WPOFFS,,,0.069*T
LSBW,5, ,
WPOFFS,,,0.061*T
LSBW,8, ,
WPOFFS,,,0.0575*T
LSBW,5, ,
WPOFFS,,,0.0515*T
LSBW,8, ,
WPOFFS,,,0.0455*T
LSBW,5, ,
WPOFFS,,,0.040*T
LSBW,8, ,
WPOFFS,,,0.035*T
LSBW,5, ,
WPOFFS,,,0.028*T
LSBW,8, ,
WPOFFS,,,0.021*T
LSBW,5, ,
WPOFFS,,,0.0172*T
LSBW,8, ,
WPOFFS,,,0.016*T
LSBW,5, ,
WPOFFS,,,0.014*T
LSBW,8, ,
WPOFFS,,,0.013*T
LSBW,5, ,
WPOFFS,,,0.0125*T
LSBW,8, ,
WPOFFS,,,0.0122*T
LSBW,5, ,
WPOFFS,,,0.012*T
LSBW,8, ,
WPOFFS,,,0.0118*T
LSBW,5, ,
WPSTYL,DEFA
WPSTYL, , , , , , 0, 0, 0,
```

```
CSYS,0
LSEL,U,LOC,X,0
LDELE,ALL,,,0
L,1,8           ! CREATE LINES FOR THE CRACK-TIP
L,8,9
L,9,10
L,10,11
L,11,17
L,17,18
L,18,19
L,19,20
L,20,21
L,21,26
L,26,27
L,27,28
L,28,29
L,29,30
L,30,31
L,31,37
L,37,38
L,38,39
L,39,40
L,40,47
L,47,48
L,48,49
L,49,50
L,50,7
ASEL,ALL
CM,EXTRUDEAREAS,AREA              ! DEFINE COMPONENT
LSEL,S,LOC,X,0.01,T
CM,DRAGLINE,LINE
VDRAG,EXTRUDEAREAS,,,,,,DRAGLINE ! EXTRUDE AREAS TO VOLUMES (cracktip area)
VEXT,66,1446,60,0,-C,             ! EXTRUDE AREAS TO VOLUMES (crack area)
WPOFFS, 0,0, 0
WPROTA,0,90,0                     ! ROTATE THE WORKING PLANE
VSBW,ALL,,DELETE
WPSTYL,DEFA
WPSTYL,,,,,,0,0,0,
VSEL,S,LOC,Y,0,-C
VDELE,ALL,,,1


!------------------------------------------------------------
!   FROM 24 TO 12 LANES OF VOLUMES
!------------------------------------------------------------
ASEL,S,AREA,,70,1450,60
VEXT,ALL,,,0,ROO-RO
KSEL,S,KP,,653,697,4
KSEL,A,KP,,654,698,4
KMODIF, ALL, ,C+ROO-0.04*T,
KSEL,S,KP,,655,699,4
KSEL,A,KP,,656,700,4
KMODIF, ALL, , C+ROO,
BLOCK, 0, T, C+ROO-0.04*T, C + ROO, 0, R
VSEL,S,VOLU,,433,456,1
VSEL,A,VOLU,,481
VSBA, ALL, 1655, , DELETE, DELETE   ! SUBTRACT AREA FROM VOLUMES
VSEL,S,LOC,Y,C+ROO-0.04*T-0.01,C+ROO
```

```
VSBV,481,ALL,,DELETE,KEEP              ! SUBTRACT VOLUMES FROM VOLUMES
ASEL,S,LOC,Y,C+ROO-0.01,C+ROO+0.01
VEXT,ALL,,,0,RT


!----------------------------
!    FROM 12 TO 6 LANES OF VOLUMES
!----------------------------
KSEL,S,KP,,784,804,4
KSEL,A,KP,,787,803,4
KSEL,A,KP,,781
KMODIF,ALL,,C+ROO+RT-0.08*T,
BLOCK,0,T,C+ROO+RT-0.08*T,C+ROO+RT, 0, R
VSEL,S,VOLU,,445,456,1
VSEL,A,VOLU,,481
VSBA, ALL, 1827, , DELETE, DELETE   ! SUBTRACT AREA FROM VOLUMES
VSEL,S,LOC,Y,C+ROO+RT-0.08*T-0.01,C+ROO+RT
VSBV,481,ALL,,DELETE,KEEP              ! SUBTRACT VOLUMES FROM VOLUMES
ASEL,S,LOC,Y,C+ROO+RT-0.01,C+ROO+RT+0.01
VEXT,ALL,,,0,W-C-ROO-RT
ALLSEL
NUMMRG, KP,


!--------------------------------------
!    MESH AREA AROUND THE CRACK-TIP
!--------------------------------------
VSEL,S,VOLU,,1,432,
VSEL,U,VOLU,,14,428,18
VSEL,U,VOLU,,15,429,18
ESIZE,,1
MSHKEY,1 ! MAPPED MESHING
VMESH,ALL


!---------------------------
!    MESH THE INNER RADIUS
!---------------------------
LSEL,S,LOC,Y,C-R-0.01,C-RI-0.01
LSEL,R,LOC,X,0,
LSEL,R,LOC,Z,0,
LESIZE,ALL,,,1
LSEL,S,LOC,Y,C-R-0.01,C-RI-0.01
LSEL,R,LOC,X,0,
LSEL,R,LOC,Z,R,
LESIZE,ALL,,,1
LSEL,S,LINE,,123,1664,67
LSEL,A,LINE,,41
LESIZE,ALL,,,1,
VSEL,S,VOLU,,14,428,18
VSWEEP,ALL


!---------------------------
!    MESH THE OUTER RADIUS
!---------------------------
LSEL,S,LINE,,126,1667,67
LSEL,A,LINE,,43
LESIZE,ALL,,,1,
LSEL,S,LINE,,128,1669,67
LSEL,A,LINE,,44
```

```
LESIZE,ALL,,,1,
LSEL,S,LINE,,130,1671,67
LSEL,A,LINE,,45
LESIZE,ALL,,,1,
VSEL,S,VOLU,,15,429,18
VSWEEP,ALL

!-----------------------------
!   MESHING THE CRACK AREA
!-----------------------------
LSEL,S,LOC,Y,0.1,C-RI-0.1
LSEL,R,LOC,X,0
LESIZE,ALL,,,6,
VSEL,S,VOLU,,457,480
VSWEEP,ALL

!-----------------------------
!   MESH THE OTHER AREAS
!-----------------------------
LSEL,S,LOC,Y,C+RO+0.1,C+ROO-0.06*T-0.01
LSEL,R,LOC,X,0
LESIZE,ALL,,,6,,,,,                    ! ROO
VSEL,S,VOLU,,506,529
VSWEEP,ALL
LSEL,S,LOC,Y,C+ROO+0.1,C+ROO+RT-0.08*T-0.1
LESIZE,ALL,,,1,,,,,                    ! RT
VSEL,S,LOC,Y,C+ROO+0.1,C+ROO+RT-0.08*T-0.1
VSWEEP,ALL
LSEL,S,LOC,Y,C+ROO+RT+0.1,W-0.1
LESIZE,ALL,,,13,,,,,                   ! W
VSEL,S,LOC,Y,C+ROO+RT+0.1,W
VSWEEP,ALL
VSEL,S,LOC,Y,C+ROO-0.04*T-0.01,C+ROO+0.01
MSHKEY,0
MSHAPE, 1,3D
VMESH,ALL
VSEL,S,LOC,Y,C+ROO+RT-0.08*T-0.01,C+ROO+RT+0.01
MSHKEY,0
MSHAPE, 1,3D
VMESH,ALL

!--------------------------------------------
!   EXTRUDE TO FULL HEIGHT AND MESH
!--------------------------------------------
ASEL,S,LOC,Z,R
VEXT,ALL, , , , ,R
ESIZE,,9
ASEL,S,LOC,Z,2*R
VEXT,ALL, , , , ,H-2*R

!-----------------------------
!   DEFINE CRACK-TIP
!-----------------------------
CMSEL,S,DRAGLINE,LINE
NSLL,S,1
CM,CRACKTIP,NODE            ! DEFINE COMPONENT FOR CRACKTIP
```

```
!--------------------------------------------------
!     BOUNDARY CONDITIONS
!--------------------------------------------------
NSEL,S,LOC,Y,0
D,ALL,UY,0                    ! CONSTRAIN UY DOF
*GET,X_CONSTR,KP,20,LOC,X  ! LOCATION TO CONSTRAIN X AT KP 20, more or less halfway T
NSEL,S,LOC,X,X_CONSTR       ! CONSTRAIN UX DOF
NSEL,R,LOC,Z,H              ! CONSTRAIN UX DOF
D,ALL,UX,0
*IF,CENTRE,EQ,0,THEN
  ASEL,S,AREA,,77,1457,60
  ASEL,A,AREA,,36,1416,60
  ASEL,A,AREA,,49,1429,60
  ASEL,A,AREA,,62,1442,60
  ASEL,A,AREA,,69,1449,60
  ASEL,A,AREA,,1745,1800,5
  ASEL,A,AREA,,1747,1802,5
  ASEL,A,LOC,Y,C,W    ! CONSTRAIN AREAS THAT ARE NOT PART OF THE CRACK
  ASEL,R,LOC,Z,0
  CM,CONSTRAINAREAS,AREA
  CMSEL,S,CONSTRAINAREAS,AREA
  NSLA,S,1
  D,ALL,UZ,0          ! CONSTRAIN UZ DOF
*ELSEIF,CENTRE,EQ,1
  NSEL,S,LOC,Y,C-0.1,W
  NSEL,R,LOC,Z,0
  D,ALL,UZ,0          ! CONSTRAIN UZ DOF
*ENDIF


!--------------------------------------------------
!   LOADS
!--------------------------------------------------
*IF,N,EQ,0,THEN             ! TENSION
  NSEL,S,LOC,Z,H
  SF,ALL,PRES,-SIGMA        ! SURFACE PRESSURE LOADING
*ELSEIF,N,EQ,1              ! BENDING
  SFGRAD,PRES,0,X,T,SIGMA/T ! PRESSURE LOAD GRADIENT
  NSEL,S,LOC,Z,H
  SF,ALL,PRES,0             ! SURFACE PRESSURE LOADING
*ENDIF
ALLSEL
FINISH

!--------------------------------------------------
!   SOLVE SYSTEM AND RETRIEVE K AND J-INTEGRAL DATA
!--------------------------------------------------
/SOLU
CINT,NEW,1                        ! CRACK ID
CINT,TYPE,SIFS                    ! DEFINE CRACK TYPE
CINT,CTNC,CRACKTIP,NODE(0,0,0),0 ! DEFINE CRACK TIP COMPONENT
CINT,NORM,0,3                     ! CRACK PLANE NORMAL - Z
CINT,NCON,5                       ! NO OF CONTOURS
CINT,SYMM,ON                      ! SYMMETRY ON
CINT,LIST
CINT,NEW,2                        ! CRACK ID
CINT,TYPE,JINT                    ! DEFINE CRACK TYPE
CINT,CTNC,CRACKTIP,NODE(0,0,0),0 ! DEFINE CRACK TIP COMPONENT
```

```
CINT,NORM,0,3                          ! CRACK PLANE NORMAL - Z
CINT,NCON,5                            ! NO OF CONTOURS
CINT,SYMM,ON                           ! SYMMETRY ON
CINT,LIST
ALLSEL,ALL
SAVE
/NERR,0,,,,
SOLVE
FINI
/POST1
EPLOT
SET,LAST,LAST
CMSEL,S,CRACKTIP,NODE
*GET,NNUM,NODE,0,COUNT
*GET,NMIN,NODE,0,NUM,MIN
*DIM,VAL,ARRAY,NNUM,8 ! CREATE ARRAY FOR VALUES
I = 1
*DO,I,1,NNUM
  NCUR = NMIN
  *GET,X_COOR,NODE,NCUR,LOC,X
  VAL(I,1) = X_COOR
  *GET,Y_COOR,NODE,NCUR,LOC,Y
  VAL(I,2) = Y_COOR
  *GET,K1,CINT,1,CTIP,NCUR,,1,,K1
  *GET,K2,CINT,1,CTIP,NCUR,,2,,K1
  *GET,K3,CINT,1,CTIP,NCUR,,3,,K1
  *GET,K4,CINT,1,CTIP,NCUR,,4,,K1
  *GET,K5,CINT,1,CTIP,NCUR,,5,,K1
  K = (K3+K4+K5)/3
  VAL(I,3) = K
  *GET,J1,CINT,2,CTIP,NCUR,,1,,JINT
  *GET,J2,CINT,2,CTIP,NCUR,,2,,JINT
  *GET,J3,CINT,2,CTIP,NCUR,,3,,JINT
  *GET,J4,CINT,2,CTIP,NCUR,,4,,JINT
  *GET,J5,CINT,2,CTIP,NCUR,,5,,JINT
  KJ1 = (J1*EMOD/(1-NU*NU))**0.5
  VAL(I,4) = KJ1
  KJ2 = (J2*EMOD/(1-NU*NU))**0.5
  VAL(I,5) = KJ2
  KJ3 = (J3*EMOD/(1-NU*NU))**0.5
  VAL(I,6) = KJ3
  KJ4 = (J4*EMOD/(1-NU*NU))**0.5
  VAL(I,7) = KJ4
  KJ5 = (J5*EMOD/(1-NU*NU))**0.5
  VAL(I,8) = KJ5
  I = I+1
  *GET,NMIN,NODE,NCUR,NXTH
*ENDDO

!-------------------------
! WRITE DATA TO .TXT FILE
!-------------------------
*CFOPEN,X_Y_K_KJ1_KJ2_KJ3_KJ4_KJ5,TXT        ! CREATE FILE
*VWRITE,VAL(1,1),VAL(1,2),VAL(1,3),VAL(1,4),VAL(1,5),VAL(1,6),VAL(1,7),VAL(1,8)
(f10.6,3x,f10.6,3x,f10.5,3x,f10.5,3x,f10.5,3x,f10.5,3x,f10.5,3x,f10.5) ! 3X BLANK SPACE
*CFCLOSE                                      ! CLOSE FILE
FINISH
```

Appendix G

Input for the numerical model

The input (Table G-1) for the models is taken from [23] for series TH, [24] for THL and from [25] for series TB. Table G-2 shows the other input values, either published with the experimental data or estimated values. The latter have no or only limited influence on the results and are only given here for completeness.

Table G-1: Input for the models

	$\Delta\sigma_m$ [MPa]	$\Delta\sigma_b$ [MPa]	$\hat{C}_C$ $\left[(\text{MPa}\sqrt{\text{m}})^{-\hat{m}}\cdot\text{m}\right]$ $\times 10^{-12}$	$\hat{m}$ [-]	a_1, c_1 [m] $\times 10^{-3}$	t [m] $\times 10^{-3}$	W [m] $\times 10^{-3}$
TH-1	211.9	0	2.45	3.11	2	10	25
TH-3	132.4	0	2.45	3.11	7	10	25
THL-1	212	0	4.05	2.94	11	25	100
TB-2	126		1.54	3.33	5	10	35
TB-3	126		1.54	3.33	5	10	35
TB-6	126		1.54	3.33	5	10	35
TB-7	126		1.54	3.33	1	10	35
TB-8	70		2.56	3.33	5	10	35
TB-9	70		2.56	3.33	5	10	35
TB-11	70		2.56	3.33	2.5	10	35

Table G-2: Other model input

	σ_y [MPa]	ν [-]	E [MPa]	ΔK_{th} [MPa$\sqrt{\text{m}}$]	K_c [MPa$\sqrt{\text{m}}$]	K_{Ic} [MPa$\sqrt{\text{m}}$]
TH, THL	824	0.3	207×10^3	12	200	200
TB	943.4	0.3	207×10^3	9 or 5	200	132

Dealing with incomplete data-sets

The data-sets of series TB are subjected to a bending stress that varies during crack development. This variation is only published as a function of crack growth and propagation at the crack initiation side of the specimen [25]. However, this variation of the bending stress ratio $\Delta\sigma_b/\Delta\sigma_m = f(c)$ is only plotted for four of the seven data-sets. In Figure H-1 the measured values as well as the fitted functions of the four known data-sets are shown as well as the assumptions for the variation of three unknown bending stress ratios. The three other curves are estimated by combining the four known curves. Another clue for the estimates is the statement that [25]:

> As the crack propagates, the bending stress decreases and approaches zero at a very high rate after penetration. The decrease of the bending stress increases as eccentricity, e, increases.

The load ratio R is varied and the load is applied with an eccentricity w.r.t. the centreline of the cracked part of the specimen. Obviously, a higher eccentricity corresponds to a larger bending stress ratio. The used e and R are given in Table H-1.

For data-set TB-2 and TB-7, both $\Delta\sigma_b/\Delta\sigma_m = f(c)$ and the calculated crack development $a/c = f(a/t)$ are plotted in [25]. To confirm that this curve fitted variation of $\Delta\sigma_b/\Delta\sigma_m = f(c)$ with a fixed value for $\Delta\sigma_m$ is indeed used in the predictive models of the data source,

Table H-1: Eccentricity and load ratio for the specimens loaded by bending and tension

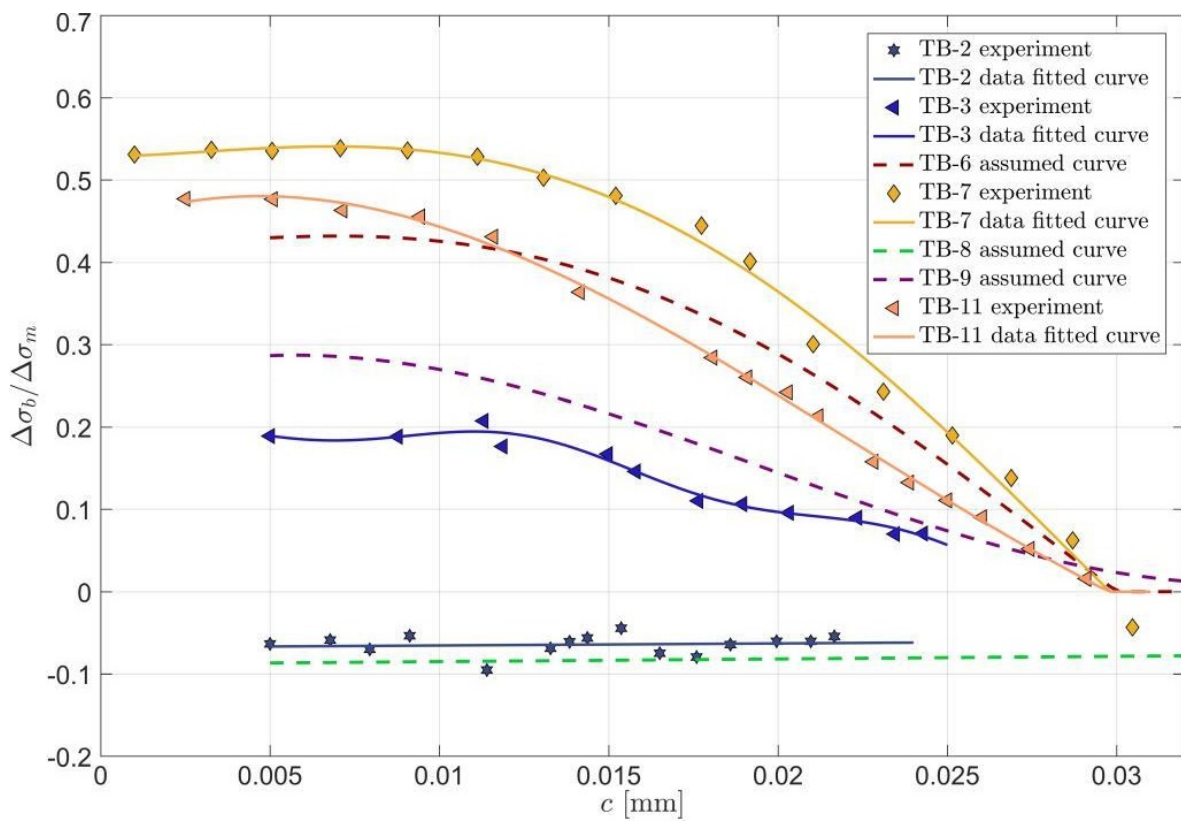|	e [mm]	R	$\Delta\sigma_b/\Delta\sigma_m = f(c)$ known?	$a/c = f(a/t)$ known?
TB-2	-0.2	0.1	✓	✓
TB-3	0.6	0.1	✓	-
TB-6	2.3	0.1	-	-
TB-7	3.0	0.1	✓	✓
TB-8	-0.1	0.5	-	-
TB-9	1.0	0.5	-	✓
TB-11	3.0	0.5	✓	-

Figure H-1: Relation between crack length at the initiation side and bending stress ratio.
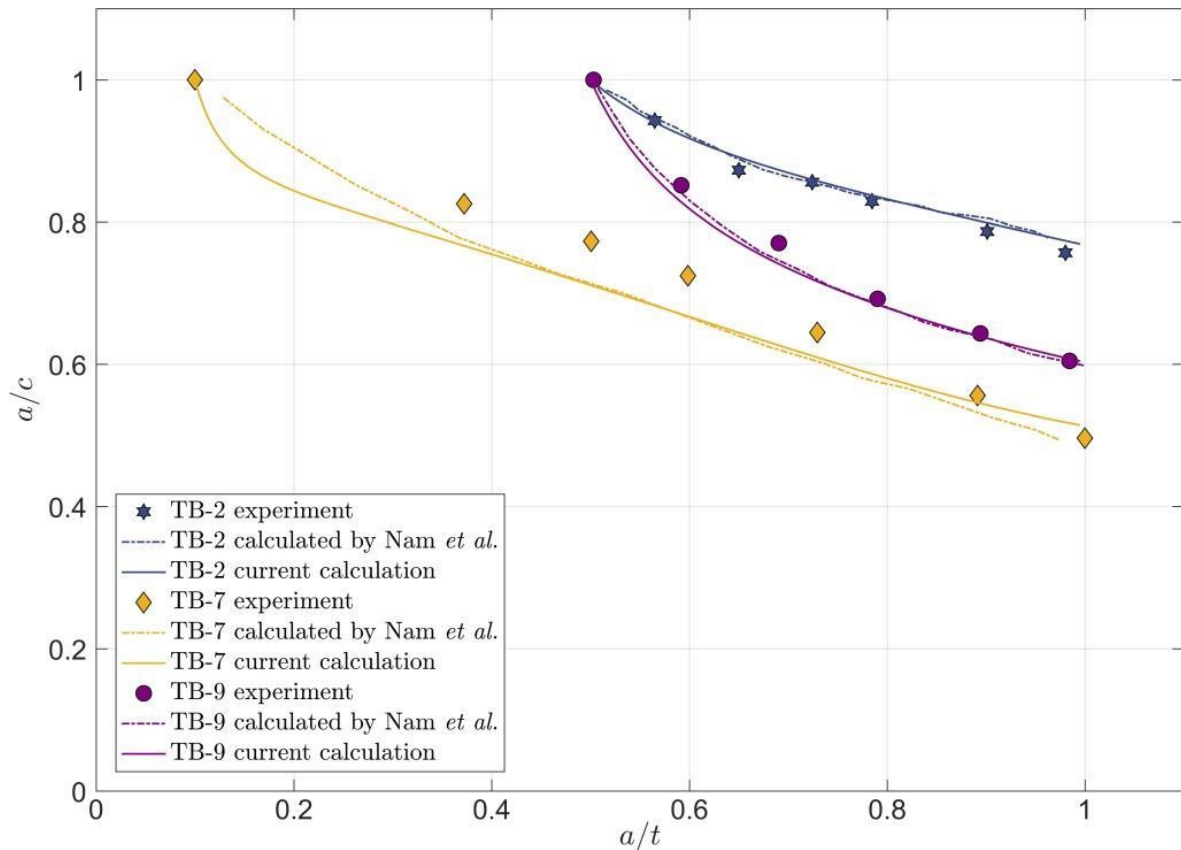
Figure H-2: Crack shape development before breakthrough

the source and current calculations of $a/c = f(a/t)$ are plotted in Figure H-2, together with the values that were measured from the experiments. Current calculations data-set TB-2 and TB-7 are in reasonable accordance with the those of Nam *et al.*. With this correspondence of calculation methods being confirmed, estimates of the bending ratio can be made for the remaining three data-sets.

By comparing the plots of TB-7 and TB-11 that both have an e of 3.0 mm, it is assumed that a higher R leads to a lower eccentricity. Therefore, it is expected that TB-8 should have approximately the same bending ratio as TB-2. By using the information of the development of $a/c = f(a/t)$, a reasonable assumption for TB-9 can be made. For instance, a rapid decrease in a/c corresponds to a high bending ratio. The curve of TB-6 is, given its e and R, expected to be positioned between TB-3 and TB-7. The estimates are optimized in such a way that they approximate the calculations of Nam *et al.* in Figures 4-7 to 4-8.

Bibliography

[1] R. Bourga, P. Moore, Y.-J. Janin, B. Wang, and J. Sharples, "Leak-before-break: Global perspectives and procedures," *International Journal of Pressure Vessels and Piping*, vol. 129 - 130, pp. 43 – 49, 2015.

[2] The British Standards Institution, "Guide to methods for assessing the acceptability of flaws in metallic structures," 31 July 2015. BS 7910:2013+A1:2015.

[3] American and Petroleum Institute, *Recommended practice 579 Fitness-For-Service*. API 579-1/ASME FFS-1 ed., June 5 2007.

[4] Structural Integrity Assessment Procedures for European Industry, *SINTAP Procedure*. November 1999. Chapter IV.5.

[5] The Marine Safety Committee, *Amendments to the international code for the construction and equipment of ships carrying liquefied gases in bulk*. Resolution MSC.370(93) ed., 22 May 2014.

[6] J. Schijve, *Fatigue of Structures and Materials*. Springer Netherlands, 2nd ed., 2009.

[7] D. Cudeiro and S. Osuna, "Engineering critical analysis of LNG cargo containments," June 2016. Lloyd's Register Marine Internal report.

[8] J. C. Newman and I. S. Raju, "An empirical stress-intensity factor equation for the surface crack," *Engineering Fracture Mechanics*, vol. 15, no. 1-2, pp. 185–192, 1981.

[9] H. Tada, P. C. Paris, and G. Irwin, *The stress analysis of cracks handbook*. ASME Press, 3rd ed., 2000.

[10] D. P. Rooke and D. J. Cartwright, *Compendium of stress intensity factors*. H.M.S.O., 1976.

[11] Y. Murakami, *Stress Intensity factors handbook*. Pergamon Oxford, 1992.

[12] T. Anderson, *Fracture Mechanics*. CRC Press, Inc., 1991.

[13] H. F. Bueckner, "Weight functions and fundamental fields for the penny-shaped and the half-plane crack in three-space," *International Journal of Solids and Structures*, vol. 23, no. 1, pp. 57 – 93, 1987.

[14] G. Shen and G. Glinka, "Determination of weight functions from reference stress intensity factors," *Theoretical and Applied Fracture Mechanics*, no. 15, pp. 237–245, 1991.

[15] G. Shen and G. Glinka, "Universal features of weight functions of cracks in mode I," *Engineering Fracture Mechanics*, vol. 40, no. 6, pp. 1135–1146, 1991.

[16] M. Isida, H. Noguchi, and T. Yoshida, "Analysis of stress intensity factors for surface cracks subjected to arbitrarily distributed surface stress," in *Stress Intensity Factor Handbook* (Y. Murakami, ed.), vol. 2, pp. 698–705, Pergamon, 1987.

[17] G. Shen and G. Glinka, "Weight functions for a surface semi-elliptical crack in a finite thickness plate," *Theoretical and Applied Fracture Mechanics*, vol. 15, pp. 247–255, 1991.

[18] X. Wang, "Stress intensity factors and weight functions for deep semi-elliptical surface cracks in finite-thickness plates," *Fatigue & Fracture of Engineering Materials & Structures*, vol. 25, no. 3, pp. 291–304, 2002.

[19] J. Sharples and A. Clayton, "A leak-before-break assessment method for pressure vessels and some current unresolved issues.," *International Journal of Pressure Vessels & Piping*, vol. 43, pp. 317 – 327, 1990.

[20] K. Shingai, N. Imamura, T. Hirata, M. Ushijima, and D. Sakai, "The fatigue crack propagation of 9% Ni-steel for the tank of LNG carriers," *Collection of papers of The Society of Naval Architects of Japan*, 1974. (in Japanese).

[21] M. Bransen, "On the crack shape development in spherical LNG tanks for a Leak-Before-Break assessment," March 2016. Research Exercise.

[22] B. Brickstad and I. Sattari-Far, "Crack shape developments for LBB applications," *Engineering Fracture Mechanics*, vol. 67, no. 6, pp. 625 – 646, 2000.

[23] K. Ando, S. Fujibashi, K. W. Nam, M. Takahashi, and N. Ogura, "The fatigue life and crack through thickness behavior of a surface-cracked plate (for the case of tensile load)," *Japan Society of Mechanical Engineers International Journal*, vol. 30, no. 270, pp. 1898–1905, 1987.

[24] K. W. Nam, K. Ando, and N. Ogura, "The effect of specimen size on the behaviour of penetrating fatigue cracks," *Fatigue and Fracture of Engineering Materials and Structures*, vol. 16, no. 7, pp. 767–779, 1993.

[25] K. W. Nam, K. Ando, N. Ogura, and K. Matui, "Fatigue life and penetration behaviour of a surface cracked plate under combined tension and bending," *Fatigue and Fracture of Engineering Materials and Structures*, vol. 17, no. 8, pp. 873–882, 1994.

[26] J. G. Kaufman, R. J. Bucci, and R. A. Kelsey, "Fracture mechanics aspects of the structural integrity technology of spherical aluminium containment vessels for LNG tankers," *Journal of Engineering Materials and Technology*, vol. 102, pp. 303–314, 1980.

[27] P. C. Paris and F. Erdogan, "A critical analysis of crack propagation law," *Transactions of the American Society of Mechanical Engineering; Journal of Basic Engineering*, vol. 85, pp. 528–539, 1963.

[28] *ANSYS Help - Mechanical APDL Documentation*, 16 March 2015. Version 16.1.0, online accessible through `https://www.sharcnet.ca/Software/Ansys/16.2.3/en-us/help/ai_sinfo/mech_intro.html`.

[29] R. J. Hartranft and G. C. Sih, "Effect of plate thickness on the bending stress distribution around through cracks," *Studies in applied mathematics*, vol. 47, no. 1-4, pp. 276–291, April 1968.

[30] P. Schreurs, *Fracture Mechanics*. Eindhoven University of Technology Department of Mechanical Engineering, Augustus 2014. `http://www.mate.tue.nl/~piet/edu/frm/pdf/frmsyl1415.pdf`.

[31] A. T. Zehnder, *Fracture Mechanics*. No. 62 in Lecture Notes in Applied and Computational Mechanics, Springer Netherlands.

[32] J. Knott, *Fundamentals of Fracture Mechanics*. Butterworth & Co Publishers Ltd, 1973.

[33] R. G. Forman, V. E. Kearney, and R. M. Engle, "Numerical analysis of crack propagation in cyclic loaded structures," *Transactions of the American Society of Mechanical Engineering; Journal of Basic Engineering*, vol. 89, pp. 459–464, 1967.

[34] S. Y. Yarema, "Correlation of the parameters of the paris equation and the cyclic crack resistance characteristics of materials," *Strength of Materials*, vol. 13, no. 9, pp. 1090–1098, 1981.

[35] K. W. Nam, F. S., K. Ando, and N. Ogura, "The fatigue life and fatigue crack through-thickness behavior of a surface-cracked plate (effect of stress concentration)," *Japan Society of Mechanical Engineers International Journal*, vol. 31, no. 2, pp. 272–279, 1988.

[36] K. W. Nam, K. Iwase, and K. Ando, "Fatigue life and surface crack penetration behaviour of an aluminium alloy," *Fatigue and Fracture of Engineering Materials and Structures*, vol. 18, no. 2, pp. 179–187, 1995.

[37] K. E. Atkinson and L. F. Shampine, "Solving Fredholm Integral Equations of the Second Kind in MATLAB," May 5 2007. `http://homepage.divms.uiowa.edu/~atkinson/ftp/Fie_paper.pdf`.

[38] M. Murthy, K. Raju, and S. Viswanath, "On the bending stress distribution at the tip of a stationarycrack from reissner's theory," *International Journal of Fracture*, vol. 17, no. 6, December 1981.